MODELLING THE IMPACT OF MAGNETOHYDRODYNAMICS (MHD) NANOFLUID FLOW ON COOLING OF ENGINEERING SYSTEMS

by

Tshivhi Khodani Sherrif

Thesis presented in fulfilment of the requirements for the degree of Masters of Military Science in Technology in the Faculty of Military Science at Stellenbosch University

Supervisor: Prof Oluwole Daniel Makinde

December 2021

DECLARATION

By submitting this thesis electronically, I declare that the entirety of the work contained therein is my own, original work, that I am the sole author thereof (save to the extent explicitly otherwise stated), that reproduction and publication thereof by Stellenbosch University will not infringe any third party rights and that I have not previously in its entirety or in part submitted it for obtaining any qualification.

December 2021

CERTIFICATE

The undersigned certify that they have read and found the thesis titled, **Modelling the Impact of Magnetohydrodynamics (MHD) Nanofluid Flow on Cooling of Engineering Systems** to be in a form acceptable for examination by Faculty of Military Science Stellenbosch University, of the requirements for the degree the Masters of Military Science in Technology (Mathematics).

Date __December 2021_

ACKNOWLEDGEMENT

I would like to thank God for His guidance throughout my studies.

I would like to thank my supervisor prof O.D. Makinde for his continues support, valuable guidance, and encouragement towards my studies. I have learned so many things from you, and I am proud of this, and my heartfelt appreciation to you for affording me this learning process. I would never have believed that I would be able to stand in front of people and share with them a productive talk about nanofluid and computational mathematics. I am proud to be an applied mathematician. Furthermore, thank you for the academic exposure and I will not forget Rhodes University and University of Cape Town.

I am grateful and thankful to my family for their continues support, keeping me motivated, and believing in me to always do my best. To my mom, Azwinndini Florah Tshivhi; my two lovely sisters, Happiness Tshivhi and Ndivhuwo Tshivhi; my son Obanzi Khodani Mamkeli; and my extended family, your prayers have carried me and have helped me to complete this thesis. To my late granny, Mma Ntsundeni Tshivhi, it was my wish to see you at my graduation, but God has decided and may your soul continue to rest in peace.

My gratitude to Maj (Dr) R.L. Monaledi for all your support you have given me and may God continue to bless you. You have planted the seed for a love of mathematics and now the seed has grown into big tree that no one can ever destroy. My love for mathematics will help me to help anyone with mathematics.

My final appreciation is to the Military Academy and the Faculty Military Science for affording me this opportunity and to the members who believed and supported me over the years.

Ndo livhuwa

ABSTRACT

The flow investigations regarding nonlinear materials are extremely important in the applied science and engineering areas to explore the properties of flow and heat transfer. Recent advancement in nanotechnology has provided a veritable platform for the emergence of a better ultrahigh-performance coolant known as nanofluid for many engineering and industrial technologies. In this study, we examine the influence of a magnetic field on the heat transfer enhancement of nanofluid coolants consisting of Cu-water, or Al_2O_3-water, or Fe_3O_4-water over slippery but convectively heated shrinking and stretching surfaces. The model is based on the theoretical concept of magnetohydrodynamics governing the equation of continuity, momentum, energy, and electromagnetism. Based on some realistic assumptions, the nonlinear model differential equations are obtained and numerically tackled using the shooting procedure with the Runge-Kutta-Fehlberg integration scheme. The existent of dual solutions in the specific range of shrinking surface parameters are found. Temporal stability analysis to small disturbances is performed on these dual solutions. It is detected that the upper branch solution is stable, substantially realistic with the smallest positive eigenvalues while the lower branch solution is unstable with the smallest negative eigenvalues. The influence of numerous emerging parameters on the momentum and thermal boundary layer profiles, skin friction, and Nusselt number are depicted graphically and quantitatively discussed.

TABLE OF CONTENTS

LIST OF FIGURES

LIST OF TABLES

NOMENCLATURE

Roman Letter

(u, v)	Velocity components
(x, y)	Cartesian Coordinates
B_0	Constant applied magnetic field
C_p	Specific heat at constant pressure
Nu	Nusselt number
Pr	Prandtl number
Ec	Eckert number
Bi	Biot Number
q_w	Dimensional heat flux
Re_x	Reynolds number
T	*T*emperature
k	Thermal conductivity
h_f	Heat transfer coefficient

Greek symbols

Ψ	Stream function
θ	Dimensionless temperature
H	Similarity variable
β	Thermal expansion coefficient
α	Thermal diffusivity
ϕ	Solid volume fraction
μ	Dynamic viscosity
υ	Kinematic viscosity
σ	Electrical conductivity
ρ	Density
τ_w	Skin friction or shear stress
λ	Stretching or shrinking
S	Slip Coefficient

Subscripts

f	Fluid
s	Solid
nf	Nanofluid

LIST OF PUBLICATIONS

K.S. Tshivhi, O.D. Makinde: Magneto-nanofluid coolants past heated shrinking/stretching surfaces: Dual solutions and stability analysis, Results in engineering, Volume 10, June 2021, 100229, doi.org/10.1016/j.rineng.2021.100229.

LIST OF CONFERENCES

K.S. Tshivhi, O.D. Makinde: presented a paper titled*:* Stagnation point flow of magneto-nanofluid towards a convectively heated stretching or shrinking sheet with Navier slip, University of Cape Town, Cape Town, RSA. 1 – 4 December 2019. (Awarded first best Price for masters presentations paper)

CHAPTER 1: INTRODUCTION AND BACKGROUND

1.1 Fluids

A fluid can be defined as a substance that continues to flow under the action of applied shear stress and that cannot resist any shear force when applied to it. The phases of matter that are assumed to be fluids include liquids, solids, gases, and plasmas as shown in Figure 1.1, respectively. Fluid mechanics is the branch of science that deals with the behaviour of fluids at rest as well as in motion. Additionally, it entails the static, kinematics, and dynamic aspects of fluids [1]. The study of fluids at rest is called fluid statics while the fluid in motion is called fluid dynamics if pressure forces are considered. The properties of fluids include the density of a substance, which is the mass per unit volume denoted by ρ; specific weight, which is the weight per unit volume of a material denoted by w; compressibility, which is a measure of the relative volume change of a fluid to a pressure change; and viscosity, which is the resistance of a fluid to a change in shape. The type of fluid that we will consider in this study is Newtonian fluids that obey Newton's law of viscosity.

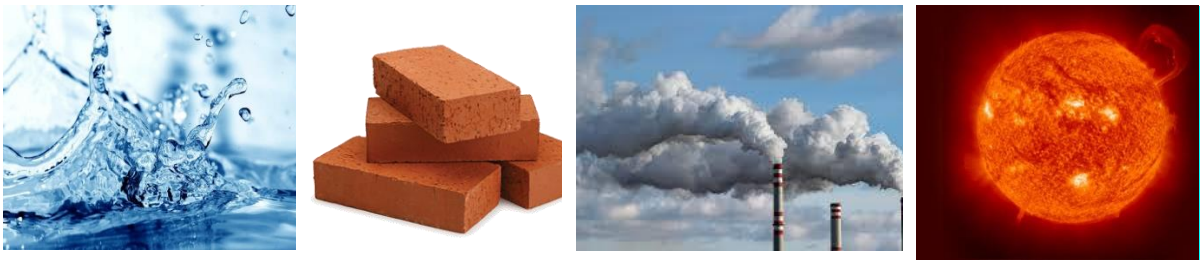

Figure 1.1: The four-common states of matter liquids, solids, gases, and plasmas. [85][86][87][88]

1.2 Heat Transfer

Heat transfer can be defined as the movement of energy from one place to another because of temperature differences. Furthermore, it is a branch of thermal science which deals with the analysis of the rate of heat transfer and temperature distribution that takes place in a system as well as the nature of heat transfer[2]. The concept of heat transfer deals with the amount of heat to be transmitted; time taken during heating/cooling; the area required for the process; the possibility of addition or removal of heat at the desired rate; and the temperature distribution existing within the system [3] [4]. It is advisable for an engineer to have a good understanding of the rate of heat transfer and the amount of heat transferred before they design boilers, condensers, evaporators, heaters, refrigerators, and heat exchangers. The fundamental laws that are applied in all major areas of heat transfer include the law of conservation of mass, Newton's second law of motion, and the first and second law of thermodynamics.

There are some useful experimental results which include Fourier's law of heat conduction, Newton's law of cooling/heating and Stefan-Boltzman's law of thermal radiation. Heat transfer can be achieved by conduction, convection or radiation as discussed below.

1.2.1 Conduction

This is a form of heat transfer that exists due to direct contact within a medium or between different mediums where heat is transferred from a region of high temperature to a region of low temperature without the actual movement of particles. In conduction, the heat is transmitted when the neighbouring particles collide with each other and cause a vibration. These vibrating particles collide with their neighbouring particles making them vibrate faster and as a result, heat is being transferred to the rest of the material as shown in Figure 1.2 below. Fourier's law of thermal conduction in differential form states that the local heat flux density q is equal to the product of thermal conductivity k and the negative local temperature gradient $-\nabla T$. The heat flux density is the amount of energy that flows through a unit area per unit of time.

$$q = -k\nabla T. \tag{1.1}$$

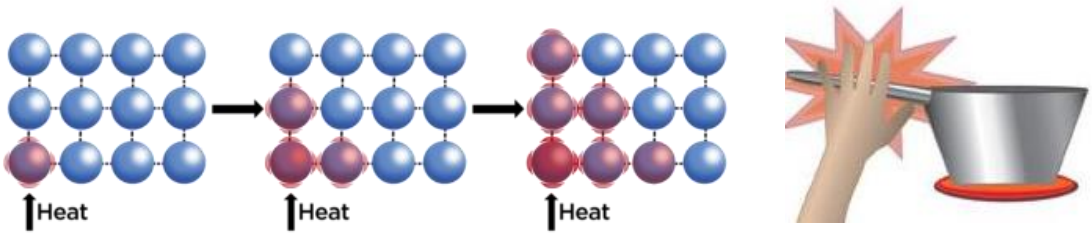

Figure 1.2: Phase of heat transfer in conduction. [89][90]

1.2.2 Convection

This form of heat transfer exists due to fluids near the heat source that gains energy and becomes less dense and rises to the top surface, whilst the fluid at the top of the surface descends near the heat source. This happens due to the mobile particle i.e. liquids and gases. The convection heat transfer may be classified into free/natural convection and forced convection as described below. The governing equation of convection heat transfer is Newton's law of cooling or heating where q is the heat transferred per unit time, A is the area of the object, h is the heat transfer coefficient, T is the surface temperature, and T_f is the fluid temperature. Newton's law of cooling is given in the equation below [5],

$$q = hA(T - T_f). \tag{1.2}$$

1.2.2.1 Free/Natural Convection

This type of convection is self-sustained and occurs when the motion within a fluid is caused due to density variations. Moreover, if the Grashof number is divided by the Reynolds number squared, and is greater than one, the fluid will then experience free convection that is due to the flow being dominated by the buoyancy force. A good example of this includes a sea and the land breeze that occurs during the day or night as shown in Figure 1.3 below.

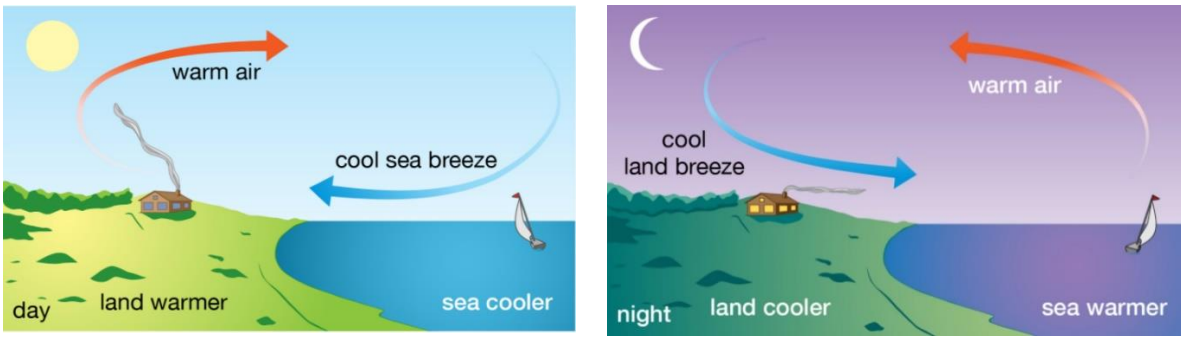

Figure 1.3: Illustration on natural convection at sea/land breeze. [91]

1.2.2.2 Forced Convection

This type of convection occurs when the motion within a fluid is caused due to an external agent like a blower for a gas or a pump for a liquid. These mechanical devices provide a definite path for the particles and set up the direction of flow that speeds up the rate of heat transfer. In addition, if the Grashof number is divided by the Reynolds number squared and it is less than one then the fluid will experience forced convection. This is due to the flow being dominated by the inertia force. Some of the examples of forced convection are shown in Figure 1.4 below.

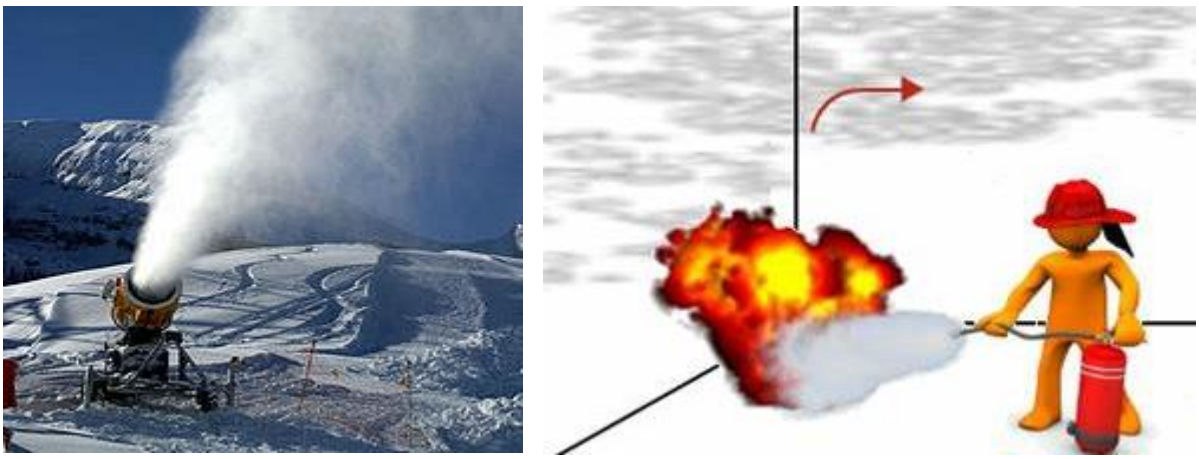

Figure 1.4: Illustration on forced convection by snow pump and fire extinguisher. [92][93]

1.2.3 Radiation

This form of heat transfer exists independent of a medium and where the heat energy is being transferred by electromagnetic waves. Moreover, this energy comes from a source, travels through space and may be able to penetrate various materials. It has been observed from experiments that a dark surface absorbs most of the thermal radiation while a silver surface reflects the thermal radiation as shown in Figure 1.5a.

$$q = \varepsilon\sigma^* A\left(T^4 - {T_f}^4\right), \tag{1.3}$$

The law of Stefan Boltzmann is useful in describing the notion of the rate heat is being transferred by emitted radiation and where in equation 1.3 ε represents the surface emissivity, A is the surface area, σ^* is the Stefan-Boltzmann constant, T is the absolute temperature of the surface and T_f is the absolute temperature of the surroundings. Lastly, some examples of radiation heat transfer are shown in Figure 1.5b, c.

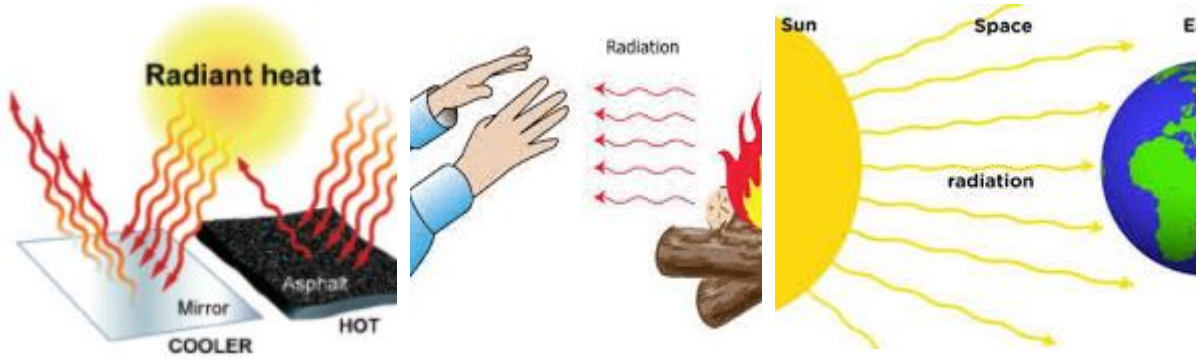

(a) (b) (c)

Figure 1.5: Visuals of radiation in heat transfer for different materials.[94][95][96]

1.3 Magnetohydrodynamics (MHD)

Magnetohydrodynamics (MHD) is the study of electrically conducting fluid motion in the presence of a magnetic field [6]. The fluid may be a gas at elevated temperatures or liquid metals like sodium or potassium. The basic equations of MHD have been proposed by Hannes Alfven who realized the usefulness of electric currents carried by plasma and a magnetic field. Magneto fluid dynamics or hydromagnetics is the study of the dynamics of electrically conducting fluids. The application of MHD was first used in astrophysics and lead to other ranges of application that includes MHD pumps, MHD generators, MHD flow meters, ship propulsion, and jet printers and many others. The equations that govern MHD flow are

equations of fluid dynamics and Maxwell's equations which connects fluids mass density ρ, the fluid velocity q , the thermodynamic pressure P and the magnetic field B. The derivation of MHD equations as discussed below, neglect the motion of electrons and consider only heavy ions.

1.3.1 Continuity Equation

This equation is based on the law of conservation of mass, which states that "mass cannot be created or destroyed" [7]. This implies that the rate of change of particle mass is zero. The equation of continuity is given by,

$$\frac{\partial \rho}{\partial t} + \nabla \rho q = 0, \tag{1.4}$$

For incompressible fluid flow, ρ = constant, hence $\frac{\partial \rho}{\partial t}$ = 0, therefore, the continuity equation for an incompressible flow becomes,

$$\nabla q = 0, \tag{1.5}$$

where ∇q is called divergence of the fluid velocity, which physically is the rate of change of volume of a moving fluid element per unit volume.

1.3.2 Momentum Equation

Newton's second law of motion state that, $F = Ma$, where F is sum of all the forces, M is the mass and a is the acceleration of any fluid element. The result of deriving at Newton's second law led to the equation of momentum equation, which is given by,

$$\rho_{nf}\left[\frac{\partial q}{\partial t} + (q \cdot \nabla)q\right] = -\nabla P + \mu_{nf}\nabla^2 q + \boldsymbol{j} \times \boldsymbol{B}\,, \tag{1.6}$$

The parameter ρ_{nf} is the density of nanofluid, μ_{nf} is the dynamic viscosity of the nanofluid, the vector j is the electrical current density. Each unit volume of fluid that has $\boldsymbol{j}$ and, experiences MHD force $\boldsymbol{j} \times \boldsymbol{B}$, known as the Lorentz force. For incompressible fluid flow the density of the fluid is constant, therefore, the momentum equation becomes,

$$\frac{\partial q}{\partial t} + (q \cdot \nabla)q = -\frac{1}{\rho_{nf}}\nabla p + \frac{1}{\rho_{nf}}\nabla\left(\mu_{nf}\nabla q\right) + \boldsymbol{j} \times \boldsymbol{B}\,. \tag{1.7}$$

1.3.3 Energy Equation

The first law of thermodynamics states that if a system is changed from one state to another, the change in the total internal energy of the system is then equal to the sum of the work done in the system and the heat gain/loss in the system [8] and is given by

$$dQ = dE + dW\ , \tag{1.8}$$

The parameter W is the work done, E is the total internal energy, and Q is the amount of heat added to a system and derives from the first law of thermodynamics. The equation of Maxwell is very useful to derive the equation of magnetic field which are defined as follows,

$$\vec{j} = \sigma(\vec{E} + \vec{q} \times \vec{B}\ \ (Ohm's\ law)\ , \tag{1.9}$$

$$\nabla \times \vec{E} = -\frac{\partial \vec{B}}{\partial t}\ \ (Faraday's\ law\ of\ induction), \tag{1.10}$$

$$\nabla \times \vec{B} = \mu_e \vec{j}\ \ (Ampere'sciricuital\ law), \tag{1.11}$$

$$\nabla \cdot \vec{B} = 0\ \ (Gauss'law\ for\ magnetism)\ , \tag{1.12}$$

assuming the fluid is incompressible we then get the energy equation in the presence of a magnetic field as given by,

$$\left(\rho C_p\right)_{nf}\left(\frac{\partial T}{\partial t} + (V \cdot \nabla)T\right) = k_{nf}\nabla^2 T + \mu_{nf}\phi + \frac{j^2}{\sigma_{nf}}, \tag{1.13}$$

where $(\rho C_p)_{nf}$ is the nanofluid heat capacity term, $\left(\frac{\partial T}{\partial t} + q\nabla T\right)$ is the convention term, $\nabla\left(K_{nf}\nabla T\right)$ is the nanofluid thermal conductivity term, $\mu_{nf}\Phi$ is the nanofluid viscous dissipation term, and $\frac{j^2}{\sigma_{nf}}$ is heat source term. The following term gives the following equations,

$$\begin{gathered}\mu_{nf} = \frac{\mu_f(T)}{(1-\phi)^{25}}\ , K_{nf} = K_f\left(\frac{K_s + 2K_f - 2\phi\left(K_f - K_s\right)}{K_s + 2K_f + 2\phi\left(K_f - K_s\right)}\right), \\ (\rho C_p)_{nf} = (1-\phi)(\rho C_p)_f + \phi(\rho C_p)_s\ ,\end{gathered} \tag{1.14}$$

where ρ_f is the density of the basefluid, ρ_s is the density of the nanoparticle, ϕ is the volume fraction of the nanoparticles, μ_f is the dynamic viscosity of the basefluid, K_f is the thermal conductivity of the basefluid, K_s is the thermal conductivity of the nanoparticle, $(\rho C_p)_s$ is the heat capacitance of the nanoparticle, and $(\rho C_p)_f$ is the heat capacitance of the basefluid.

1.4 Nanofluids

The term nanofluids was given by Choi after he pioneered the newly innovative class of heat transfer fluids that depend on suspending nanoscale particles of metallic origin with an average particle size of less than 100 nm into conventional heat transfer fluids [9]**.** Nanofluids are fluids that are engineered by suspending small amounts of nanometre-sized (10–50 nm) solid materials having high thermal conductivity such as nanoparticles, nanofibers, nanotubes, nanowires, nanorods, nanosheet, or droplets in the basefluids. The literature search into nanofluids has been described by, Bhanvase *et al.* [10] " as the future of heat transfer fluids in various heat transfer applications". Nanofluids have been found to enhanced thermophysical properties such as thermal conductivity, thermal diffusivity, viscosity, and convective heat transfer coefficients compared to traditional basefluids like oil or water [11] as shown in Figure 1.6 below. With the rising demands of modern technology for process intensification and device miniaturization, there is a need to develop new types of fluids that are more effective in terms of heat exchange performance.

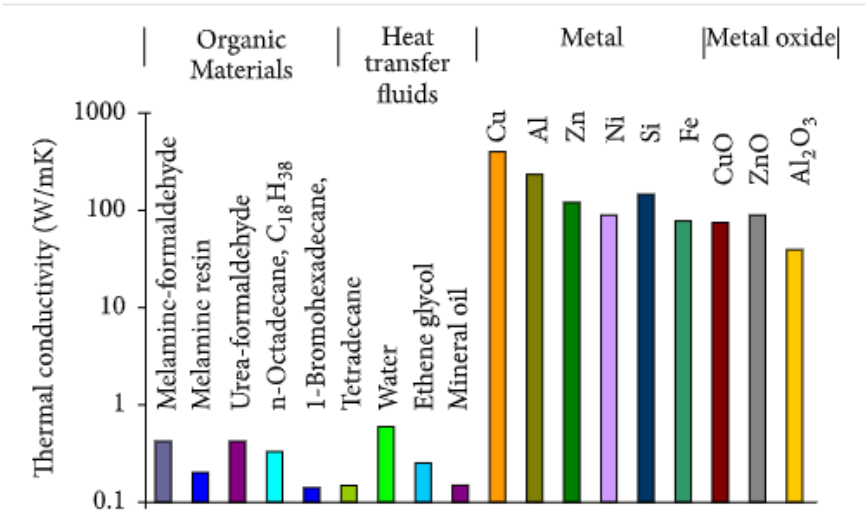

Figure 1.6: Thermal conductivity for different materials. [97]

1.5 Application of Nanofluid

Some useful applications of nanofluids include industrial cooling, heating buildings and reducing pollution, nuclear system cooling, Space, and defence of which some are being discussed below.

1.5.1 Heat Transfer Intensification

This is the theoretical or experimental study of enhancing or improving heat transfer performance by using nanofluids. Various review articles have been written on how to intensify heat transfer. In future, more heat transfer can be enhanced by increasing the heat transfer coefficient. The purpose of heat transfer intensification is to reduce the size and cost of heat exchanger equipment or to increase the heat duty for a given size heat exchanger based on the geometrical characteristics of the shell and tube exchangers.

1.5.2 Cooling of Electronics

The rapid development of modern technology has led designers of electronic components with more compact and higher-density chips which have made heat dissipation more difficult and that leads to a disturbance in normal performance, reduces reliability and the lifespan of devices [11]. Advanced electronic devices face thermal management challenges from the high level of heat generation and the reduction of available surface area for heat removal. Furthermore, a reliable thermal management system is vital for the smooth operation of the advanced electronic devices. Decreasing the temperature of electronic components, it increases their performance as well as their reliability. Therefore, an efficient cooling system is one of the most vital aspects when designing electronic components. There are two approaches to improve the heat removal for electronic equipment. One has to either find the optimum geometry of the cooling devices or to increase the heat transfer capacity. Nanofluid is commonly used due to its enhancement in heat transfer to reduce the temperature on electronic devices.

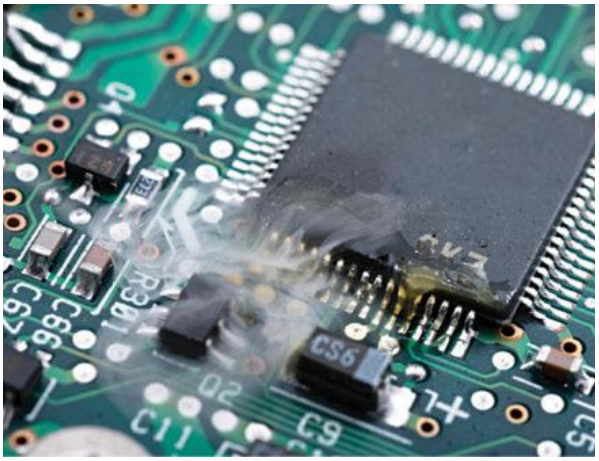

Figure 1.7: Basic Nanofluids cooling system used in cars, buildings, and electronics. [98][99]

1.5.3 Military application

Most military devices and systems require high-heat-flux cooling to the level of tens of MW/m^2. Moreover, cooling with conventional fluids is challenging due to their poor thermal conductivity. Furthermore, military applications include the cooling of power electronics and directed energy weapons [11]. In directed-energy weapons and power electronics involving high-heat-fluxes, it is critical to have an adequate cooling system. Nanofluids have the potential to provide the required cooling in such applications as well as in other military systems, including military vehicles, submarines, and high-power laser diodes. In some cases, nanofluid research for defence applications includes multifunctional nanofluids with added thermal energy storage or energy harvesting through chemical reactions [12].

Figure 1.8: Application of Nanofluids in the Military department. [100]

1.5.4 Transportation Cooling

Nanofluids have great potential to enhance automotive and heavy-duty engine cooling rates by increasing efficiency, lowering weight, and reducing the complexity of thermal management systems. In transportation departments, thermal management is highly important because it directly or indirectly affects engine performance, fuel economy, safety and reliability, aerodynamics, driver/passenger comfort, materials selection, emissions, maintenance, and component life [13]. Choi showed that nanofluids have the potential of being recognized as a new coolant for transportation departments due to their significantly higher thermal

conductivities than base fluids [10]. Since transportation is becoming more advance, it is beneficial to design more compact cooling systems with smaller and lighter radiators.

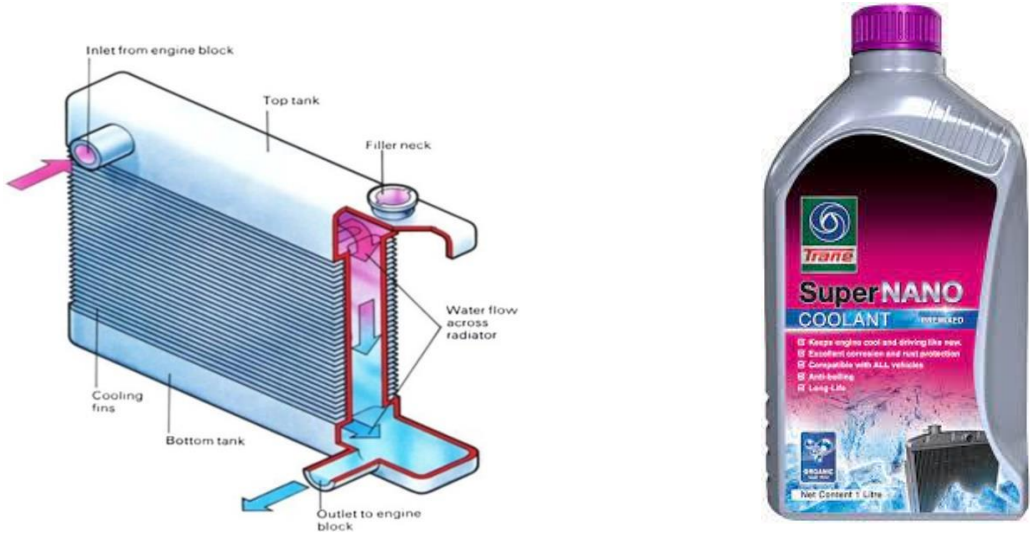

Figure 1.9: Application of nanofluids in the transportation department. [101][102]

1.6 Boundary Layer

A boundary layer is defined as a thin layer of viscous fluid close to the solid surface of a wall in contact with a moving stream in which the flow velocity varies from zero at the wall up to U_0 at the boundary. This approximately corresponds to the free stream velocity as shown in Figure 1.10. Also, the value of δ is an arbitrary value because of the friction force, depending on the molecular interaction between fluid and the solid body, it decreases with the distance from the wall and becomes equal to zero at infinity [14].

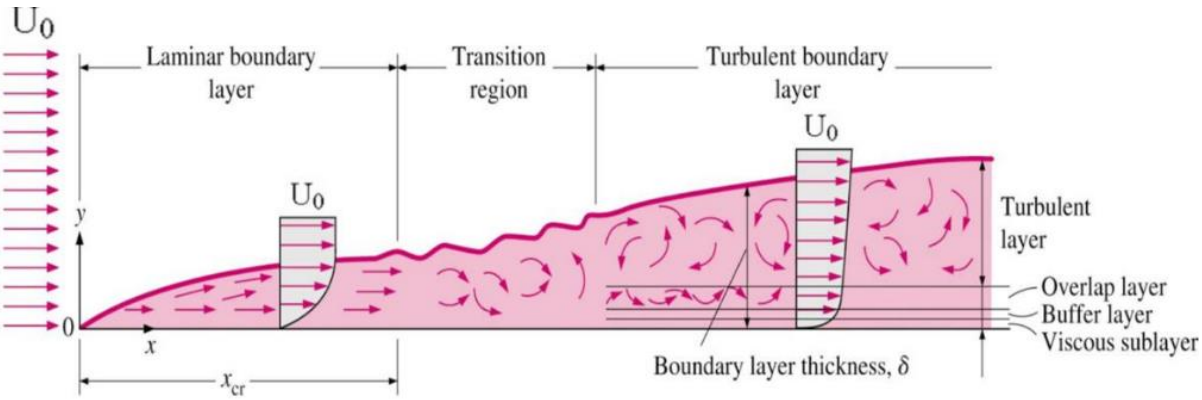

Figure 1.10: The development of the boundary layer for flow over a flat plate from laminar to turbulent boundary. [103]

The concept of the boundary layer was suggested by Prandtl in 1904 and defines the boundary layer as a layer of fluid developing in flows with a very high Reynolds number Re, that has a

relatively low viscosity compared to inertia forces [15]. In fluids that have a relatively small viscosity, the effect of internal friction in a fluid will be appreciable only in a narrow region surrounding the fluid boundaries. Since the fluid at the boundaries has zero velocity, there is a steep velocity gradient from the boundary into the flow. This velocity gradient in a real fluid sets up shear forces near the boundary that reduces the flow speed to that of the boundary [14].

Figure 1.11: Visualization of the flow around the car with a thin layer along the body caused by the viscosity of the fluid. [104]

The fluid layer that has its velocity affected by the boundary shear is called the boundary layer. For smooth upstream boundaries, the boundary layer starts as a laminar boundary layer in which the fluid particles move in smooth layers. As the laminar boundary layer increases in thickness, it becomes unstable and finally transforms into a turbulent boundary layer in which the fluid particles move in haphazard paths [15] . The laminar sub layer is when the boundary layer has become turbulent, and there is still a very thin layer next to the boundary layer that has laminar motion.

1.7 Stagnation Point Flow

The stagnation point flow is a fundamental aspect of fluid mechanics. A stagnation point is the study of fluid flow in the immediate neighbourhood of a solid surface. Furthermore, the fluid is stagnant everywhere on the solid surface due to the non-slip condition and thus their local fluid velocity is zero [16]. As the fluid approaches, the surface divides into two streams. The

application can be seen when air is flowing around an aeroplane wing, where there is often a spot just in front of the wing where the airflow is brought to a halt at a stagnation point.

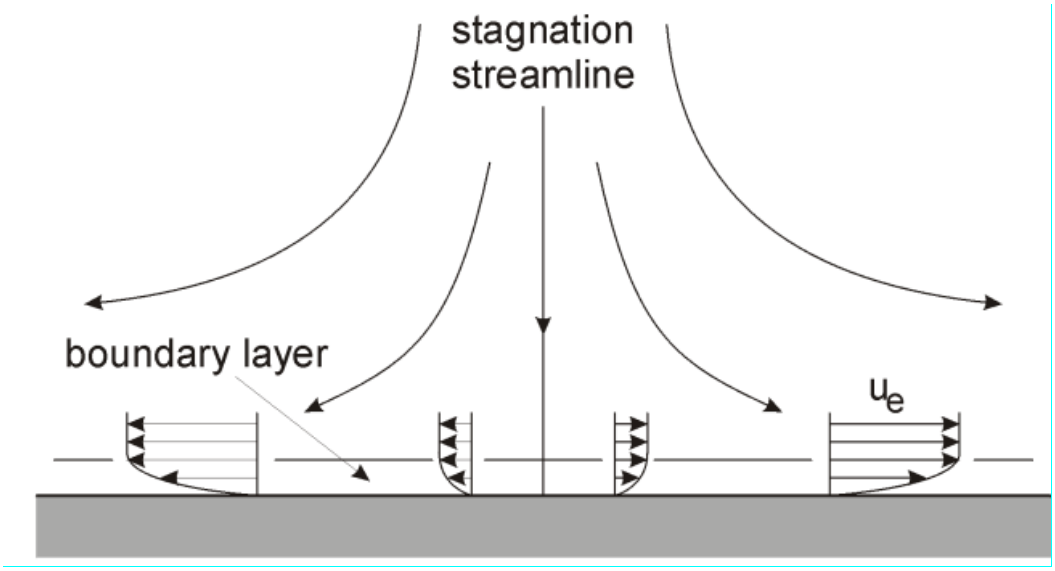

Figure 1.12: Nanofluid flowing toward the stagnation point to form a boundary layer. [105]

1.8 Navier Slip Condition

It is universally accepted that non-slip conditions at the boundary of a sold surface impose the interface between a solid and a liquid. The idea of a slip boundary condition was first proposed by Navier in 1823 [17] in his model in which he assumed the velocity u at a solid surface is proportional to its shear rate. Navier's proposed slip boundary condition is given as (1.15) where μ is the dynamic viscosity and β is the slip parameter.

$$\mu \frac{\partial u}{\partial y} = \beta u, \tag{1.15}$$

Ken *et al.* [18] used the Navier scalar slip properties to derive the effective slip boundary conditions for an arbitrary periodic surface.

1.9 Motivation of the Study

The motivation for this study is based on the lower production in the field of engineering where most of the time is spent on the cooling of the product due to high temperatures used during production. Nanofluids have been discovered to be the best coolant because of their high thermal conductivity; consequently, the heat transfer capacity of the fluid is enhanced during the flow process. Moreover, mathematical modelling and computations provide an excellent cost-effective platform to tackle real-life problem like the cooling of a heated surface.

Therefore, a mathematical model was designed to analyse the impact of magnetic nanofluid on the cooling of engineering systems. Relevant information on how to enhance the cooling of heated stretching, fixed and shrinking surfaces will be obtained.

From the literature research, it appears the problem of spray cooling stagnation point flow of magneto-nanofluid over a convectively heated slippery stretching, fixed or shrinking sheet has not been adequately investigated theoretically. Therefore, an attempt has been made in the present study to fill this missing gap. In the following chapters, the problem is formulated with respect to the basic flow equations, tackled both analytically and numerically. The equations describing the temporal development of small disturbances are developed and solved. The numerical solutions are obtained and displayed graphically and in tabular form. Pertinent results are discussed quantitatively.

1.10 Research Objectives

- To formulate a single phase nonlinear mathematical model for the impact of magnetic nanofluid flow over convectively heated stretching and shrinking slippery surfaces.
- To derive a similarity model equation by using appropriate similarity transformation.
- To develop appropriate numerical algorithms based on the shooting method coupled with the Runge-Kutta-Fehlberg integration scheme to solve the obtained nonlinear boundary value problem.
- To investigate the effects of various thermophysical parameters on the magnetic nanofluid velocity and temperature profiles.
- To investigate the effects of various thermophysical parameters on skin friction and Nusselt number.
- To obtain the critical values of the shrinking parameters at which no real solution exists (i.e. the surface can no longer shrink).
- To perform a hydromagnetic stability analysis on the basic dual solutions of the model problem for the case of shrinking surface.

1.11 Significance of the Study

Several engineering and industrial devices generate heat during operation. The accumulation of heat in these systems may lead to thermal runaway, inefficient operation and destruction of life and properties. This study is aimed at demonstrating the efficient way of removing high-heat-flux from heated surfaces using magnetic nanofluid. Moreover, spray cooling of heated surfaces using magnetic nanofluid for electronic devices, which is essentially a stagnation point flow problem, is an emerging area of research.

1.12 Research Methodology

In this study, the theoretical concept based on Continuum Mechanics, thermodynamics, electromagnetic theory, nanofluid thermophysical properties and numerical simulation techniques are employed. Equations that govern the fundamental of fluid dynamics are the continuity equation, momentum equation (NSE) and energy equations. The fundamental equations of electromagnetism are the modified electrodynamics equations called Maxwell's equation.

1.12.1 The Shooting Method

This study used the shooting method to solve the boundary value problem, since it has many advantages such as ease of programming in a general form, less storage that is required, and its suitability for automatic procedures. The shooting method is an iterative algorithm that reformulates the original boundary value problem to a related initial value problem (IVPs) with its appropriate initial conditions [19]. The new problem requires the solution of the IVP with the initial conditions arbitrary guessed to approximate the boundary conditions at the endpoints. If these boundary conditions are not satisfied to the required accuracy, the procedure is repeated with a new set of initial conditions until the required accuracy is acquired or a limit to the iteration is reached [20]. The resultant IVP is solved numerically using any appropriate method for solving linear ordinary differential equations. This study used the fourth-order-Runge-Kutta-Fehlberg integration scheme, which provided high accuracy results. The solution of the IVP should converge to that of the BVP. The algorithm for the above procedure is achieved by using Maple programming language. The computed results are presented in graphical form. A two-point boundary value problem was considered,

$$y'' = f(x, y, y'), \qquad y(a) = \alpha \ \ and \ \ y(b) = \beta. \tag{1.16}$$

Where $a < b$ and $x \in [a, b]$. The requirement of the shooting method is to convert the BVP to an IVP with appropriate initial condition. Thus, we have $y'' = f(x, y, y')$ with $y\ (a) = \alpha$ and

first guess for the initial value $y'(a) = s$. Introducing the notations $u(x;s) = y(x;s), v(x;s) = \frac{\partial}{\partial x}y(x;s)$ to equation (1.16) and rewritten the system of first order ODEs as,

$$\frac{\partial}{\partial x}u(x;s) = v(x;s), \qquad u(a;s) = \alpha \quad \frac{\partial}{\partial x}v(x;s) = f(x;u(x;s)), \quad v(a;s) = \beta, \tag{1.17}$$

The solution $u(x;s)$ of the IVP (1.20), will coincide with the solution $y(x)$ of the BVP (1.16), if a value for s is found, such that, $\phi(s) = u(b;s) - \beta = 0$. Equation (1.17) is solvable if and only if there exists $s\epsilon\mathbb{R}$, so that $\phi(s) = 0$. The essence of the shooting method for the solution of the BVP (1.16) is to find a root to the equation (1.17). A standard root-finding technique such as the Bisection method or Newton-Raphson method is used.

1.12.2 Newton's Raphson Method

This method is one of the most powerful and well-known methods used for finding a root of $f(x) = 0$. The formula may be derived in many ways. The simplest way to derive this formula will be to compute a sequence $\{s_n\}_{n=1}^{\infty}$ generated by $s_{n+1} = s_n - \frac{\phi(s_n)}{\phi'(s_n)}$ starting with a value s_n arbitrary guessed to calculate $\phi'(s_n)$. New independent variables $\xi(x;s) = \frac{\partial u(x;s)}{\partial x}, \eta(x;s) = \frac{\partial v(x;s)}{\partial x}$ are introduced and differentiate the IVP (1.19) with respect to s to obtain a second IVP,

$$\begin{aligned} \frac{\partial \xi(x;s)}{\partial x} &= \eta(x;s), \qquad \xi(a;s) = 0, \\ \frac{\partial \eta(x;s)}{\partial x} &= p(x;s)\,\xi(x;s) + q(x;s)\eta(x), \quad \eta(a;s) = 1, \end{aligned} \tag{1.18}$$

where $p(x;s) = \frac{\partial f(x,u(x;s),v(x;s))}{\partial u}$ and $q(x;s) = \frac{\partial f(x,u(x;s),v(x;s))}{\partial v}$. We assign the value s_n to $s, n \geq 0$ then the IVP can be solved using a numerical method for IVPs such as the fourth-order-Runge-Kutta-Fehlberg integration scheme in the interval $[a,b]$. Thus, an approximation of $u(b,s_n)$ is obtained to calculate $\phi(s_n) = u(b;\ s_n) - \beta$ and an approximation $\xi(b,s_n) = \phi'(s_n)$ is also obtained. The values $\phi(s_n)$ and $\phi'(s_n)$ gives the next Newton-Raphson iterate s_{n+1} from $s_{n+1} = s_n - \frac{\phi(s_n)}{\phi'(s_n)}$. The process is repeated until the iterate s_n settle to a fixed number of digits. The problem with the shooting method is that it assumes that the BVP has a unique solution and there is no guarantee that the IVP has a solution in the interval $[a,b]$.

1.12.3 Runge-Kutta-Fehlberg Integration Method

In 1992, Press and Teukolsky stated that "many years later, it is still true that Runge-Kutta-Fehlberg is our favourite integration method for ordinary differential equations" and the reason is that the method is of accuracy of order 5×10^{-5} [21]. The Runge-Kutta method is a numerical technique used to solve ordinary differential equations. It is based on the first five terms of the Taylors series. The formula used is [22];

$$y_{i+1} = y_i + \frac{1}{6}(k_1 + 2k_2 + 2k_3 + k_4), \tag{1.19}$$

where

$$k_1 = f(x_i, y_i), \qquad k_2 = f\left(x_i + \frac{1}{2}h, y_i + \frac{1}{2}k_1 h\right),$$
$$k_3 = f\left(x_i + \frac{1}{2}h, y_i + \frac{1}{2}k_2 h\right), \qquad \text{and } k_4 = f(x_i + h, y_i + k_3 h). \tag{1.20}$$

1.13 Literature Review

The analysis of fluid flow in a boundary layer over convectively stretching or shrinking heated surfaces are encountered in various engineering and industrial systems such as extrusion of plastic and rubber sheets, polymer processing and metallurgy [23]. In addition, in some of these applications, a heat source is placed at a distance from the top edge of the surface; such an application is commonly seen in the cooling of electronic components, air-conditioning, nuclear plant reactors, and automobiles. The operating temperatures of these thermal systems are very significant for their performance, reliability, and lifespan and consequently, lowering the operating temperature is crucial to enhance the life of electronic components. Innovative research in the field of nanotechnology has recently led to the production of a new thermal management technology known as nanofluids [9] to improve the thermal system performance and reliability by removing the high-heat-flux. Nanofluids are primarily used for their enhanced thermal properties as coolants in heat transfer equipment such as heat exchangers, electronic cooling systems, and radiators. The theoretical approach is necessary to improve the experimental technique to build some standards for determining an optimal condition to obtain a higher thermal conductivity. Pang *et al.* [12] suggested that more theoretical investigation should be carried out to support the reported experimental results in their extensive review study on nanofluid flow with heat and mass transfer characteristics.

The research on nanofluids has mainly focused on the prediction and measurement techniques to evaluate their thermal conductivity. Since Choi discovered the term nanofluid [13], the energy conversion problem is of interest to many researchers. Numerous experimental and theoretical studies on the heat transfer enhancement capability of nanofluids have been

conducted by researchers including Makinde *et al.* [24], Mutuku-Njane and Makinde [25], Lund *et al.* [26], Khan *et al.* [27], Omar *et al.* [28], Raju *et al.* [29], and Mansur *et al.* [30]. Pillai and Yoshie [31] were interested in the effect of convective heat transfer coefficient from the velocity and surface temperature of urban canopy surfaces. Their results showed that a change in velocity affects the convective heat transfer coefficient while a change in surface temperature does not affect the convective heat transfer coefficient. The study of heat and mass transfer in a steady two-dimensional magnetohydrodynamic boundary layer flow of an incompressible electrically conducting fluid over a vertical stretching sheet was carried out by Rostami *et al.* [32]. Rostam*i et al.* used the homotopy analysis method to investigate the physical effects of a magnetic field, suction, Prandtl number, Grashof number, Schmidt number, Boit number and radiation parameter on the velocity, temperature, and concentration profiles. Ganesan *et al.* [33], performed a numerical study on a single and two-phase model of turbulent force convection of Cu-water nanofluid in a heated pipe. They reported that an increase in the Reynolds number and nanoparticles concentration might result in an upsurge in the Nusselt number. In addition, it was found that the examination of the single-phase model problem is more reliable than the two-phase problem to predict the Nusselt number.

The flow investigations regarding nonlinear materials are extremely important in the applied sciences and engineering areas and to explore the properties of flow and heat transfer, several theological models have been proposed. Hayat *et al.* used the homotopic analysis technique together with convergence analysis to solve the nonlinear ordinary differential equation model problem of the Cattaneo-Christov heat flux model in flow of variable thermal conductivity fluid over a variable thick surface[34]. Their results predicted the impact of various parameters on the velocity, temperature, and concentration distributions. Khan [35] studied the nonlinear thermal radiative flow of hybrid nanofluid on a preamble rotating disk and analysed it with consideration of velocity and thermal slip conditions on boundaries. Khan *et al.* [36] investigated the behaviour of Casson fluid in the presence of homogeneous-heterogeneous reactions together with a homogeneous heat effect subject to a resistive force of electromagnetic origin. Khan *et al.* [37] considered a nonlinear dissipative slip flow of Jeffrey nanomaterial towards a curved surface with entropy generation and activation energy and computational results of the differential equations were recorded through the shooting method. Khan and Alzahrani [38] model nonlinear mixed convection of Darcy-Forchheimer radiated flow near the stagnation point to analyse the change in activation energy.

Free convection and radiation effects of nanofluid consisting of Silicon dioxide and Molybdenum disulphide with second-order velocity slip was analysed by Khan and Alzahrani [39] in a Darcy-Forchheimer porous medium effect on entropy generation was shown

graphically. Awan *et al.* theoretically investigated the thermal analysis of oblique stagnation point flow with slippage on second-order fluid [40]. Ahmad *et al.* combined two different nanoparticles AA7075 and AA7072 alloys to form a hybrid fluid with water as a basefluid to analyse mixed convection hybridized micropolar nanofluid with triple stratification and the Cattaneo-Christov heat flux model[41]. Yasin *et al.* used the finite element method to get the solutions of the partial differential equations in their study of free convective flow of Lorentz forces and partially thermal walls [42]. Hussain *et al.* used the homotopy perturbation and variation iteration method to solve the ordinary differential equations of their study on combined convection of the Carreau-Yasuda Nanofluid model over a convective heated surface near a stagnation point [43]. Abbas *et al.* investigated the exponentially stretching sheet of modified nanofluid flow with time-dependent viscosity over a Riga plate [44]. Khan *et al.* analysed the flow and heat transfer of bio-convective hybrid nanofluid with triple stratification effects [45]. Akhtar's *et al.* studied the scientifically brake down of non-Newtonian blood flow of Jeffret fluid inside a tube with multi-thrombosis [46]. Saleem's *et al.* mathematical study of electroosmotically driven peristaltic flow of Casson fluid inside a tube having systematically contracting and relaxing sinusoidal heated walls used lubrication approximation to simplify the dimensionless form of the model equation [47]. Furthermore, Yildirim and Sezer [48], has studied analytically the stagnation point flow using the homotopy perturbation method. The study of boundary layer flow over a continuously moving heated flat surface with the momentum and the energy equations coupled through the viscous dissipation term was theoretically analysed by Mureithi *et al.* [49]. A theoretical model of the steady boundary layer flow of nanofluid due to an exponentially permeable stretching sheet with an external magnetic field was analysed by Bhattacharyya and Layek [50]. The purpose of this study is to theoretically investigate the steady of two-dimensional magnetohydrodynamic (MHD) boundary layer flow over a shrinking or stretching sheet.

CHAPTER 2: COMPUTATIONAL MODELLING OF MHD NANOFLUID FLOW OVER A STRETCHING HEATED SURFACE

2.1 Summary

The recent advancement in nanotechnology has provided a real platform for the emergence of a better ultrahigh-performance coolant known as nanofluid for many engineering and industrial technologies due to the miniaturization era of technology. In this chapter, the influence of magnetic field on heat transfer enhancement of nanofluid coolants consisting of Cu-water, Al_2O_4-water, and Fe_3O_4-water over a slippery but convectively heated stretching surface is examined. Based on some realistic assumptions, the model's partial differential equation will be transformed to an ordinary differential equation by using Blasius's similarity transformation. Furthermore, the nonlinear model differential equations are obtained and numerically tackled by using the shooting procedure with the Runge-Kutta-Fehlberg integration scheme. The influence of numerous emerging parameters on the momentum and thermal boundary layer profiles, skin friction and Nusselt number are depicted graphically in tables and figures, and quantitatively discussed.

2.2 Introduction

The flow over convectively heated stretching surfaces is globally increasing in multiple dynamical applications in the miniaturization-era of engineering and thermal sciences. There are an exponential increase in the theoretical and experimental studies of heat transfer enhancement after Maxwell's theoretical and Choi's experimental work was published about the dispersions of the small nanoparticles solids in a base fluid known as nanofluid [9][51] and their results validated that nanofluid enhances the heat transfer in the system. In addition, nanofluids are used in cooling/heating materials, heat production, energy resources, and bio-medical sciences like cancer treatment, destroying of damaged cells, and brain tumours. The study of cooling/heating surface by using nanofluid has been researched either experimental or numerical which include the study by Ferdows [52], Saha *et al*. [53], Makinde [54], Ajala *et al*. [55], Mondal *et al*. [56] and Jafar *et al*. [57].

Mohamed *et al.* conducted a numerical analysis by studying the boundary layer flow of Carreau nanofluid. In this study, the flow was a convectively heated non-linear stretched surface with chemical reaction and the heat generation/absorption in a porous medium [58]. This study focussed on the effect of the Brownian motion and thermophoresis. A numerical study of

Casson nanofluid was also conducted by Kamran *et al.* [59] that considered the case of flow past a horizontal stretched surface in the presence of magnetic and joule heating. They considered the Keller box numerical technique to analyse the slip and thermal convective boundary conditions. The purpose of the study by Tasawar *et al.* [60] was to investigate the impact of relevant parameters like power-law indices, dimensionless radius of curvature, nanoparticle volume fraction and Hartmann number on the velocity, temperature, skin friction, and Nusselt number profile of MHD mixed convection flow of copper or silver nanofluid in the presence of Joule heating and nonlinear thermal radiation.

According to the author's information and reviews, the mutual effects of magnetic field, surface slipperiness, nanoparticles volume fraction, viscous and thermal dissipation on the heat transfer enhancement rate in a boundary layer flow of nanofluids consisting of Cu-water, Al_2O_4-water, and Fe_3O_4-water past a convectively heated stretching surface has not been studied yet. Therefore, the objective of this thesis is to fill this missing gap in the literature. In the next section, the applicable model equations for the problem are obtained and numerically solved. The consequences of diverse rooted parameters on the velocity, temperature profile, skin friction, and Nusselt number are provided graphically and discussed.

2.3 Model Problem

The influence of magnetic field of strength B_0 on the heat transfer enhancement capability of nanofluids coolants consisting of either Cu-water, Al_2O_4-water, or Fe_3O_4-water over a slippery but convectively heated stretching surfaces as shown in Figure 2.1 below are studied:

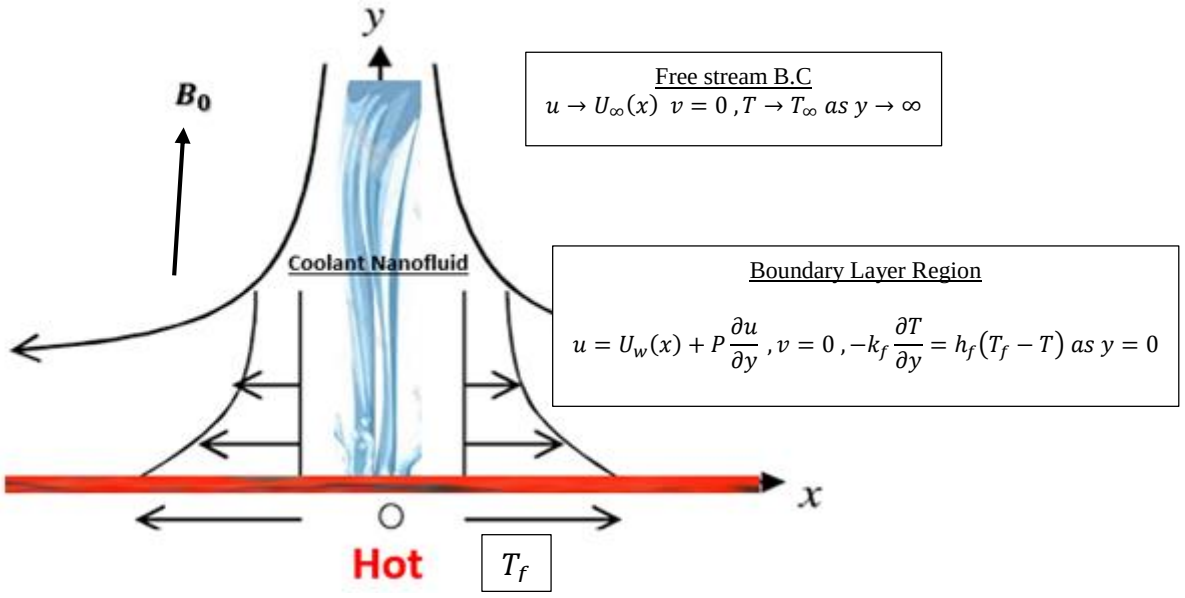

Figure 2.1: Problem geometry of fixed and stretching sheet.

The sheet is aligned with the x-axis and the y-axis where (u, v) are the velocity components of the nanofluid in the (x, y) directions respectively; h_f is the heat coefficient; $U_w(x) = ax$ is the sheet fixed/stretching velocity; $U_\infty(x) = bx$ is the free stream velocity; T_∞ is the free stream temperature; and T_f is the temperature of the hot fluid below the sheet. It is assumed that the flow is two dimensional i.e., $q(u, v)$, steady i.e., $\frac{\partial q}{\partial t} = 0$ and incompressible, density of a fluid particle as it moves along is assumed to be constant i.e., $\frac{D\rho}{Dt} = 0$. The partial differential equation of continuity and Navies Stokes equation (NSE) is given by [61],

$$\nabla q = 0, \tag{2.1}$$

$$\frac{\partial q}{\partial t} + (q \cdot \nabla)q = -\frac{1}{\rho_{nf}}\nabla p + \frac{\mu_{nf}}{\rho_{nf}}\nabla^2 q + \frac{1}{\rho_{nf}} j \times B. \tag{2.2}$$

Form equation (2.2) the term of unsteady acceleration, $\frac{\partial q}{\partial t} = 0$ since we are considering a steady flow. The convective acceleration term can be simplified as $(q \cdot \nabla)q = \left((u, v) \cdot \left(\frac{\partial}{\partial x}, \frac{\partial}{\partial y}\right)\right)(u, v) = \left(u\frac{\partial}{\partial x} + v\frac{\partial}{\partial y}\right)(u, v)$, the pressure gradient term is given by $\nabla p = \left(\frac{\partial p}{\partial x}, \frac{\partial p}{\partial y}\right)$, the viscous term is given by $\nabla^2 q = \left(\frac{\partial^2}{\partial x^2} + \frac{\partial^2}{\partial y^2}\right)(u, v)$ and lastly the body force term which is derived from Maxwell's where $E = 0$ since there is no presence of an electric field $q(u, v, 0)$ and $B(0, B_0, 0)$ starting with Ohm's law we have $\vec{j} = \sigma_{nf}(E + V \times B)$ and finally simplify to $j \times B = -\sigma_{nf} {B_0}^2 u$ along x. Then NS equation can be simplified as shown in equations (2.3) and (2.4) along x and y respectively.

$$u\frac{\partial u}{\partial x} + v\frac{\partial u}{\partial y} = -\frac{1}{\rho_{nf}}\frac{\partial p}{\partial x} + \frac{\mu_{nf}}{\rho_{nf}}\left(\frac{\partial^2 u}{\partial x^2} + \frac{\partial^2 u}{\partial y^2}\right) - \frac{\sigma_{nf}}{\rho_{nf}} {B_0}^2 u,$$

$$u\frac{\partial v}{\partial x} + v\frac{\partial v}{\partial y} = -\frac{1}{\rho_{nf}}\frac{\partial p}{\partial y} + \frac{\mu_{nf}}{\rho_{nf}}\left(\frac{\partial^2 v}{\partial x^2} + \frac{\partial^2 v}{\partial y^2}\right), \tag{2.3}$$

The characteristics scales were chosen as $x \sim L$, $y \sim \delta$ and $u \sim U_\infty$ and from the scaling analysis of the continuity equation (2.1) we get that $v \sim \frac{U_\infty \delta}{L}$. We assume that that $\frac{\delta}{L} \ll 1$, and $p \sim \rho U_\infty^2$ and let $\upsilon = \frac{\mu_{nf}}{\rho_{nf}}$. Considering y in the momentum equation (2.4) and its scaled analysis in (2.5),

$$u\frac{\partial v}{\partial x} + v\frac{\partial v}{\partial y} = -\frac{1}{\rho_{nf}}\frac{\partial p}{\partial y} + \upsilon\left(\frac{\partial^2 v}{\partial x^2} + \frac{\partial^2 v}{\partial y^2}\right),$$

(2.4)

$$\frac{{U_\infty}^2\delta}{L^2} \quad \frac{{U_\infty}^2\delta}{L^2} \quad \frac{{U_\infty}^2}{\delta} \quad \frac{\partial^2 v}{L^2} + \frac{\partial^2 v}{\delta^2}, \tag{2.5}$$

$$\delta \ll L \implies \frac{1}{L^2} \ll \frac{1}{\delta^2} \implies \frac{\partial^2 v}{\partial x^2} \ll \frac{\partial^2 v}{\partial y^2}, \tag{2.6}$$

Form the assumption $\delta \ll L \implies \frac{1}{L^2} \ll \frac{1}{\delta^2} \implies \frac{\partial^2 v}{\partial x^2} \ll \frac{\partial^2 v}{\partial y^2}$ thus $\frac{\partial^2 v}{\partial x^2}$ since it is of order $\frac{1}{\delta^2}$. Order of magnitude of $\frac{inertia\ term}{pressure\ gradient} \sim \frac{\left(\frac{{U_\infty}^2\delta}{L^2}\right)}{\left(\frac{{U_\infty}^2}{\delta}\right)} \sim \left(\frac{\delta}{L}\right)^2$ thus we will neglect inertia terms. Furthermore, order of magnitude of $\frac{viscous\ term}{pressure\ gradient} \sim \frac{\left(\frac{\upsilon U_\infty}{\delta L}\right)}{\left(\frac{{U_\infty}^2}{\delta}\right)} \sim \frac{\upsilon}{LU_\infty} \sim \frac{1}{Re}$ which lead to neglecting of viscous terms assuming that Re is very large within the boundary layer, The y momentum equation will be dominated by pressure gradient,

$$-\frac{1}{\rho_{nf}}\frac{\partial p}{\partial y} = 0 \implies \frac{\partial p}{\partial y} = 0. \tag{2.7}$$

Pressure is not function of y within the boundary layer then $p \neq p(y)$. In the x momentum equation (2.4) we neglect $\frac{\partial^2 u}{\partial x^2}$ since is of order $\frac{1}{\delta^2}$ the equation will reduce to (2.8),

$$u\frac{\partial u}{\partial x} + v\frac{\partial u}{\partial y} = -\frac{1}{\rho_{nf}}\frac{\partial p}{\partial x} + \frac{\mu_{nf}}{\rho_{nf}}\left(\frac{\partial^2 u}{\partial y^2}\right) - \frac{\sigma_{nf}}{\rho_{nf}}{B_0}^2 u, \tag{2.8}$$

As $y \to \infty$ at the free stream $u = U_\infty$ and $v = 0$ then we will have equation (2.9) and (2.10),

$$U_\infty\frac{dU_\infty}{dx} = -\frac{1}{\rho_{nf}}\frac{\partial p}{\partial x} - \frac{\sigma_{nf}}{\rho_{nf}}{B_0}^2 U_\infty, \tag{2.9}$$

$$-\frac{1}{\rho_{nf}}\frac{\partial p}{\partial x} = U_\infty\frac{dU_\infty}{dx} + \frac{\sigma_{nf}}{\rho_{nf}}{B_0}^2 U_\infty. \tag{2.10}$$

Substitute equation (2.10) into equation (2.8) then the momentum equation becomes,

$$u\frac{\partial u}{\partial x} + v\frac{\partial u}{\partial y} = U_\infty\frac{dU_\infty}{dx} + \frac{\sigma_{nf}}{\rho_{nf}}{B_0}^2 U_\infty + \frac{\mu_{nf}}{\rho_{nf}}\left(\frac{\partial^2 u}{\partial y^2}\right) - \frac{\sigma_{nf}}{\rho_{nf}}{B_0}^2 u, \tag{2.11}$$

And its future simplifies as,

$$u\frac{\partial u}{\partial x} + v\frac{\partial u}{\partial y} = U_\infty\frac{dU_\infty}{dx} + \frac{\mu_{nf}}{\rho_{nf}}\left(\frac{\partial^2 u}{\partial y^2}\right) - \frac{\sigma_{nf}}{\rho_{nf}}{B_0}^2 (u - U_\infty), \tag{2.12}$$

From the Partially Differential Equation (PDE) in (2.12) with its Boundary Condition (BC) $u(x,0) = U_w(x) + P\frac{\partial u}{\partial y}$, $v(x,0) = 0$ and $u(x,\infty) \to U_\infty(x)$ where P is the slip length coefficient we now translate it to Ordinary Differential Equation (ODE) using similarity transformation defined in (2.13).

$$U_w(x) = ax, \qquad U_\infty(x) = bx, \quad where\ a,b \in (s^{-1})\left(\frac{1}{t}\right),$$
$$u = \frac{\partial \psi}{\partial y}, \qquad v = -\frac{\partial \psi}{\partial x} \text{ where } \psi = x\sqrt{\nu_f b}F(\xi)\ and\ \xi = y\sqrt{\frac{b}{\nu_f}}. \tag{2.13}$$

Note that ψ is the stream function. The terms in equation (2.12) are expanded as follows in equation (2.14).

$$u = \frac{\partial \psi}{\partial \xi}\frac{\partial \xi}{\partial y} = \left(x\sqrt{\nu_f b}F'(\xi)\right)\left(\sqrt{\frac{b}{\nu_f}}\right) = xbF'(\xi,$$

$$v = -\frac{\partial \psi}{\partial x} = -\sqrt{\nu_f b}F(\xi),$$

$$\frac{\partial u}{\partial y} = \frac{\partial u}{\partial \xi}\frac{\partial \xi}{\partial y} = (xbF''(\xi))\left(\sqrt{\frac{b}{\nu_f}}\right) = xb\sqrt{\frac{b}{\nu_f}}F''(\xi), \tag{2.14}$$

$$\frac{dU_\infty}{dx} = b,$$

$$\frac{\partial^2 u}{\partial y^2} = \frac{\partial}{\partial y}\left(\frac{\partial u}{\partial y}\right) = \frac{\partial}{\partial y}\left(xb\sqrt{\frac{b}{\nu_f}}F''(\xi)\right) = \left(xb\sqrt{\frac{b}{\nu_f}}F'''(\xi)\right)\left(\sqrt{\frac{b}{\nu_f}}\right) = \frac{xb^2}{\nu_f}F'''(\xi),$$

Substituting the expanded equation (2.14) into (2.12) and simplifying it we get the ODE of the momentum equation as (2.15)

$$F'''(\xi) + \frac{\rho_{nf}\mu_f}{\mu_{nf}\rho_f}(F(\xi)F''(\xi) - F'(\xi)^2 + 1) - \frac{\mu_f \sigma_{nf} B_0^2}{\mu_{nf} b \rho_f}\frac{\sigma_f}{\sigma_f}\frac{\mu_f}{\mu_f}(F'(\xi) - 1) = 0, \tag{2.15}$$

reducing the equation (2.15) by introducing some new parameters shown in equation (2.16)

$$\nu_f = \frac{\mu_f}{\rho_f}, \qquad A_1 = \frac{\mu_f}{\mu_{nf}}\frac{\rho_{nf}}{\rho_f}, \qquad M = \frac{\sigma_f B_0^2}{\rho_f b}, \quad A_2 = \frac{\sigma_{nf}\mu_f}{\sigma_f \mu_{nf}}, \qquad \gamma = \frac{\sigma_s}{\sigma_f},$$

$$S = P\sqrt{\frac{b}{\nu_f}}, Bi = \frac{h_f}{k_f}\sqrt{\frac{\nu_f}{b}}, \quad \lambda = \frac{a}{b}, \qquad \frac{\sigma_{nf}}{\sigma_f} = 1 + \frac{3(\gamma - 1)\phi}{(\gamma + 2) - (\gamma - 1)\phi}, \tag{2.16}$$

$$\rho_{nf} = (1-\phi)\rho_f + \phi\rho_s,\ \ \mu_{nf} = \frac{\mu_f}{(1-\phi)^{2.5}},$$

Then the ODE momentum equation is given by equation (2.17) below with its boundary conditions,

$$F'''(\xi) + A_1\left(F(\xi)F''(\xi) - F'(\xi)^2 + 1\right) - A_2 M(F'(\xi) - 1) = 0,$$

$$F(0) = 0\ ,\ F'(0) = \lambda + S\,F''(0)\ \text{ and } F'(\infty) = 1. \qquad (2.17)$$

The parameters used are defined as ρ_{nf} and is the nanofluid density, ρ_f is the basefluid density, ρ_s is the nanoparticle density, μ_{nf} is the nanofluid dynamic viscosity, μ_f is the basefluid dynamic viscosity, σ_{nf} is the nanofluid electrical conductivity, σ_f is the basefluid electrical conductivity, σ_s is the nanoparticle electrical conductivity, ν_f is the kinematic viscosity of the basefluid and ϕ is the nanoparticle volume fraction. The partial differential equation of the energy equation is given by,

$$(\rho C_p)_{nf}\left(\frac{\partial T}{\partial t} + (V\cdot\nabla)T\right) = k_{nf}\nabla^2 T + \mu_{nf}\phi + \frac{j^2}{\sigma_{nf}} + q'''. \qquad (2.18)$$

From equation (2.18) the local energy change with time $\frac{\partial T}{\partial t} = 0$ since it is a steady flow, the convective term $(V\cdot\nabla)T = \left((u,v)\cdot\left(\frac{\partial}{\partial x},\frac{\partial}{\partial y}\right)\right)(T) = u\frac{\partial T}{\partial x} + v\frac{\partial T}{\partial y}$, the diffusion term is given by $\nabla^2 T = \left(\frac{\partial^2}{\partial x^2} + \frac{\partial^2}{\partial y^2}\right)(T) = \frac{\partial^2 T}{\partial x^2} + \frac{\partial^2 T}{\partial y^2}$, $\phi = 2\left(\frac{\partial u}{\partial x}\right)^2 + 2\left(\frac{\partial v}{\partial y}\right)^2 + \left(\frac{\partial u}{\partial y} + \frac{\partial v}{\partial x}\right)^2$, from the momentum derivation $\overrightarrow{j^2} = {\sigma_{nf}}^2 {B_0}^2 u^2$ and $q''' = 0$. Then the PDE of energy equation becomes,

$$(\rho C_p)_{nf}\left(u\frac{\partial T}{\partial x} + v\frac{\partial T}{\partial y}\right) = k_{nf}\left(\frac{\partial^2 T}{\partial x^2} + \frac{\partial^2 T}{\partial y^2}\right) + \mu_{nf}\left(2\left(\frac{\partial u}{\partial x}\right)^2 + 2\left(\frac{\partial v}{\partial y}\right)^2 + \left(\frac{\partial u}{\partial y} + \frac{\partial v}{\partial x}\right)^2\right) + \sigma_{nf}\,{B_0}^2 u^2. \qquad (2.19)$$

The characteristics scales was chosen as, $x \sim L\ \ y \sim \delta_T\ u \sim \frac{\delta_T}{\delta}\,U_\infty$ and $T \sim \Delta T$ and from the scaling analysis of the continuity equation we get that $v \sim \frac{\delta_T U_\infty}{\delta}\,\frac{\delta_T}{L}$, we assume that that $\frac{\delta_T}{\delta} \ll 1$. Then we scale the energy equation (2.19),

$$(\rho C_p)_{nf}\left(u\frac{\partial T}{\partial x} + v\frac{\partial T}{\partial y}\right) = k_{nf}\left(\frac{\partial^2 T}{\partial x^2} + \frac{\partial^2 T}{\partial y^2}\right) + \mu_{nf}\left(2\left(\frac{\partial u}{\partial x}\right)^2 + 2\left(\frac{\partial v}{\partial y}\right)^2 + \left(\frac{\partial u}{\partial y} + \frac{\partial v}{\partial x}\right)^2\right),$$

$$\frac{\delta_T U_\infty \Delta T}{\delta L},\quad \frac{\delta_T U_\infty \Delta T}{\delta L},\quad \frac{\Delta T}{L^2},\quad \frac{\Delta T}{{\delta_T}^2},\quad \left(\frac{\delta_T}{\delta}\right)^2\frac{U_\infty}{L^2},\quad \left(\frac{\delta_T}{\delta}\right)^2\frac{U_\infty}{L^2},\quad \left(\frac{\delta_T}{\delta}\frac{U_\infty}{\delta_T}\quad \frac{\delta_T}{\delta}\frac{U_\infty \delta_T}{L^2}\right)^2. \qquad (2.20)$$

Suppose that L is significantly large $\Rightarrow \frac{\delta_T}{L} \ll 1 \Rightarrow \frac{1}{L^2} \ll \frac{1}{{\delta_T}^2}$, neglect $\frac{\partial^2 T}{\partial x^2}$, $\left(\frac{\partial u}{\partial x}\right)^2$, $\left(\frac{\partial v}{\partial y}\right)^2$ and $\frac{\partial v}{\partial x}$ since are of order $\frac{1}{L^2}$, the equation reduced to,

$$\left(\rho C_p\right)_{nf}\left(u\frac{\partial T}{\partial x}+v\frac{\partial T}{\partial y}\right)=k_{nf}\frac{\partial^2 T}{\partial y^2}+\mu_{nf}\left(\frac{\partial u}{\partial y}\right)^2+\sigma_{nf}\,{B_0}^2u^2, \tag{2.21}$$

As $y \to \infty$ at the free stream $u = U_\infty$, $v = 0$ and T =constant then we will have,

$$0=\sigma_{nf}\,{B_0}^2{U_\infty}^2, \tag{2.22}$$

then to balance the system we subtract equation (2.21) from equation (2.22) to get equation (2.23) with its boundary condition,

$$\left(\rho C_p\right)_{nf}\left(u\frac{\partial T}{\partial x}+v\frac{\partial T}{\partial y}\right)=k_{nf}\frac{\partial^2 T}{\partial y^2}+\mu_{nf}\left(\frac{\partial u}{\partial y}\right)^2+\sigma_{nf}B_0^2(u-U_\infty)^2,$$

$$u(x,0)=U_w(x)+P\frac{\partial u}{\partial y},\quad v(x,0)=0,\quad -k_f\frac{\partial T}{\partial y}(x,0)=h_f\left[T_f-T(x,0)\right], \tag{2.23}$$
$$u(x,\infty)\to U_\infty(x),\qquad T(x,\infty)\to T_\infty.$$

Now from PDE in (2.23) we translate it to ODE using similarity transformation define in (2.24).

$$U_w(x)=ax,\ U_\infty(x)=bx\quad where\ a,b\in(s^{-1})\left(\frac{1}{t}\right),\ T=\theta(\xi)\left(T_f-T_\infty\right)+T_\infty,$$

$$u=\frac{\partial\psi}{\partial y},v=-\frac{\partial\psi}{\partial x},\quad \psi=x\sqrt{\nu_f b}F(\xi),\quad \xi=y\sqrt{\frac{b}{\nu_f}},\qquad \theta(\xi)=\frac{T-T_\infty}{T_f-T_\infty}. \tag{2.24}$$

Note that ψ is the stream function. The terms in equation (2.23) are expanded in equation (2.25).

$$u=\frac{\partial\psi}{\partial\xi}\frac{\partial\xi}{\partial y}=\left(x\sqrt{\nu_f b}F'(\xi)\right)\left(\sqrt{\frac{b}{\nu_f}}\right)=xbF'(\xi,\ \ v=-\frac{\partial\psi}{\partial x}=-\sqrt{\nu_f b}F(\xi),$$

$$\frac{\partial T}{\partial x}=\frac{\partial T}{\partial\xi}\frac{\partial\xi}{\partial x}=\left(\theta'(\xi)\left(T_f-T_\infty\right)\right)(0)=0,$$

$$\frac{\partial T}{\partial y}=\left(\theta'(\xi)\left(T_f-T_\infty\right)\right)\left(\sqrt{\frac{b}{\nu_f}}\right), \tag{2.25}$$

$$\frac{\partial^2 T}{\partial y^2}=\frac{\partial}{\partial y}\left(\frac{\partial T}{\partial y}\right)=\left(\left(\theta''(\xi)\left(T_f-T_\infty\right)\right)\sqrt{\frac{b}{\nu_f}}\right)\left(\sqrt{\frac{b}{\nu_f}}\right)=\left(\theta''(\xi)\left(T_f-T_\infty\right)\right)\frac{b}{\nu_f},$$

$$\frac{\partial u}{\partial y} = \frac{\partial u}{\partial \xi}\frac{\partial \xi}{\partial y} = (xbF''(\xi))\left(\sqrt{\frac{b}{\nu_f}}\right) = xb\sqrt{\frac{b}{\nu_f}}F''(\xi),$$

Substituting the expanded equation (2.25) into (2.23) and simplifying we get the ODE of energy equation as (2.15),

$$\theta''(\xi) + \frac{\mu_f(\rho C_p)_{nf}}{\rho_f k_{nf}}\frac{k_f}{k_f}\frac{(\rho C_p)_f}{(\rho C_p)_f}F(\xi)\theta'(\xi) + \frac{\mu_{nf}x^2b^2}{k_{nf}(T_f - T_\infty)}\frac{k_f}{k_f}\frac{(C_p)_f}{(C_p)_f}\frac{\mu_f}{\mu_f}F''(\xi)^2$$
$$+\frac{\mu_f\sigma_{nf}B_0^2x^2b}{\rho_f k_{nf}(T_f - T_\infty)}\frac{k_f}{k_f}\frac{\sigma_f}{\sigma_f}\frac{(C_p)_f}{(C_p)_f}\frac{b}{b}(F'(\xi) - 1)^2 = 0. \quad (2.26)$$

We will reduce the equation (2.26) by introducing some new parameters shown in equation (2.27),

$$A_3 = \frac{(\rho C_p)_{nf}k_f}{(\rho C_p)_f k_{nf}}, \quad A_4 = \frac{\mu_{nf}k_f}{\mu_f k_{nf}}, \quad A_5 = \frac{\sigma_{nf}k_f}{\sigma_f k_{nf}}, \quad \nu_f = \frac{\mu_f}{\rho_f}, \quad \lambda = \frac{a}{b},$$

$$M = \frac{\sigma_f B_0^2}{\rho_f b}, \quad Pr = \frac{\mu_f C_{pf}}{k_f}, \quad Ec = \frac{x^2b^2}{(C_p)_f(T_f - T_\infty)}, \quad S = P\sqrt{\frac{b}{\nu_f}},$$

$$(\rho C_p)_{nf} = (1-\phi)(\rho C_p)_f + \phi(\rho C_p)_s, \quad \gamma = \frac{\sigma_s}{\sigma_f}, \quad Bi = \frac{h_f}{k_f}\sqrt{\frac{\nu_f}{b}}, \quad (2.27)$$

$$\rho_{nf} = (1-\phi)\rho_f + \phi\rho_s,$$

$$\mu_{nf} = \frac{\mu_f}{(1-\phi)^{2.5}}, \quad \frac{\sigma_{nf}}{\sigma_f} = 1 + \frac{3(\gamma-1)\phi}{(\gamma+2) - (\gamma-1)\phi}.$$

Then the ODE energy equation is given by equation (2.28) below with its boundary conditions,

$$\theta''(\xi) + A_3PrF(\xi)\theta'(\xi) + A_4PrEcF''(\xi)^2 + A_5PrEcM(F'(\xi) - 1)^2 = 0,$$
$$F(0) = 0, \quad F'(0) = \lambda + S\,F''(0), \quad F'(\infty) = 1, \quad \theta'(0) = Bi(\theta(0) - 1), \quad (2.28)$$
$$and \quad \theta(\infty) = 0.$$

The parameters used are defined as ρ_{nf} as the nanofluid density, ρ_f is the basefluid density, ρ_s is nanoparticle density, μ_{nf} is the nanofluid dynamic viscosity, μ_f is the basefluid dynamic viscosity, σ_{nf} is the nanofluid electrical conductivity, σ_f is the basefluid electrical conductivity, σ_s is the nanoparticle electrical conductivity, $(\rho C_p)_{nf}$ is the nanofluid heat capacitance, ν_f is the kinematic viscosity of the basefluid, S is slip, Bi is Boit number, M is the magnetic field,

Pr is the Prandtl number, Ec is the Eckert number and ϕ is the nanoparticle volume fraction and future elaborated by Table 2.1.

Table 2.1: The Relationship between Nanoparticle and basefluids.

Properties	Nanofluid
Density	$\rho_{nf} = (1-\phi)\rho_f + \phi\rho_s$
Heat Capacity	$(\rho C_p)_{nf} = (1-\phi)(\rho C_p)_f + \phi(\rho C_p)_s$
Viscosity	$\mu_{nf} = \frac{\mu_f}{(1-\phi)^{2.5}}$
Thermal Conductivity	$\frac{k_{nf}}{k_f} = \frac{(k_s+2k_f)-2\phi(k_f-k_s)}{(k_s+2k_f)+\phi(k_f-k_s)}$
Electrical Conductivity	$\frac{\sigma_{nf}}{\sigma_f} = 1 + \frac{3\left(\frac{\sigma_s}{\sigma_f}-1\right)\phi}{\left(\frac{\sigma_s}{\sigma_f}+2\right)-\left(\frac{\sigma_s}{\sigma_f}-1\right)\phi}$

The density, heat capacity, thermal conductivity, and electrical conductivity of H_2O, Al_2O_3 and Fe_3O_4 are shown in Table 2.2 below,

Table 2.2: Nanoparticles and basefluid Thermophysical Properties.

Physical Properties	$\rho\left(\frac{kg}{m^3}\right)$	$c_p\left(\frac{J}{Kg\ K}\right)$	$k\left(\frac{W}{m\ K}\right)$	$\sigma\left(\frac{S}{m}\right)$
H_2O	997.1	4179	0.613	5.5×10^{-6}
Cu	8933	385	401	59.6×10^{6}
Al_2O_3	3970	765	40	35×10^{6}
Fe_3O_4	5180	670	9.7	2.5×10^{6}

Other quantities of interest are the skin friction coefficients(C_f) and the Nusselt number (Nu) which can be expressed as,

$$C_f\sqrt{Re_x} = \frac{F''(0)}{(1-\phi)^{2.5}}, \qquad \frac{Nu}{\sqrt{Re}} = -\frac{k_{nf}}{k_f}\theta'(0), \tag{2.29}$$

where

$$C_f = \frac{T_w}{\rho_f U_\infty^2}, \qquad Nu = \frac{xq_w}{k_f(T_f - T_\infty)}, \qquad T_w = \mu_{nf}\frac{\partial u}{\partial y}\Big|_{y=0}, \tag{2.30}$$

$$q_w = -k_{nf}\frac{\partial T}{\partial y}\,|_{y=0}\,,\quad Re_x = \frac{xU_\infty}{\upsilon_f}.$$

2.4 Numerical Procedure

The numerical method based on the shooting technique together with the Runge-Kutta-Fehlberg integration scheme was utilized to solve the model equations. From the obtained boundary value problem (BVP) in equations (2.17) and (2.28), we constructed the initial value problem (IVP) by letting $x_1 = F(\xi)\,,\ x_2 = F'(\xi),\ x_3 = F''(\xi),\ x_4 = \theta(\xi),\ \ x_5 = \theta'(\xi),$

$$x_1{}' = x_2, \qquad x_2{}' = x_3, \qquad x_3{}' = A_2M(x_2 - 1) - A_1\,(x_1x_3 - x_2{}^2 + 1), \tag{2.31}$$

$$x_4{}' = x_5, \qquad x_5{}' = -A_3Prx_1x_5 - A_4PrEcx_3{}^2\ - A_5PrEcM(x_2 - 1)^2, \tag{2.32}$$

with the initial conditions,

$$x_1\,(0) = 0\,, x_2\,(0) = \lambda + \delta x_3(0),\ x_3(0) = a_1, x_4(0) = a_2, x_5(0) = Bi(a_2 - 1). \tag{2.33}$$

The unknown values of a_1 and a_2 are first guessed and subsequently obtained via the shooting numerical procedure using the Newton Raphson root finding method. Thereafter, the system of first order ODEs is then solved by applying the Runge-Kutta-Fehlberg integration scheme [62].

2.5 Results and Discussion

Numerical results representing the impact of emerging thermophysical parameters on the nanofluids velocity and temperature profiles, skin friction and Nusselt number are displayed graphically and in tabular form, as shown in Figures 2.2 – 2.13 and Tables 3-5. In all our computations the Prandtl number is taken as $Pr = 6.2$ which corresponds to that of basefluid (water). To validate the numerical results obtained, we compare our results with those reported by Wang. [63] and Ishak [64] where the parameters $M = S = \phi = 0$, which showed a favorable agreement, as presented in Table 2.3 below,

Table 2.3: Computations Showing Comparison with [63] [64] for Stretching Sheet.

λ	Ref [63] $\sqrt{Re_x}C_f$	Ref. [64] $\sqrt{Re_x}C_f$	Present results $\sqrt{Re_x}C_f$
0	1.232588	1.232588	1.23258765
0.1	1.14656	1.146561	1.14656100
0.2	1.05133	-	1.05112999
0.5	0.71330	0.713295	0.71329496
0.8	-	0.306095	0.30609476
1	0	0	0
2	–1.88731	-1.887307	-1.88730667

2.5.1 Velocity Profile

The impact of various parameters on the velocity profile are presented in Figure 2.2 – 2.4 where it is noticeable that velocity increases from surface velocity to free stream velocity. Furthermore, this observation was overserved in all cases of nanofluid flow consisting of either Cu-water, Fe_3O_4-water, or Al_2O_3-water nanofluid. Figure 2.2 shows that the Cu-water velocity boundary layer thickness is the smallest followed by Fe_3O_4-water and then Al_2O_3-water nanofluid, respectively. This implies that Cu-water nanofluid closely interacts with the sheet surface more than Fe_3O_4-water and Al_2O_3-water as shown in Figure 2.2. The impact of parameters ϕ, S, M, and λ on the velocity profiles $F'(\xi)$ will be generalized using Cu-water nanofluid as it shows the same impact using either Fe_3O_4-water or Al_2O_3-water nanofluid. Figure 2.2 - 2.6 are velocity profiles that reveal a decline in the velocity boundary layer thickness with increasing nanoparticles volume fraction(ϕ), surface slipperiness (S), magnetic field intensity (M), and surface stretching rate (λ), respectively. It is noteworthy that a decrease in velocity boundary layer thickness boosts the interaction between the Cu-water, Fe_3O_4-water, and Al_2O_3-water nanofluid and the heated stretching surface leading to an enhancement in heat transfer rate.

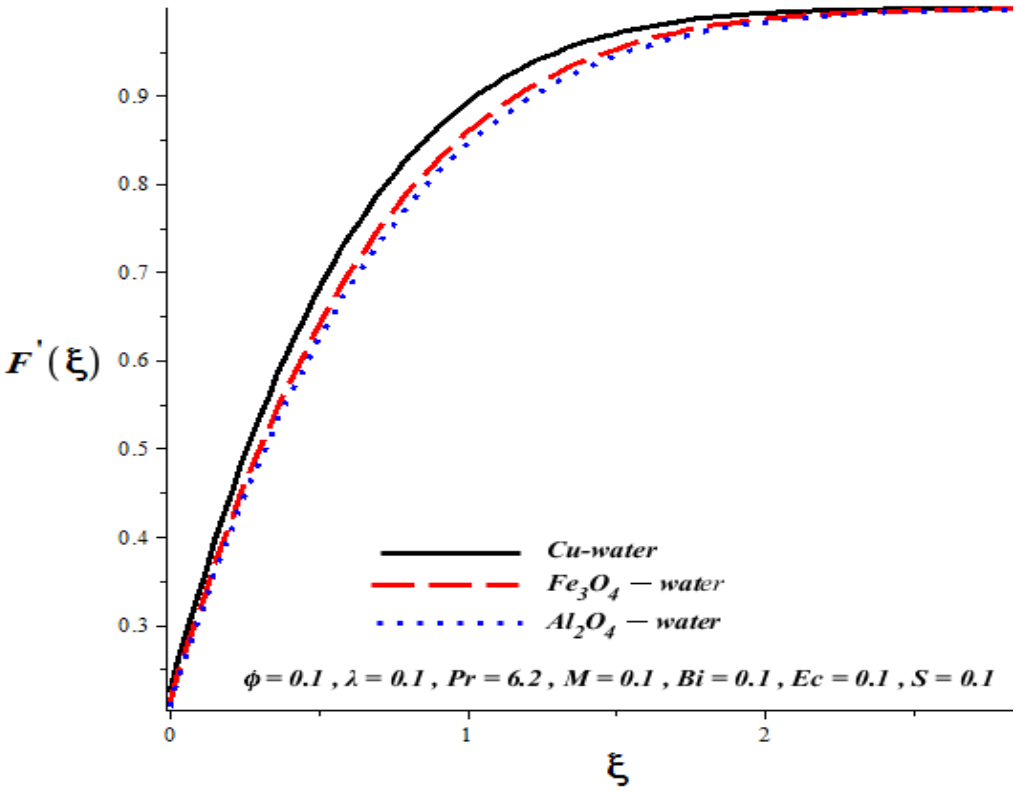

Figure 2.2: Impact of Cu-water, Fe_3O_4-water, and Al_2O_3-water nanofluid on the velocity profiles of the flow.

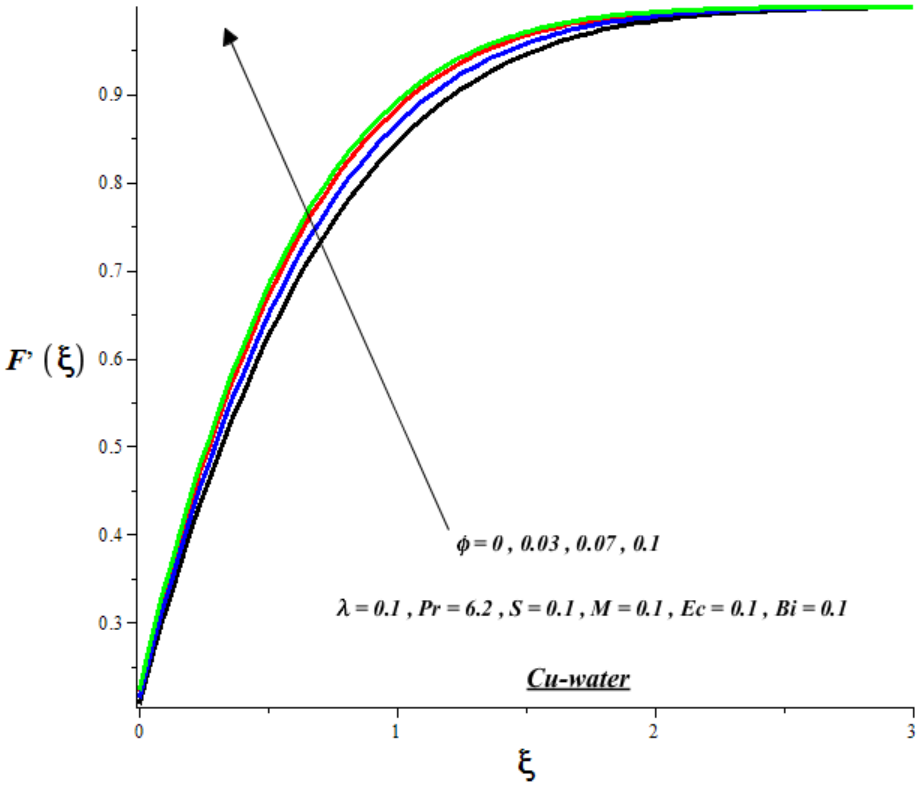

Figure 2.3: Impact of ϕ on the velocity profiles of Cu-water nanofluid flow.

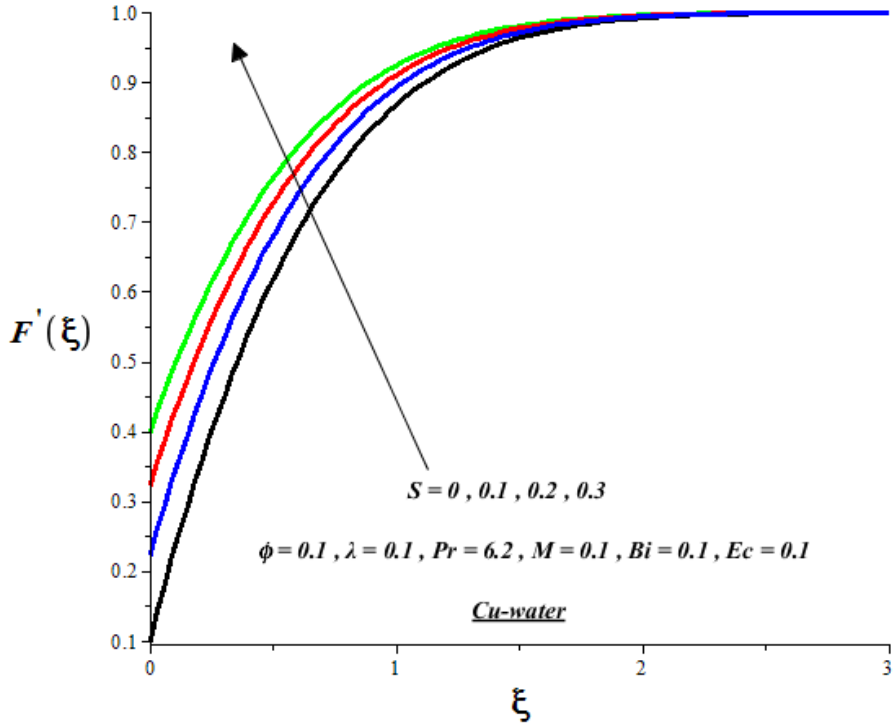

Figure 2.4: The impact of S on the velocity profile of Cu water nanofluid flow.

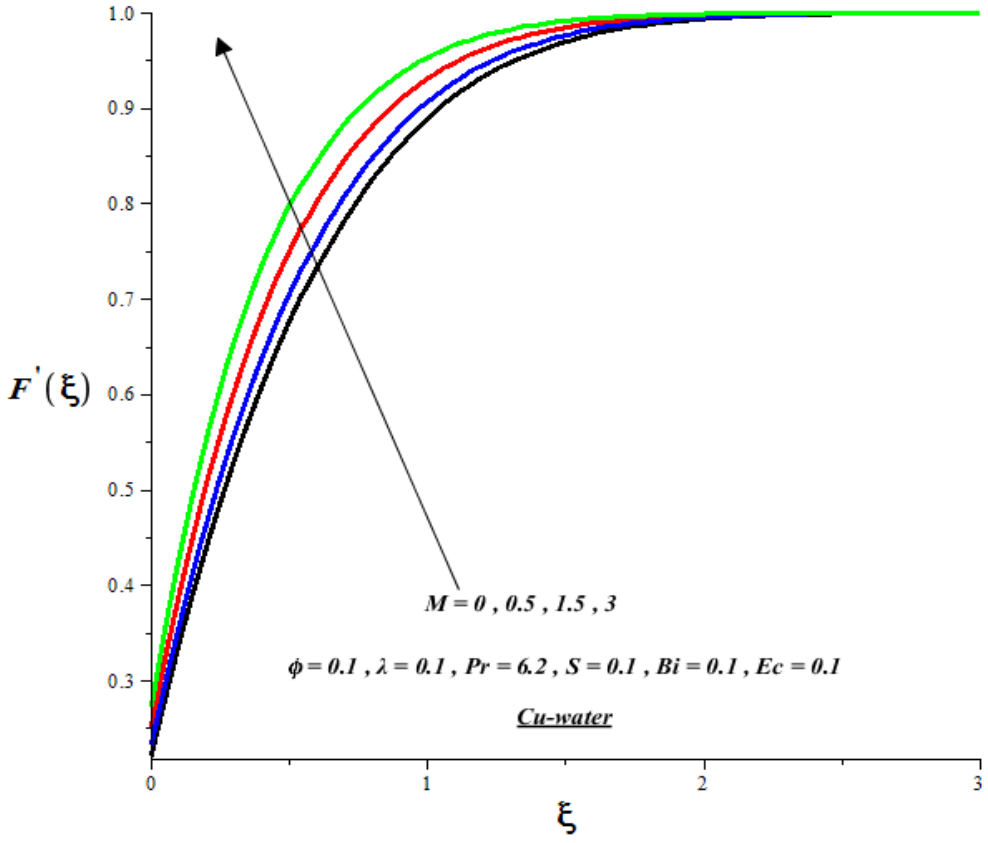

Figure 2.5: The impact of M on the velocity profile of Cu water nanofluid flow.

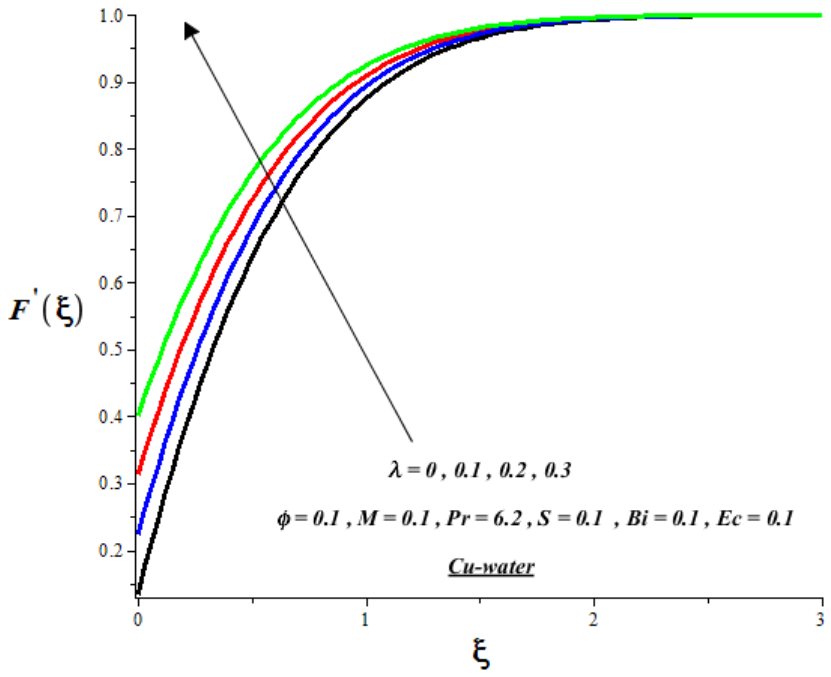

Figure 2.6: The impact of λ in the velocity profile of Cu water nanofluid flow.

2.5.2 Temperature Profile

Figures 2.7 – 2.13 demonstrate the numerical results obtained from the impact of thermophysical parameters on the temperature profiles of a Cu-water, Fe_3O_4-water, or Al_2O_3-water nanofluid flow past a heated stretching surface. From the observation in general the temperature of the nanofluids is higher at the sheet surface due to convective heating and decreases gradually towards the free stream temperature value far away from the surface. The author decides to show the figures for Cu-water nanofluid, whilst the impact is the same for Fe_3O_4-water, and Al_2O_3-water nanofluid. In Figure 2.7, it is noticeable that the thermal boundary layer thickness of Cu-water is the largest followed by Fe_3O_4-water and Al_2O_3-water, respectively. This implies that Cu-water takes more heat from the surface as compared to Fe_3O_4-water and Al_2O_3-water. From Figures 2.8 – 2.13 an increase in the Cu-water temperature is noticed with an increase in values of nanoparticles volume fraction (ϕ), magnetic field intensity (M), Eckert number (Ec), and Biot number (Bi). The rise in nanofluid temperature may be attributed to the combined effects of the convective heating of the surface due to hot fluid underneath; viscous dissipation; Joule heating due to the magnetic field; and nanoparticles thermal conductivity. Consequently, the thermal boundary layer thickness is enhanced. It is observed that an increase in sheet surface slipperiness (S) and surface stretching rate (λ) lessened the Cu-water nanofluid temperature profiles.

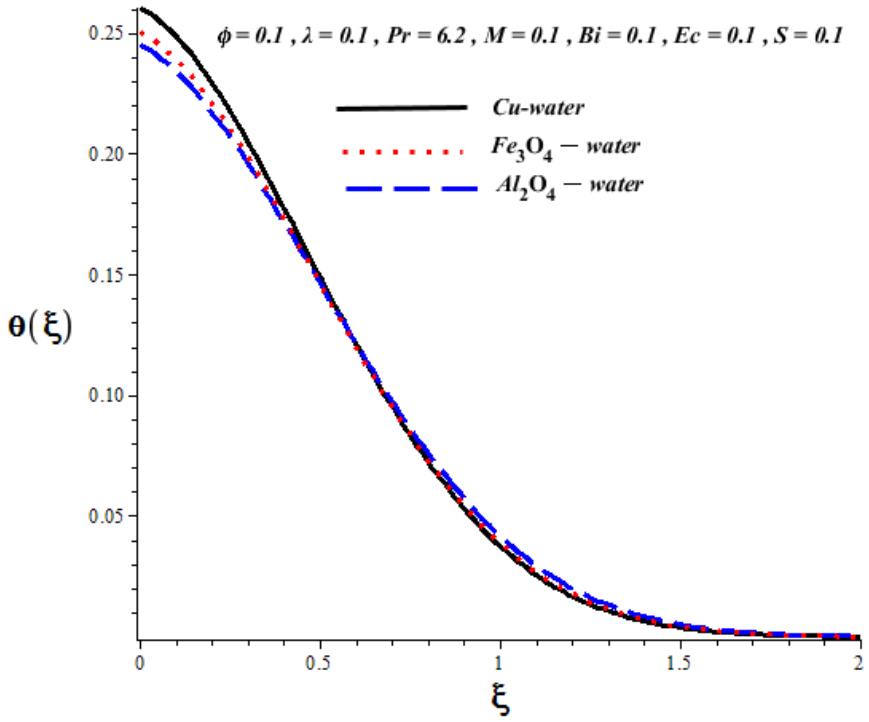

Figure 2.7: Impact of Fe_3O_4-water, and Al_2O_3-water nanofluid and ϕ on the temperature profiles of the flow.

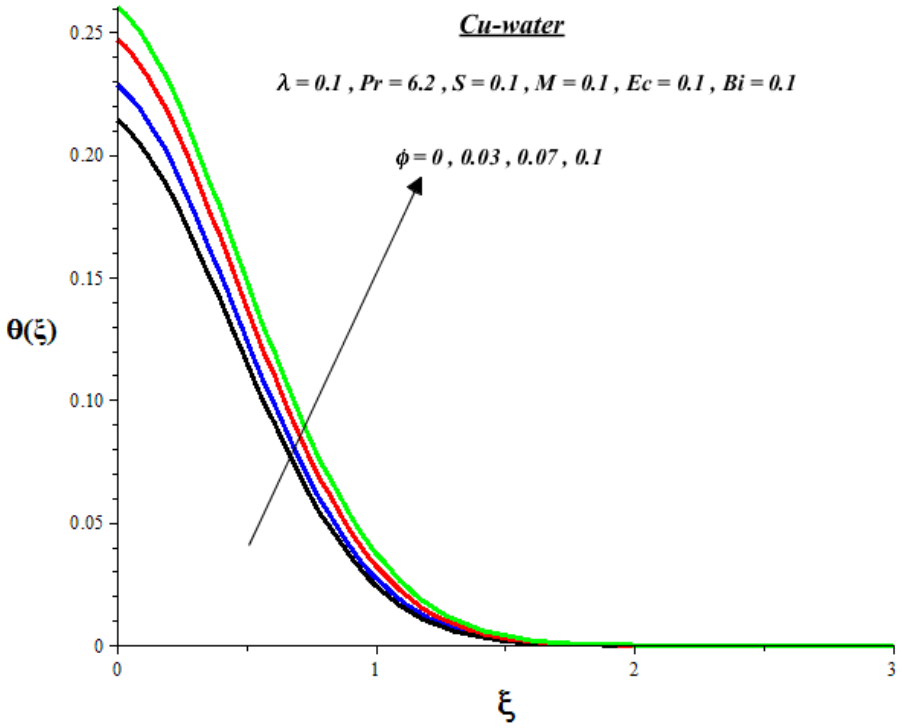

Figure 2.8: Impact of ϕ on the temperature profiles of Cu-water nanofluid flow.

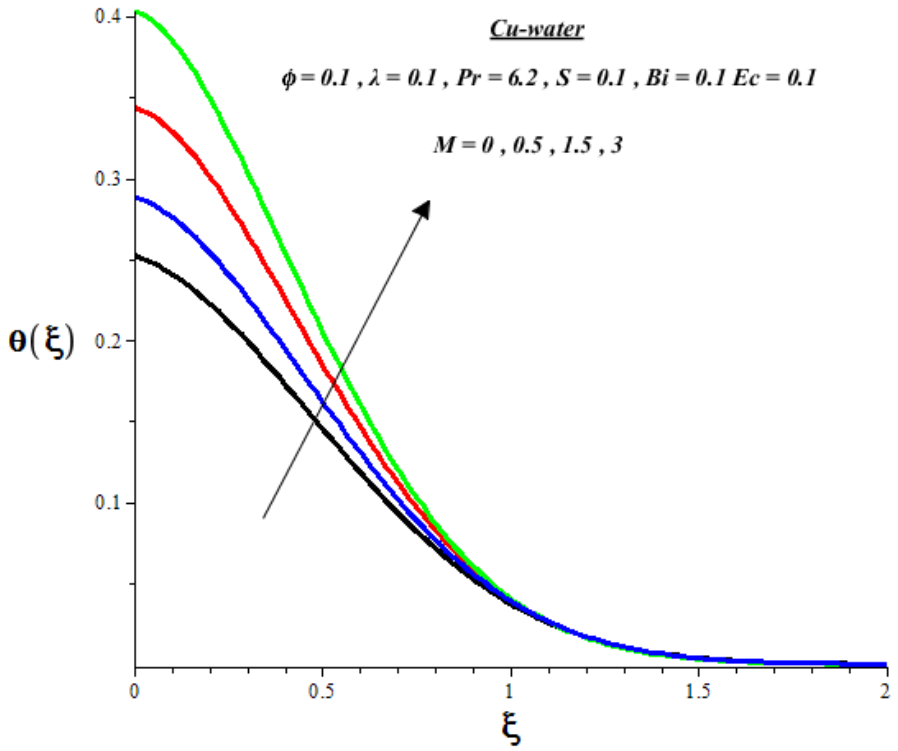

Figure 2.9: The impact of M on the temperature profile of Cu-water nanofluid flow.

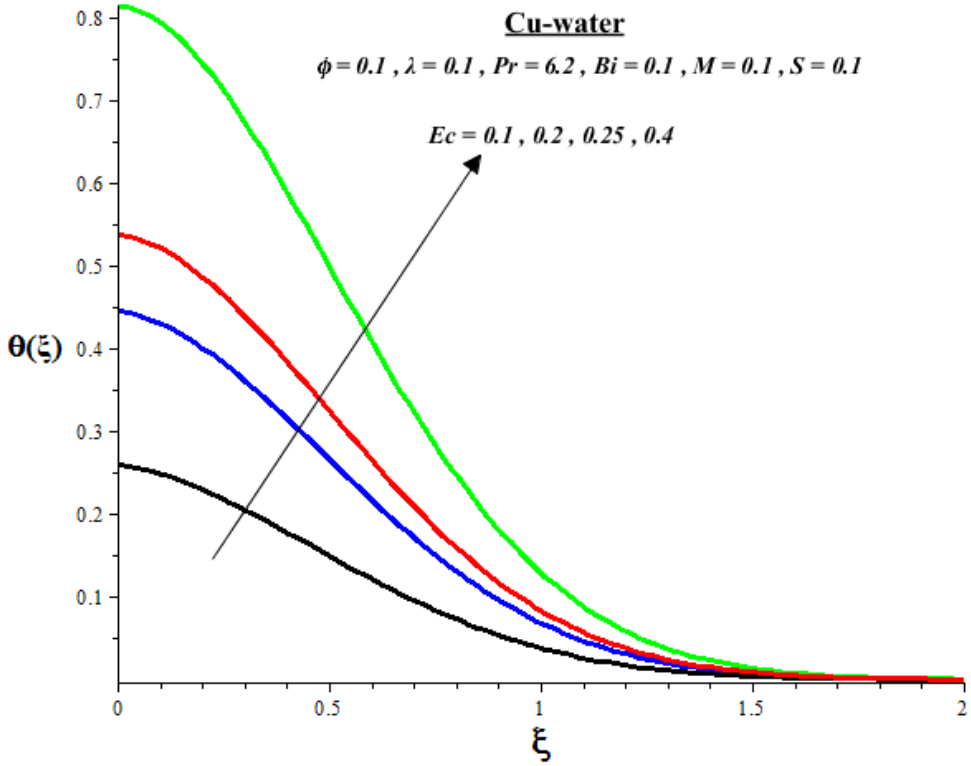

Figure 2.10: The impact of Ec on the temperature profile of Cu-water nanofluid flow.

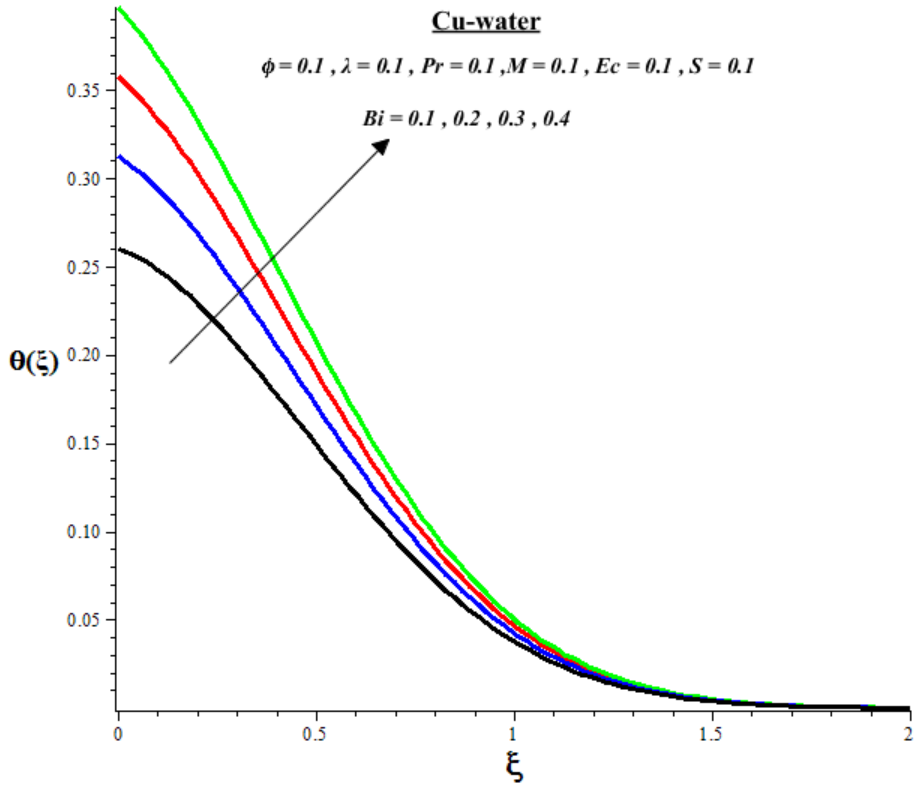

Figure 2.11: The impact of Bi on the temperature profile of Cu-water nanofluid flow.

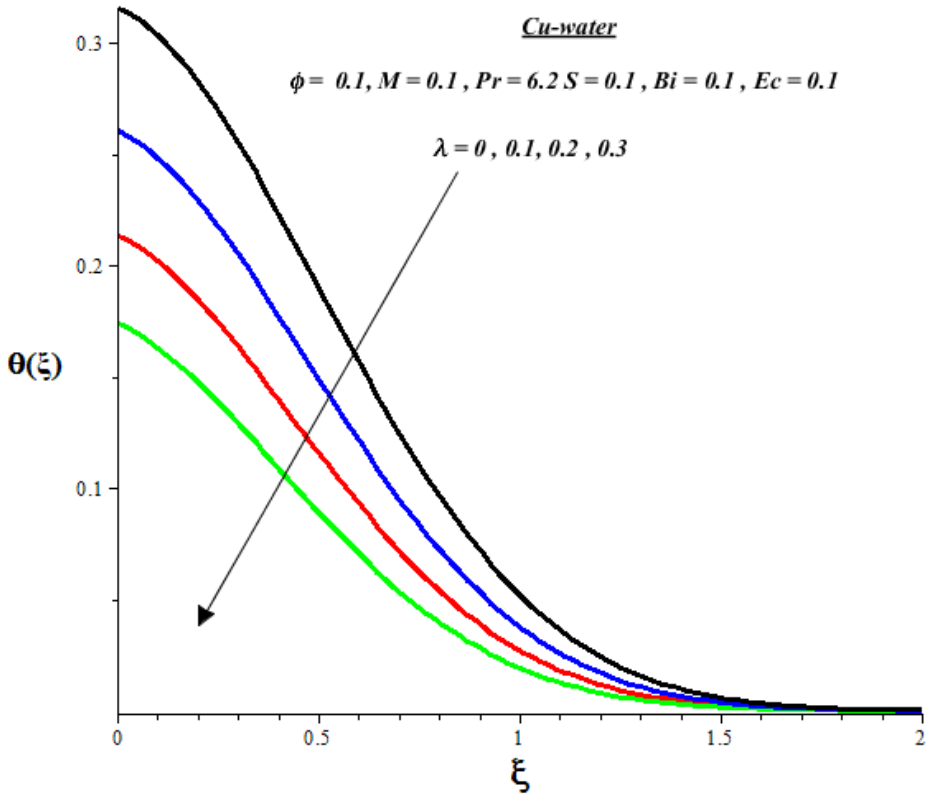

Figure 2.12: The impact of λ on the temperature profile of Cu-water nanofluid flow.

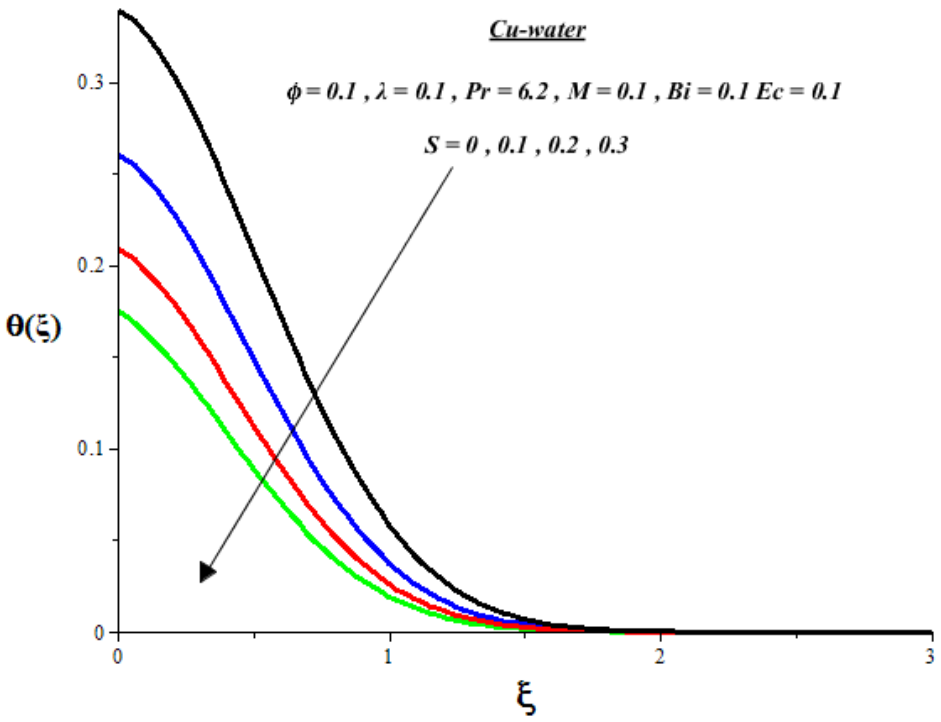

Figure 2.13: The impact of S on the temperature profile of Cu-water nanofluid flow.

2.5.3 Skin friction

The skin friction coefficient $\boldsymbol{C_f\sqrt{Re_x}}$ for Cu-water nanofluid is plotted against the nanoparticles volume fraction($\boldsymbol{\phi}$) for stretching surface as shown in Figures 2.14 and 2.16. Interestingly, the skin friction escalates with an upsurge in nanoparticles volume fraction ($\boldsymbol{\phi}$) and magnetic field ($\boldsymbol{M}$) but diminishes with a rise in sheet surface slipperiness ($\boldsymbol{S}$) and surface stretching rate ($\boldsymbol{\lambda}$) as illustrated in Figure 2.14 – 2.16 below.

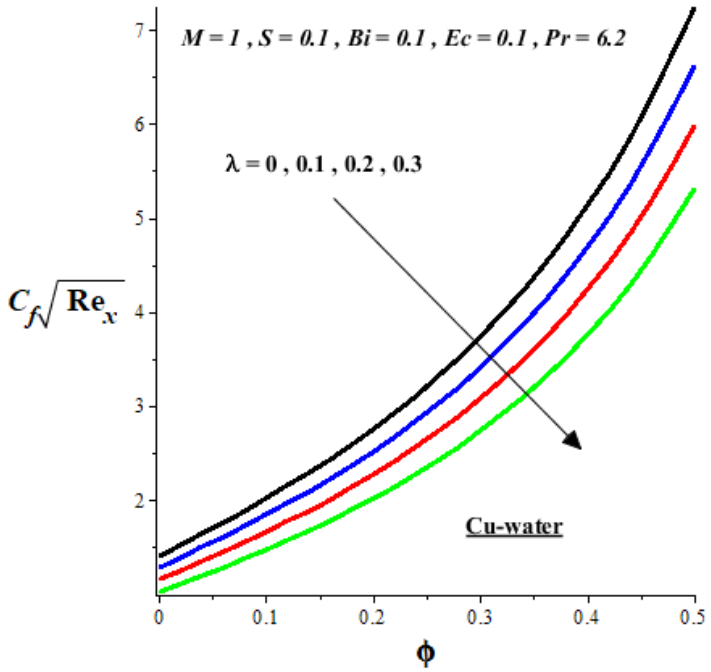

Figure 2.14: The impact of λ in the $C_f\sqrt{Re_x}$ of Cu-water nanofluid flow

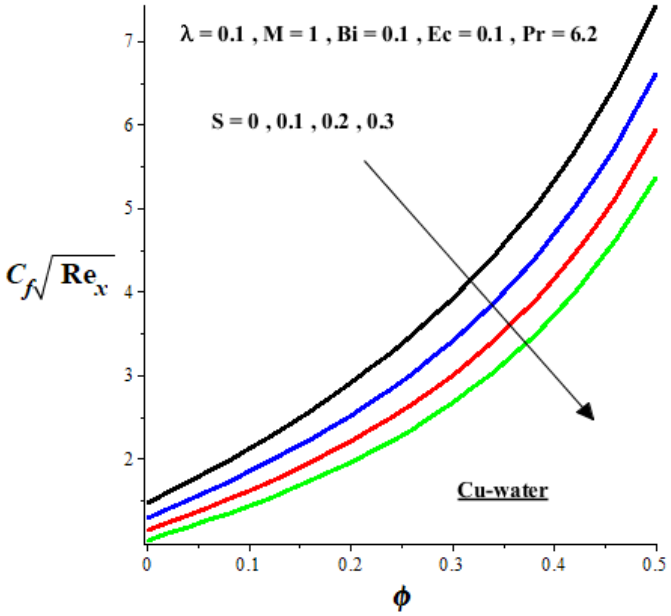

Figure 2.15: The impact of S in the $C_f\sqrt{Re_x}$ of Cu-water nanofluid flow.

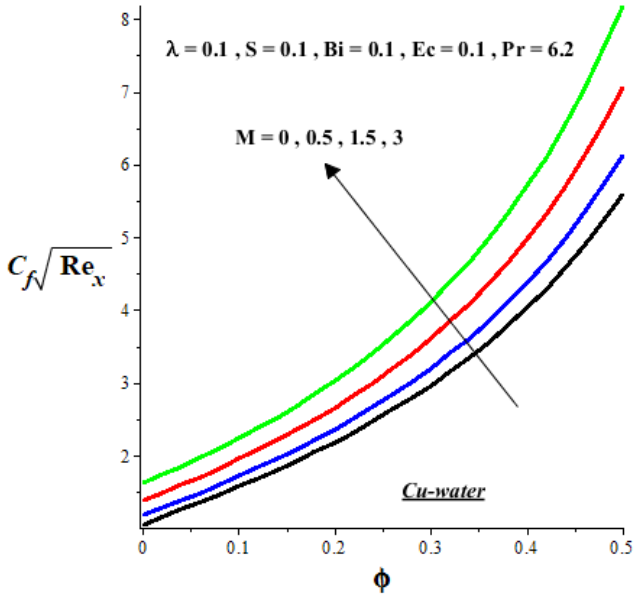

Figure 2.16: The impact of M in the $\boldsymbol{C_f\sqrt{Re_x}}$ of Cu-water nanofluid flow.

2.5.4 Nusselt number

The heat transfer rate of the stretching surfaces with Cu-water as working nanofluid reveals the effects of various emerging parameters and is displayed in Figures 2.17 – 2.19. It is notable that an increase in surface stretching rate ($\boldsymbol{\lambda}$), Biot number ($\boldsymbol{Bi}$), surface slipperiness ($\boldsymbol{S}$), and nanoparticles volume fraction ($\boldsymbol{\phi}$) due to convective heating of the sheet surface boosts heat transfer rate, while a rise in magnetic field intensity ($\boldsymbol{M}$) and Eckert number ($\boldsymbol{Ec}$) will diminish the Nusselt number due to viscous dissipation.

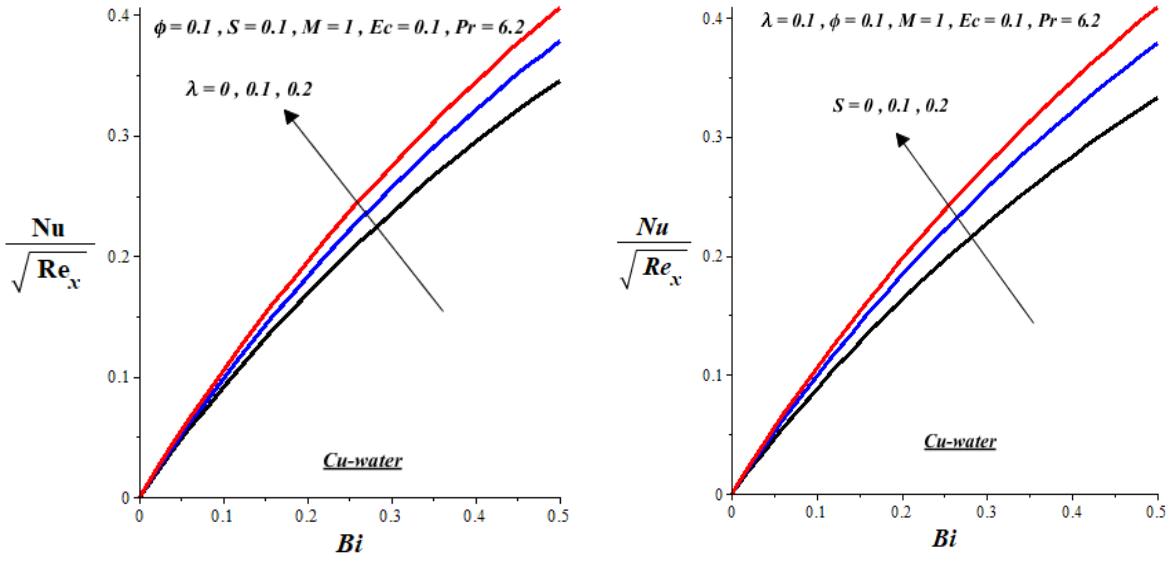

A B

Figure 2.17: The impact of λ and S in the $\frac{Nu}{\sqrt{Re}}$ profile of Cu-water nanofluid flow.

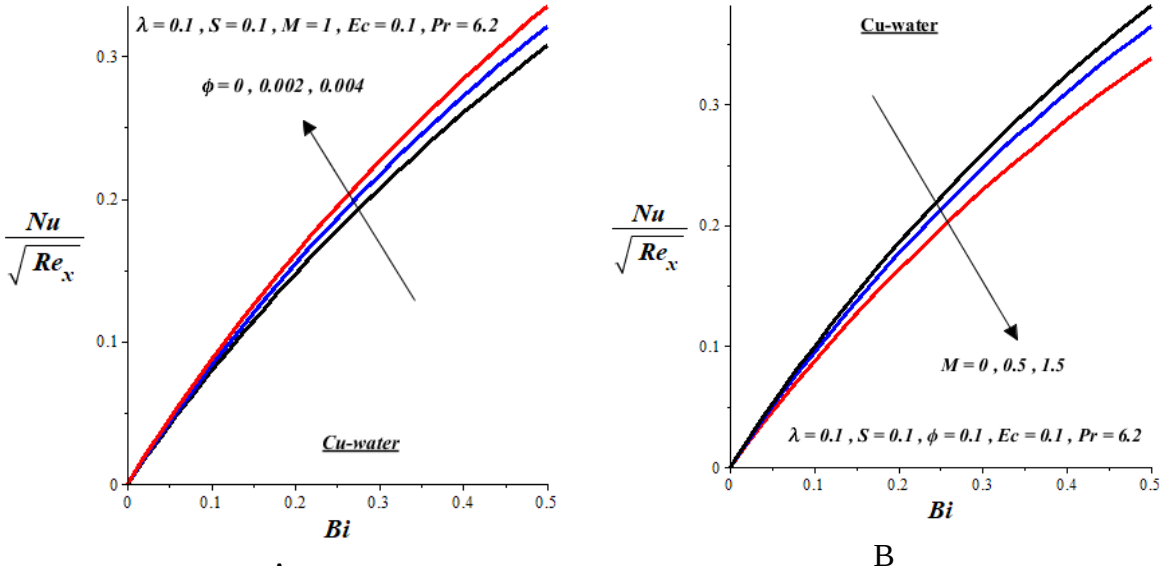

A B

Figure 2. 18: The impact of ϕ and M in the $\frac{Nu}{\sqrt{Re}}$ profile of Cu-water nanofluid flow.

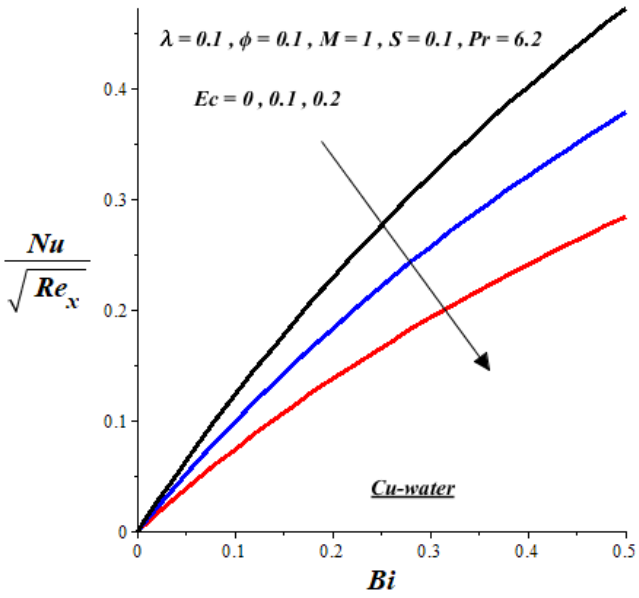

Figure 2.19: The impact of Ec in the $\frac{Nu}{\sqrt{Re}}$ profile of Cu-water nanofluid flow.

CHAPTER 3: ANALYSIS OF DUAL SOLUTIONS FOR MHD STAGNATION POINT OF NANOFLUID TOWARDS A HEATED SHRINKING SURFACE

3.1 Summary

This chapter examines the heat transfer enhancement of incompressible two-dimensional steady magnetohydrodynamics (MHD) flow consisting of either Cu-water, Al_2O_4-water, or Fe_3O_4-water over slippery but convectively heated shrinking surfaces. The derived partial differential equations based on Newton's law of motion and the first law of thermodynamics are obtained, and based on the realistic assumptions the PDE will be transformed to nonlinear ordinary differential equations using a suitable similarity transformation. Furthermore, the nonlinear model differential equations are obtained and numerically tackled using the shooting procedure with the Runge-Kutta-Fehlberg integration scheme. Analytical solutions are obtained for the nanofluids velocity, temperature, local skin friction, and local Nusselt number and are depicted graphically and quantitatively discussed. A critical value of a shrinking parameter exists below which no real solution can be found. The existence of a dual solution in the specific range of shrinking surface parameters is found.

3.2 Introduction

Magnetohydrodynamic (MHD) refers to the interaction of a magnetic field with electrically conducting fluids during the flow process. This interaction may enhance the flow control and the heat transfer capability of a system. The use of magnetic fields and nanofluids in a heat transfer problem are becoming more common due to its wide range of applications. For example, Heidary *et al.* [66] conducted a mathematical model to study the impact of a magnetic field on the forced convection of a nanofluid in a straight channel. Khan *et al.* [27] numerically examined the joint effects of Navier slip and magnetic field on bio-convection of water-based nanofluid in the presence of gyrotactic microorganisms over an upright sheet surface. Their study validates the fact that nanofluid and magnetic field enhances heat and mass transfer. The concerns by Rashidi *et al*. [67] lead to the investigation of the mixed convection heat transfer of nanofluid flow in an upright channel with sinusoidal walls under a magnetic field. Their results revealed that an increase in the magnetic field intensity lessened the velocity profiles while the Nusselt number is augmented.

Akbar *et al.* [68] discussed the behaviours of various values of emerging parameters such as the power-law index, Weissenberg number, Hartmann number and suction/blowing parameter on the model of MHD stagnation point flow of carreau fluid toward a permeable shrinking sheet. In addition, their study reveals a dual solution for both skin friction coefficient and velocity profile. Rostami *et al.* [69] analytically modelled the problem of the steady laminar MHD mixed convection boundary layer flow of a SiO_2- and Al_2O_3-water hybrid nanofluid near the stagnation point on a vertical permeable flat plate. Additionally, they observed a dual solution for both assisting and opposing regimes. The theoretical study of the boundary layer stagnation point flow of the Prandtl fluid model towards a shrinking sheet in the presence of a magnetic field was studied by Akbar *et al.* [70]. They showed that dual solutions exist for the proposed Prandtl fluid model and investigated the effect of the suction/injection parameter, Prandtl parameter, elastic parameter, and magnetic parameter on the skin friction and velocity profile. Dhanai *et al.* [71] investigated the multiple solutions for critical values in slip flow and heat transfer analysis of Newtonian nanofluid utilizing heat source/sink and variable magnetic field where the dual solutions are obtained for skin friction, rate of heat transfer, velocity and temperature profile. The numerical calculation exhibited the existence of dual solutions for the velocity and the temperature fields while Bhattacharyya *et al.* [72] investigated the stagnation point flow and heat transfer over an exponentially shrinking sheet. Bhattacharyya [73] presented a study of dual nature of solution of mass transfer with order chemical reaction in boundary layer stagnation point flow over a stretching/shrinking sheet. His study revealed that the dual solution of velocity and concentration exist for certain values of velocity ration parameter.

In this chapter, the mutual effects of magnetic field, surface slipperiness, nanoparticles volume fraction, viscous and thermal dissipation on the heat transfer enhancement rate in a boundary layer flow of nanofluids consisting Cu-water, Al_2O_4-water, and Fe_3O_4-water past a convectively heated shrinking surface are discussed. To the best of the authors' knowledge, no such investigation has been carried out yet. The main objective of the chapter is to discuss the dual solutions on the velocity, temperature profile, skin friction, and Nusselt number for both stagnation points and shrinking flows.

3.3 Model Problem

The effect of magnetic field of strength B_0 on the heat transfer enhancement capability of nanofluids coolants consisting of either Cu-water, Al_2O_4-water, or Fe_3O_4-water over a slippery but convectively heated shrinking surfaces as shown in Figure 3.1 below are studied:

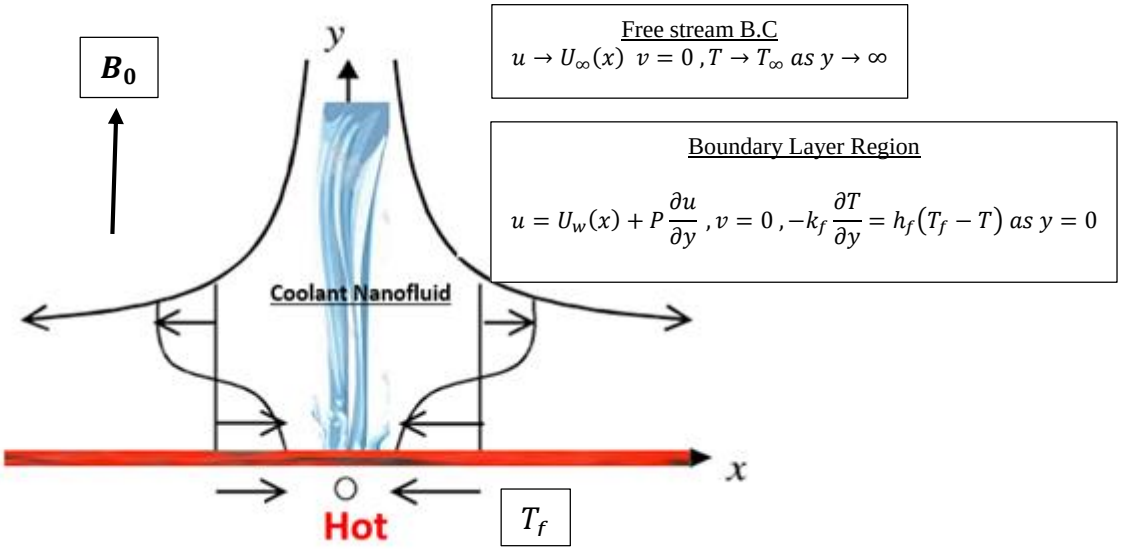

Figure 3.1: Problem geometry of shrinking sheet.

Based on the above assumptions to the model in Figure 3.1, the magnetohydrodynamics governing equations can be written as the boundary layer equation below,

$$\frac{\partial u}{\partial x} + \frac{\partial v}{\partial y} = 0, \tag{3.1}$$

$$u\frac{\partial u}{\partial x} + v\frac{\partial u}{\partial y} = U_\infty \frac{dU_\infty}{dx} + \frac{\mu_{nf}}{\rho_{nf}}\left(\frac{\partial^2 u}{\partial y^2}\right) - \frac{\sigma_{nf}}{\rho_{nf}}{B_0}^2(u - U_\infty), \tag{3.2}$$

$$\left(\rho C_p\right)_{nf}\left(u\frac{\partial T}{\partial x} + v\frac{\partial T}{\partial y}\right) = k_{nf}\frac{\partial^2 T}{\partial y^2} + \mu_{nf}\left(\frac{\partial u}{\partial y}\right)^2 + \sigma_{nf}{B_0}^2(u - U_\infty)^2, \tag{3.3}$$

with Boundary Condition (BC),

$$\begin{aligned} u(x,0) &= U_w(x) + P\frac{\partial u}{\partial y}, \qquad v(x,0) = 0, \quad T(x,\infty) \to T_\infty, \\ -k_f\frac{\partial T}{\partial y}(x,0) &= h_f\left[T_f - T(x,0)\right], \quad u(x,\infty) \to U_\infty(x), \end{aligned} \tag{3.4}$$

where (u, v) are the velocity components of the nanofluid in the (x, y) directions respectively; U_∞ represent the free stream velocity; h_f is the heat coefficient; T represent the temperature; T_∞ is the free stream temperature; T_f is the temperature of the hot fluid below the sheet; ρ_{nf} is

the nanofluid density; μ_{nf} is the nanofluid dynamic viscosity; k_{nf} is the nanofluid thermal conductivity; $(\rho C_p)_{nf}$ is the nanofluid heat capacitance; σ_{nf} is the nanofluid electrical conductivity; and P is the slip length coefficient. From the Partially Differential Equation (PDE) in (3.1) to (3.3) with its Boundary Condition (3.4) we translate it now to the Ordinary Differential Equation (ODE) using similarity transformation as defined in (3.5).

$$U_w(x) = ax,\ U_\infty(x) = bx \quad where\ a, b \in (s^{-1})\left(\frac{1}{t}\right),\ T = \theta(\xi)\left(T_f - T_\infty\right) + T_\infty,$$

$$u = \frac{\partial \psi}{\partial y},\ v = -\frac{\partial \psi}{\partial x}, \quad \psi = x\sqrt{\nu_f b}F(\xi), \quad \xi = y\sqrt{\frac{b}{\nu_f}}, \qquad \theta(\xi) = \frac{T - T_\infty}{T_f - T_\infty}. \tag{3.5}$$

Note that ψ is the stream function. The terms in equations (3.2) to (3.3) are expanded in equation (3.6).

$$u = \frac{\partial \psi}{\partial \xi}\frac{\partial \xi}{\partial y} = \left(x\sqrt{\nu_f b}F'(\xi)\right)\left(\sqrt{\frac{b}{\nu_f}}\right) = xbF'(\xi,\ \ v = -\frac{\partial \psi}{\partial x} = -\sqrt{\nu_f b}F(\xi),$$

$$\frac{\partial T}{\partial x} = \frac{\partial T}{\partial \xi}\frac{\partial \xi}{\partial x} = \left(\theta'(\xi)\left(T_f - T_\infty\right)\right)(0) = 0,$$

$$\frac{\partial T}{\partial y} = \left(\theta'(\xi)\left(T_f - T_\infty\right)\right)\left(\sqrt{\frac{b}{\nu_f}}\right), \tag{3.6}$$

$$\frac{\partial^2 T}{\partial y^2} = \frac{\partial}{\partial y}\left(\frac{\partial T}{\partial y}\right) = \left(\left(\theta''(\xi)\left(T_f - T_\infty\right)\right)\sqrt{\frac{b}{\nu_f}}\right)\left(\sqrt{\frac{b}{\nu_f}}\right) = \left(\theta''(\xi)\left(T_f - T_\infty\right)\right)\frac{b}{\nu_f},$$

$$\frac{\partial u}{\partial y} = \frac{\partial u}{\partial \xi}\frac{\partial \xi}{\partial y} = \left(xbF''(\xi)\right)\left(\sqrt{\frac{b}{\nu_f}}\right) = xb\sqrt{\frac{b}{\nu_f}}F''(\xi).$$

Substituting the expanded equation (3.6) into equations (3.2) to (3.3) and simplifying we get the ODE of momentum and energy equation as (3.7) and (3.8),

$$F'''(\xi) + \frac{\rho_{nf}\mu_f}{\mu_{nf}\rho_f}\left(F(\xi)F''(\xi) - F'(\xi)^2 + 1\right) - \frac{\mu_f \sigma_{nf} B_0^2}{\mu_{nf} b \rho_f}\frac{\sigma_f}{\sigma_f}\frac{\mu_f}{\mu_f}\left(F'(\xi) - 1\right) = 0, \tag{3.7}$$

$$\theta''(\xi) + \frac{\mu_f\left(\rho C_p\right)_{nf}}{\rho_f k_{nf}}\frac{k_f}{k_f}\frac{\left(\rho C_p\right)_f}{\left(\rho C_p\right)_f}F(\xi)\theta'(\xi) + \frac{\mu_{nf}x^2b^2}{k_{nf}\left(T_f - T_\infty\right)}\frac{k_f}{k_f}\frac{\left(C_p\right)_f}{\left(C_p\right)_f}\frac{\mu_f}{\mu_f}F''(\xi)^2 \tag{3.8}$$

$$+\frac{\mu_f \sigma_{nf} B_0^2 x^2 b}{\rho_f k_{nf}\left(T_f - T_\infty\right)} \frac{k_f}{k_f} \frac{\sigma_f}{\sigma_f} \frac{\left(C_p\right)_f}{\left(C_p\right)_f} \frac{b}{b} (F'(\xi) - 1)^2 = 0.$$

We will reduce the equations (3.7) and (3.8) by introducing some new parameters shown in equation (3.9),

$$A_1 = \frac{\mu_f}{\mu_{nf}} \frac{\rho_{nf}}{\rho_f}, A_2 = \frac{\sigma_{nf} \mu_f}{\sigma_f \mu_{nf}}, A_3 = \frac{\left(\rho C_p\right)_{nf} k_f}{\left(\rho C_p\right)_f k_{nf}}, A_4 = \frac{\mu_{nf} k_f}{\mu_f k_{nf}}, \gamma = \frac{\sigma_s}{\sigma_f},$$

$$A_5 = \frac{\sigma_{nf} k_f}{\sigma_f k_{nf}}, M = \frac{\sigma_f B_0^2}{\rho_f b}, Pr = \frac{\mu_f C_{pf}}{k_f}, \nu_f = \frac{\mu_f}{\rho_f}, Ec = \frac{x^2 b^2}{\left(C_p\right)_f \left(T_f - T_\infty\right)}, Bi = \frac{h_f}{k_f} \sqrt{\frac{\nu_f}{b}},$$

$$\frac{k_{nf}}{k_f} = \frac{(k_s + 2k_f) - 2\phi(k_f - k_s)}{(k_s + 2k_f) + \phi(k_f - k_s)}, \left(\rho C_p\right)_{nf} = (1 - \phi)\left(\rho C_p\right)_f + \phi\left(\rho C_p\right)_s, S = L \sqrt{\frac{b}{\nu_f}}, \quad (3.9)$$

$$\rho_{nf} = (1 - \phi)\rho_f + \phi\rho_s, \ \ \mu_{nf} = \frac{\mu_f}{(1 - \phi)^{2.5}}, \frac{\sigma_{nf}}{\sigma_f} = 1 + \frac{3(\gamma - 1)\phi}{(\gamma + 2) - (\gamma - 1)\phi}, \lambda = \frac{a}{b},$$

where ρ_f is the density of the basefluid; ρ_s is the density of the solid nanoparticle; m is the nanoparticles shape factor; k_f is the basefluid thermal conductivity; k_s is the nanoparticles thermal conductivity; σ_f is the basefluid electrical conductivity; σ_s is the nanoparticles electrical conductivity; ϕ is the nanoparticles volume fraction; μ_f is the basefluid dynamic viscosity; C_{pf} is the basefluid specific heat capacity; and C_{ps} is the nanoparticles specific heat capacity as shown in Table 3.1. Then the ODE momentum and energy equations are given by equations (3.10) and (3.11) below with its boundary conditions (3.12),

$$F'''(\xi) + A_1 \left(F(\xi)F''(\xi) - F'(\xi)^2 + 1\right) - A_2 M(F'(\xi) - 1) = 0, \quad (3.10)$$

$$\theta''(\xi) + A_3 PrF(\xi)\theta'(\xi) + A_4 PrEcF''(\xi)^2 + A_5 PrEcM(F'(\xi) - 1)^2 = 0, \quad (3.11)$$

$$F(0) = 0, F'(0) = \lambda + SF''(0), F'(\infty) = 1, \theta'(0) = Bi(\theta(0) - 1), \theta(\infty) = 0. \quad (3.12)$$

where Pr is the basefluid Prandtl number $Pr = 6.2$; Bi is the Biot number; Ec is the Eckert number; M is the magnetic field parameter; S is the slip parameter; and λ is the shrinking parameter. Other quantities of interest are the skin friction coefficients(C_f) and the Nusselt number (Nu) which can be expressed as,

$$C_f\sqrt{Re_x} = \frac{F''(0)}{(1-\phi)^{2.5}}, \qquad \frac{Nu}{\sqrt{Re}} = -\frac{k_{nf}}{k_f}\theta'(0), \tag{3.13}$$

where

$$C_f = \frac{T_w}{\rho_f U_\infty^2}, \qquad Nu = \frac{xq_w}{k_f\left(T_f - T_\infty\right)}, \qquad T_w = \mu_{nf}\frac{\partial u}{\partial y}\,|_{y=0},$$
$$q_w = -k_{nf}\frac{\partial T}{\partial y}\,|_{y=0}, \quad Re_x = \frac{xU_\infty}{\upsilon_f} \tag{3.14}$$

3.4 Analytical Solution Procedure

From the obtained nonlinear ODE momentum equation in (3.10) we suppose that the exact solution is given by $F(\xi) = B + C\xi + De^{-n\xi}$. Solving for unknowns using boundary conditions in equation (3.12) we find that $B = \frac{\lambda-1}{Sn^2+n}$, $C = 1$ and $D = \frac{1-\lambda}{Sn^2+n}$, then the momentum equation becomes,

$$F(\xi) = \frac{\lambda-1}{Sn^2+n}\left(1 - e^{-n\xi}\right) + \xi. \tag{3.15}$$

It also follows that the axial velocity which is the derivative of $F(\xi)$ with respect to ξ is given by,

$$F'(\xi) = 1 + \frac{\lambda-1}{Sn+1}e^{-n\xi}. \tag{3.16}$$

To obtain the solution for nonlinear ODE energy equation in (3.11) we suppose that the exact solution is given by $\theta(\xi) = Ae^{-r\xi}$ where r >0 the prescribed free stream condition is satisfies. Using the sheet surface boundary condition in equation (3.12) we obtain the $A = \frac{Bi}{Bi+r}$ and the solution for temperature equation becomes,

$$\theta(\xi) = \frac{Bi}{Bi+r}e^{-r\xi}, \tag{3.17}$$

Remark The expression for n and r in the solutions for the velocity and temperature profiles can easily be obtained from the model similarity equations (3.15) and (3.17). Using equation (3.13), we obtain the expression for the skin friction $\delta = \frac{F''(0)}{m} = -\frac{(\lambda-1)n}{m(Sn+1)}$, where the parameter $\delta = C_f Re^{\frac{1}{2}}$ and $m = (1-\phi)^{2.5}$ and the expression for the n can be obtained

as $n = -\frac{\delta m}{S\delta m+\lambda-1}$. Substitute the exact solution equation (3.15) in the momentum equation (3.10) and evaluate $\xi = 0$ at the free stream, using maple program we get that,

$$Sn^3 + n^2 - (A_2MS + 2A_1S)n - (A_1\lambda + A_2M + A_1) = 0. \tag{3.18}$$

Replace n to the momentum equation (3.18) and making use of maple program to simplify we get equation (3.19) also note that $\delta = C_f Re^{\frac{1}{2}}$ is a local skin friction and will be solved using maple program and results will be plotted and discussed.

$$A_1S^3m^3\delta^3 + m^2(3A_1\lambda S^2 + A_2MS^2 - A_1S^2 - 1)\delta^2 + Sm(\lambda-1)(3A_1\lambda + 2A_2M + A_1)\delta \tag{3.19}$$
$$+(\lambda-1)^2(A_1\lambda + A_2M + A_1) = 0.$$

From the Nusselt number equation (3.13) we let $\chi = NuRe^{-\frac{1}{2}}$ and $p = \frac{k_{nf}}{k_f}$ and the expression for the r can be obtained as $r = \frac{\chi Bi}{Bip-\chi}$. Substitute the exact solution equation (3.17) in the momentum equation (3.11) and evaluate $\xi = 0$ at the free stream, using maple program we get that,

$$Bi(Sn+1)^2r^2 + EcPr(\lambda-1)^2(A_4n^2 + A_5M)(Bi + r) = 0. \tag{4.20}$$

Replace r to the energy equation (4.20) and making use of maple program to simplify we get equation (3.21). Also note that $\chi = NuRe^{-\frac{1}{2}}$ which is a local Nusselt number and will be solved using maple program and results will be plotted and discussed.

$$Bi(Sn+1)^2\chi^2 + pEcPr(\lambda-1)^2(A_4n^2 + A_5M)(pBi - \chi) = 0. \tag{4.21}$$

3.5 Results and Discussion

3.5.1 Velocity Profile

The impact of various parameters on the velocity profile are presented in Figure 3.2 – 3.3 where it is noticeable that velocity increases from surface velocity to free stream velocity. Note that this observation was overserved in all cases of nanofluid flow consisting of either Cu-water, Fe_3O_4-water, or Al_2O_3-water nanofluid. There is an existence of dual solution where from the figure the solid line represents the upper branch solution and dotted line represents the lower branch solution. Figure 3.2 A show that within the velocity boundary layer the Cu-water nanofluid interact closer to the surface for both upper and lower branch solution followed by Fe_3O_4-water nanofluid and lastly Al_2O_3-water nanofluid. The impact of parameters ϕ, S, M, and λ on the velocity profiles $F'(\xi)$ will be generalized using Cu-water nanofluid as it shows the same impact using either Fe_3O_4-water or then Al_2O_3-water nanofluid.

It is furthermore noticeable that the upper branch solution interacts closely to the surface compared to the lower branch solution. From Figure 3.2 B and 3.3 the upper solution branch for velocity profiles revealed a decline in the momentum boundary layer thickness with increasing nanoparticles volume fraction(ϕ), magnetic field intensity (M) and surface slipperiness (S) which boosts the interaction between the nanofluids and the heated surface leading to an enhancement in heat transfer rate. However, the lower branch solution revealed that an incline in the momentum boundary layer thickness with increasing nanoparticles volume fraction(ϕ) while there was a decline with an increase in surface slipperiness (S), and magnetic field intensity (M).

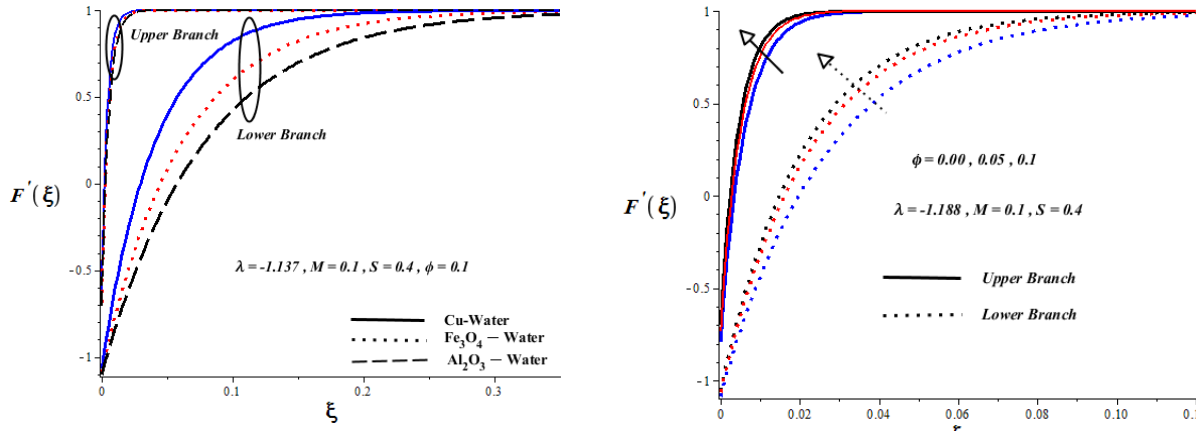

Figure 3.2: Velocity profiles for different nanofluids and increasing values of ϕ.

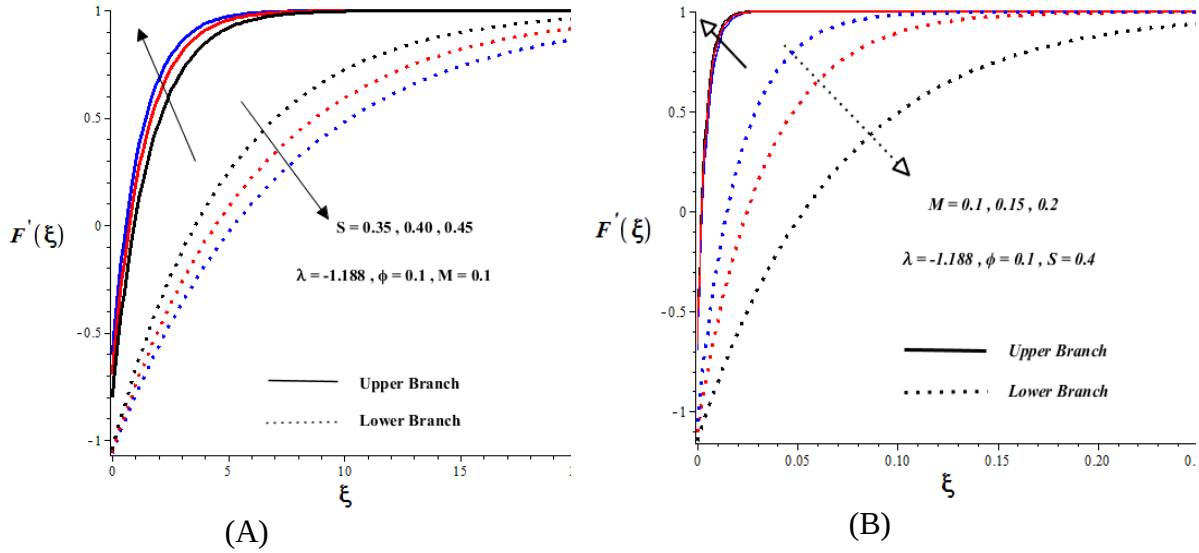

Figure 3.3: Velocity profiles for increasing values of S and M.

3.5.2 Temperature Profile

The impact of thermophysical parameters on the temperature profiles of a Cu-water, Fe_3O_4-water, or Al_2O_3-water nanofluid are presented in Figure 3.4 – 3.6. Observation in general indicates that the nanofluids' temperature is higher at the surface due to convective heating and decreases gradually towards the free stream temperature value far away from the surface. There is a similar observation of the existence of a dual solution like in the velocity profile where the solid line represents the upper branch solution and dotted line represents the lower branch solution. Figure 3.4 A shows that within the thermal boundary layer the Cu-water nanofluid interacts closer to the surface for both upper and lower branch solution followed by Al_2O_3-water nanofluid and lastly Fe_3O_4-water nanofluid. This implies that Cu-water takes more heat from the surface as compared to Fe_3O_4-water and Al_2O_3-water. The author decided to show the figures for Cu-water nanofluid, as the impact for Fe_3O_4-water, and Al_2O_3-water nanofluid is the same. From Figures (3.4 B), (3.5), and (3.6) an increase in the Cu-water temperature is noticed with an increase in values of magnetic field intensity(M), Biot number (Bi), nanoparticles volume fraction (ϕ) and Eckert number (Ec) for both cases of upper and lower branch solution. The rise in nanofluid temperature may be attributed to the combined effects of convective heating of the surface due to hot fluid underneath, viscous dissipation, Joule heating due to magnetic field, and nanoparticles thermal conductivity. Consequently, the thermal boundary layer thickness is enhanced. We observed that an increase in sheet surface slipperiness (S) and stretching rate (λ) lessened the Cu-water nanofluid temperature profiles.

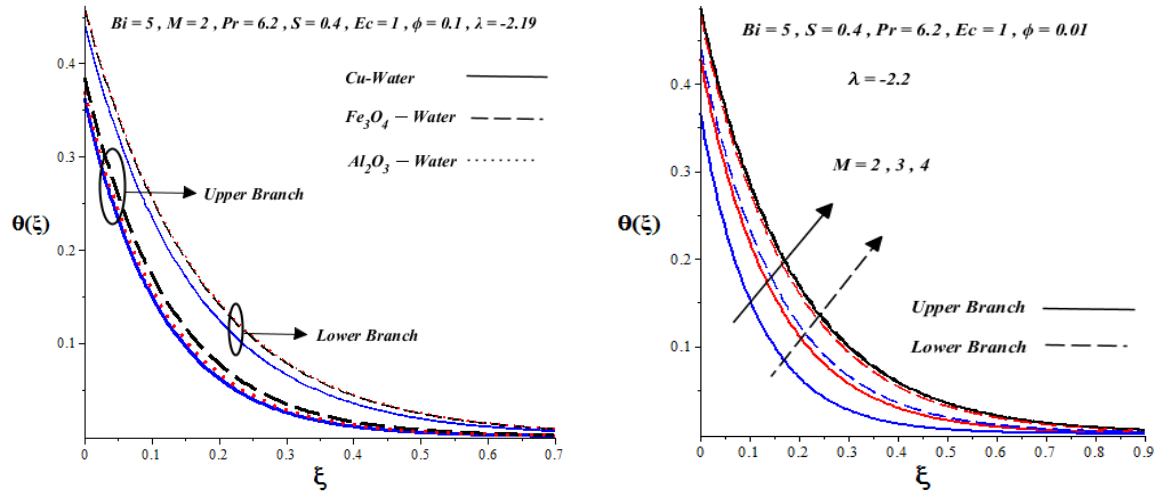

(A) (B)

Figure 3.4: Temperature profiles for different nanofluids and increasing values of M.

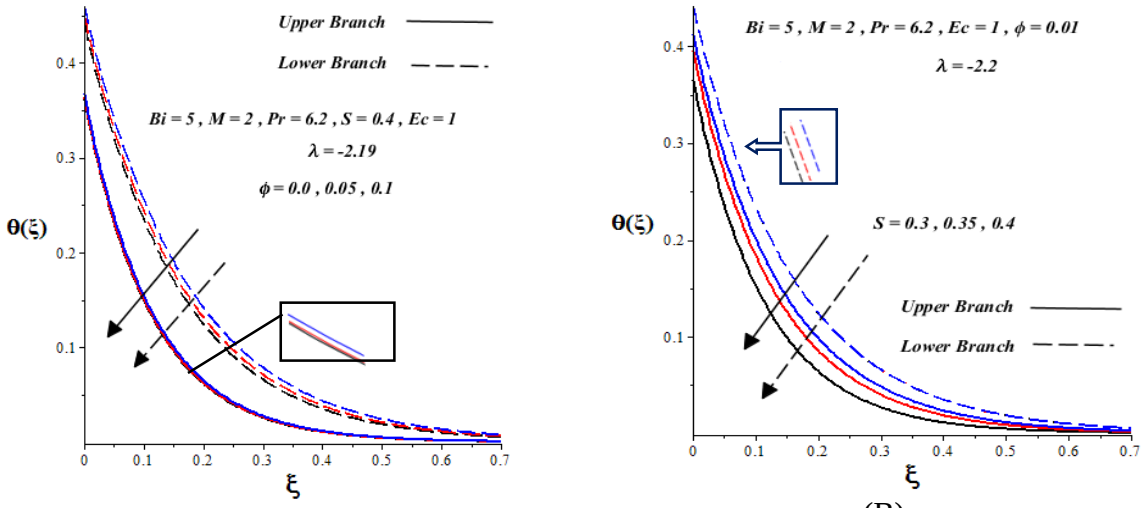

Figure 3.5: The impact of (ϕ) and S on the temperature profile of Cu-water nanofluid flow.

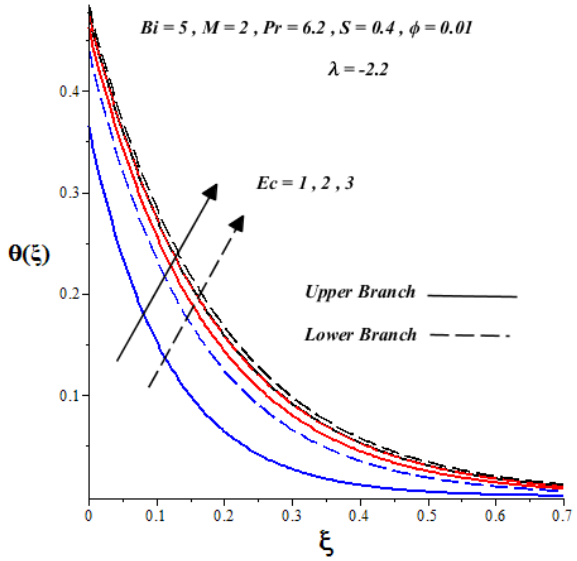

Figure 3.6: The impact of Ec and ϕ on the temperature profile of Cu-water nanofluid flow.

3.5.3 Skin friction

The impact of the skin friction coefficient $\boldsymbol{C_f\sqrt{Re_x}}$ for Cu-water, Fe_3O_4-water, or Al_2O_3-water nanofluid are plotted against $\boldsymbol{\lambda}$ for shrinking surface as shown in Figures 3.7 and 3.8. There is a similar observation of an existence of dual solution as observed in the velocity and temperature profile where the solid line represents the upper branch solution and dotted line represents the lower branch solution. A critical shrinking surface parameter $\boldsymbol{\lambda_c}$ exists below which no real solution can be found for. Dual solution is only apparent for $\boldsymbol{\lambda_c} < \boldsymbol{\lambda} < 0$. Table 3.1 depicts the influence of parameters variation on the dual solutions for skin friction in the case of shrinking sheet surface with Cu-water as working nanofluid. Interestingly, the skin friction on the upper and lower solution branches heightened with a rise in nanoparticles volume fraction $(\boldsymbol{\phi})$ as shown in Figure 3.7A.

However, for an increase in magnetic field intensity (***M***) and surface slipperiness (***S***) in the upper branch solution the skin friction will increase while the lower branch solution decreases the skin friction as referred to in figure 3.7 B and 3.8 A. Figure 3.8 B compares the skin friction of different nanofluids and it is notable that on the upper branch solution Cu- water nanofluid has a higher skin friction followed by Fe_3O_4-water and Al_2O_3-water nanofluid, respectively; while on the lower branch solution Al_2O_3-water nanofluid has a higher skin friction followed by Fe_3O_4-water and Cu-water nanofluid.

Table 3.1: The impact of Ec and ϕ on the temperature profile of Cu water nanofluid flow.

S	M	ϕ	λ_c	λ	Upper branch $\sqrt{Re_x}C_f$	Lower branch $\sqrt{Re_x}C_f$
0.35	0.10	0.10	- 1.232612111	-1.088	1.43950	0.52960
0.40	0.10	0.10	- 1.274458888	-1.088	1.59115	0.43142
0.45	0.10	0.10	- 1.319296881	-1.088	1.67897	0.36855
0.40	0.10	0.00	-1.254358635	-1.188	0.99780	0.25842
0.40	0.10	0.05	-1.265294597	-1.188	1.29155	0.35041
0.40	0.15	0.10	-1.318321364	-1.188	1.70023	0.27270
0.40	0.20	0.10	-1.362282074	-1.188	1.78908	0.13397

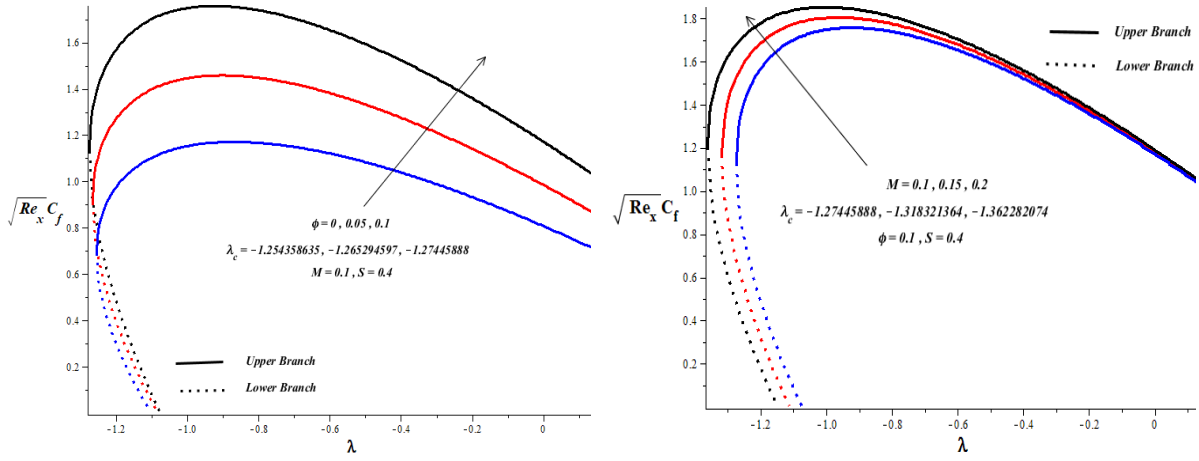

(A) (B)

Figure 3.7: Skin friction for shrinking sheet with increasing values of ϕ and M.

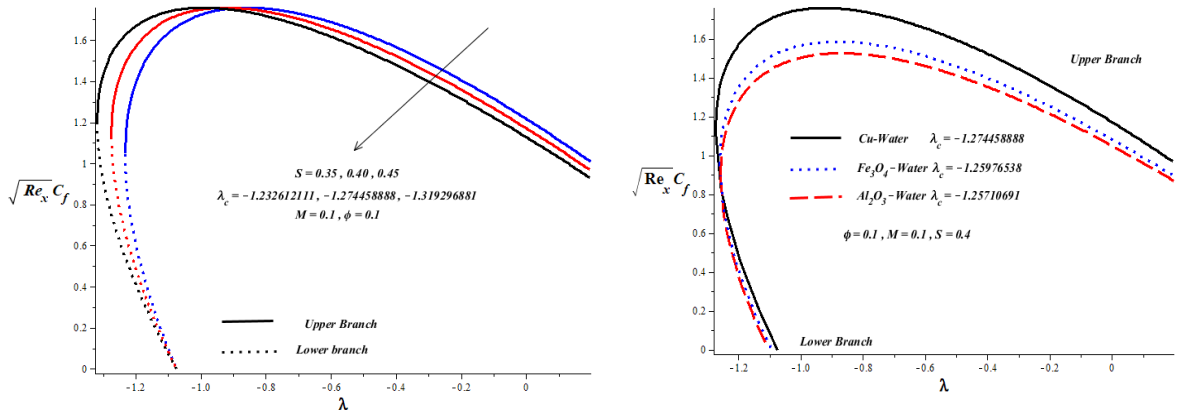

(A) **(B)**

Figure 3.8: Skin friction for shrinking surface with increasing values of S and different nanofluid.

3.5.4 Nusselt number

The heat transfer rate at the shrinking surfaces with Cu-water as working nanofluid are displayed in Figures 3.9 - 3.10 including Table 3.2. The results show the same impact using Fe_3O_4-water and Al_2O_3-water nanofluid as a working fluid. It is remarkable that the Nusselt number exhibits dual solution for $\boldsymbol{\lambda_c} < \boldsymbol{\lambda} < 0$ where the sold line indicates the upper branch solution and the dotted line indicates the lower branch solution as shown in the figures. This is expected since the model momentum and energy equations are coupled together. It is notable that an increase in nanoparticles volume fraction ($\boldsymbol{\phi}$), Biot number ($\boldsymbol{Bi}$), magnetic field intensity ($\boldsymbol{M}$) due to convective heating of the sheet surface boosts heat transfer rate, while a rise inEckert number (Ec), surface slipperiness (S) and shrinking parameter ($\boldsymbol{\lambda}$) diminishes the Nusselt number. Figure (3.11 A) shows that the Cu-water nanofluid has a higher heat transfer followed by Fe_3O_4-water and Al_2O_3-water nanofluid, respectively.

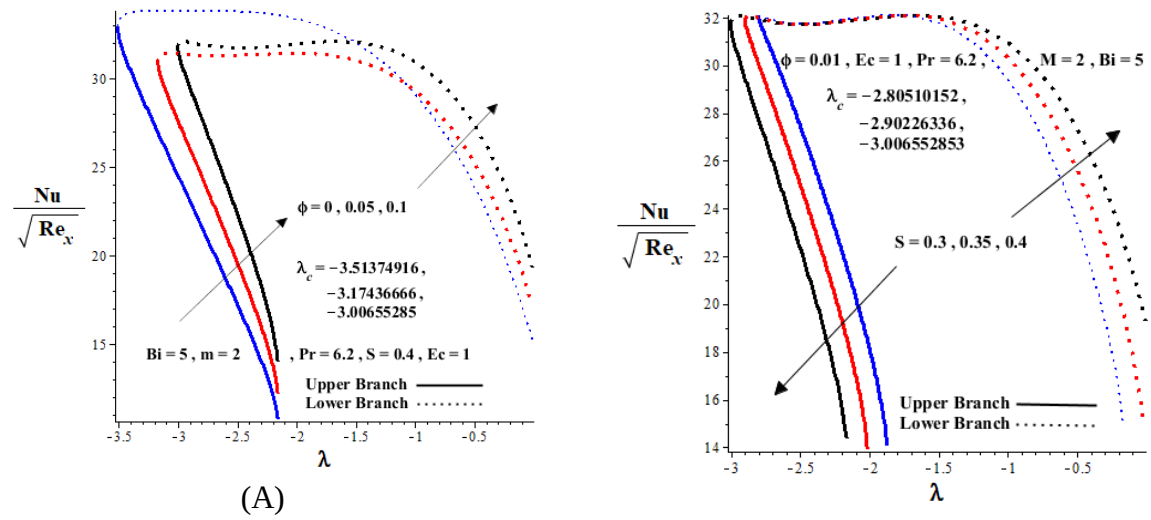

(A) (B)

Figure 3.9: Nusselt number for shrinking sheet with increasing values of ϕ and S.

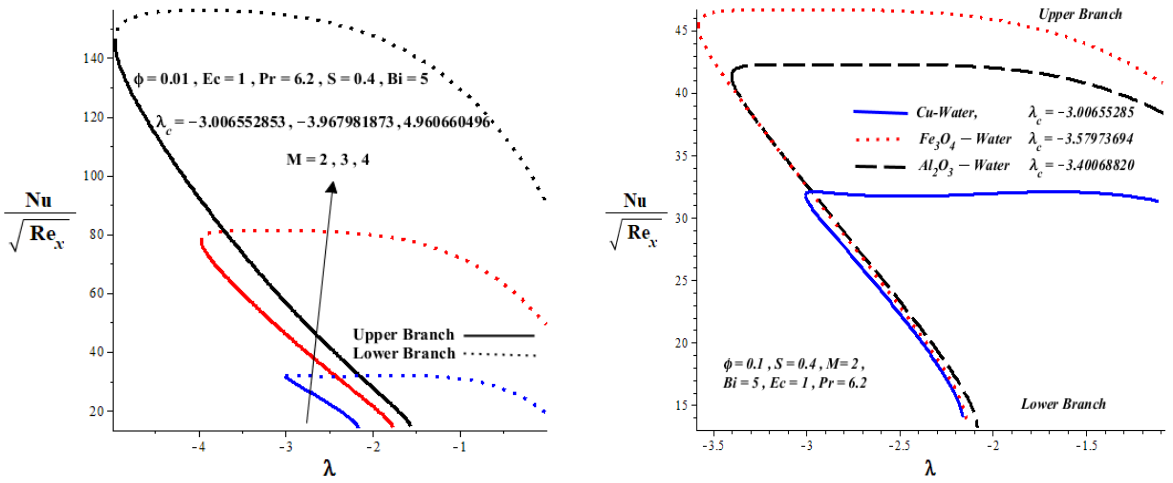

(A) (B

Figure 3.10: Nusselt number for shrinking sheet with increasing values of M and different nanoparticle.

CHAPTER 4: ANALYSIS OF HYDROMAGNETIC STABILITY FOR STAGNATION POINT FLOW OF NANOFLUID TOWARDS A HEATED SHRINKING SURFACE

4.1 Summary

In this chapter, the two-dimensional unsteady magnetohydrodynamics (MHD) flow of a conducting incompressible nanofluid over a convectively heated shrinking and slippery surface (S) is numerically investigated. It is assumed that working water-based nanofluid contains either Copper (Cu) nanoparticles, Alumina nanoparticles (Al_2O_4) or Iron Oxide nanoparticles (Fe_3O_4). The model's partial differential equations (PDE) based on the conservation laws of mass, momentum and energy are obtained and converted to nonlinear ordinary differential equations (ODE) by using a suitable similarity transformation. The obtained ODE will be reformulated from boundary value problem to a related initial value problem using the shooting method where after it is solved numerically using the Runge-Kutta-Fehlberg method to solve nonlinear obtained equation. The numerical solutions for the velocity and temperature profile together with their thermophysical properties skin friction and local Nusselt number have been discussed in the previous section. It was found that the dual solution exits for some value shrinking (λ). In this section, the stability of lower and upper branch solution for temporal development of small disturbances is analysed, and it was found that the upper branch solution is stable and achievable.

4.2 Introduction

The study of stability related to small disturbances in the fluid's flow provide much insight into the complexity involved in the fluid flow process and can be helpful to advice the engineer and decision makers. There are many theoretical and numerical studies about stability in counted on dual solutions and includes the work by Makinde [74] who investigated the small disturbance eigenvalue functions to analyse the temporal stability of ferro fluid past a permeable shrinking sheet. The effect of partial slip condition on the shrinking sheet was analysed by Lund *et al.* [75] on the temporal stability of unsteady magnetized hybrid nanofluid flow. Makinde and Tshehla [76] used a special type of Hermite-Pade approximation technique to analyse thermal stability in a convecting and radiating two-step reactive slab. The Hermite-Pade approximation and perturbation technique was used by Makinde [77] to study the thermal stability of a reactive viscous flow through a porous saturated channel with convective boundary condition. More work has been done by Makinde [78] to exploit important properties of velocity and temperature

together with perturbation and Hermite-Pade approximation technique to investigate thermal stability of a reactive third grade fluid in a cylindrical pipe. It is notable that Makinde [79] analysed the stability MHD of plane Poiseuille flow by using a multideck asymptotic technique.

The perturbation method is one of the best techniques used to analyse the stability caused by small disturbances in the system. Makinde [80] also used the method on the thermal stability of a reactive third grade fluid in a channel with convective cooling of the walls. The stability analysis was carried out by Liaquat *et al.* [81] on the multiple solution of Cu-Al2/H2O nanofluid containing hybrid nanomaterials over a shrinking surface in the presence of viscous dissipation. The transonic small disturbance equation was used by Liu *et al.* [82] to investigate multiple solutions and stability of the steady flow. The eigenvalue plays an important role in the study of stability. Mustafa [83] used the idea of stability analysis for a multiple solution of boundary layer flow towards a shrinking sheet and the analytical solution was obtained using a least square method. Furthermore, the idea of eigenvalue was also used by Lund et al. [28] to analyse stability and dual solutions of micropolar nanofluid over the inclined stretching/shrinking surface with convective boundary condition. The linear stability analysis method was used by Samanta *et al.* [84] to analyse the heat transfer and stability of MHD natural convection above a horizontal plate with a heat flux boundary condition.

4.3 Model Problem

A 2-dimensional unsteady flow of conducting incompressible water-based nanofluid containing either Cu, Al_2O_4 or Fe_3O_4 nanoparticles over a convectively heated shrinking sheet under the influence of a transversely imposed magnetic field of strength B_0 is considered. The sheet is aligned with the x-axis while the y -axis is normal to it as shown in Figure 4.1 below.

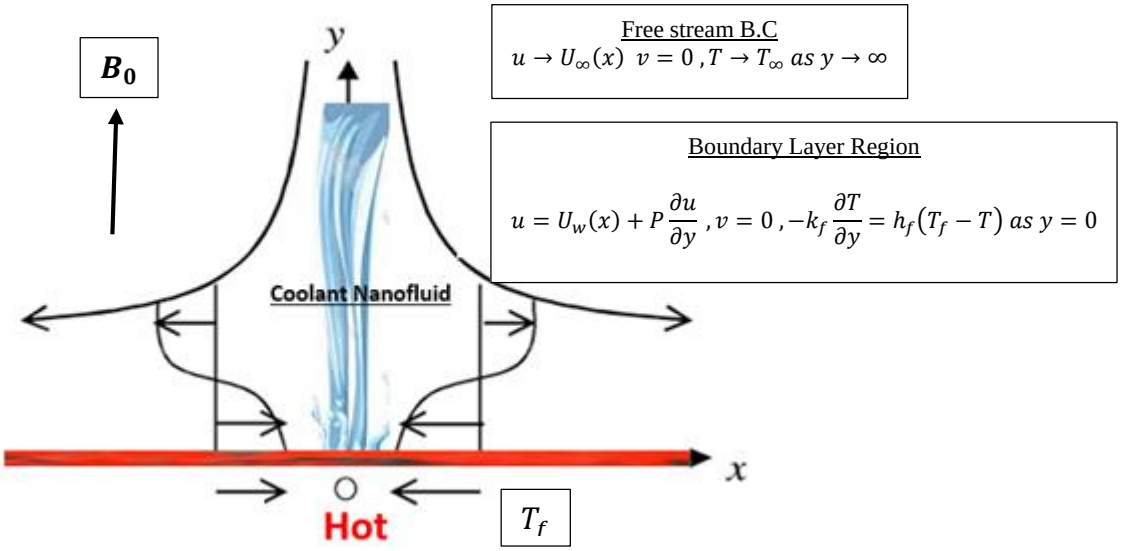

Figure 4.1: Problem geometry of shrinking sheet.

Under these conditions, the continuity, momentum and energy equations governing the problem in two dimensions may be written as;

$$\frac{\partial u}{\partial x} + \frac{\partial v}{\partial y} = 0, \tag{4.1}$$

$$\frac{\partial u}{\partial t} + u\frac{\partial u}{\partial x} + v\frac{\partial u}{\partial y} = U_\infty \frac{dU_\infty}{dx} + \frac{\mu_{nf}}{\rho_{nf}}\left(\frac{\partial^2 u}{\partial y^2}\right) - \frac{\sigma_{nf}}{\rho_{nf}}{B_0}^2(u - U_\infty), \tag{4.2}$$

$$(\rho C_p)_{nf}\left(\frac{\partial T}{\partial t} + u\frac{\partial T}{\partial x} + v\frac{\partial T}{\partial y}\right) = k_{nf}\frac{\partial^2 T}{\partial y^2} + \mu_{nf}\left(\frac{\partial u}{\partial y}\right)^2 + \sigma_{nf}B_0^2(u - U_\infty)^2, \tag{4.3}$$

with Boundary Condition,

$$u(x,0,t) = U_w(x) + P\frac{\partial u}{\partial y}, \qquad v(x,0,t) = 0, \qquad T(x,\infty,t) \to T_\infty,$$
$$-k_f\frac{\partial T}{\partial y}(x,0,t) = h_f\left[T_f - T(x,0,t)\right], \qquad u(x,\infty,t) \to U_\infty(x), \tag{4.4}$$

where (u, v) are the velocity components of the nanofluid in the (x, y) directions respectively; h_f is the heat coefficient; $U_w(x)$ is the sheet shrinking velocity; $U_\infty(x)$ is the free stream velocity; T_∞ is the free stream temperature; T_f is the temperature of the hot fluid below the sheet; ρ_{nf} is the nanofluid density; μ_{nf} is the nanofluid dynamic viscosity; k_{nf} is the nanofluid thermal conductivity; $(\rho C_p)_{nf}$ is the nanofluid heat capacitance; σ_{nf} is the nanofluid electrical conductivity; and t represents time since it is the unsteady flow.

From the Partially Differential Equation (PDE) in (4.1) to (4.3) with its Boundary Condition (4.4) we can translate it to the Ordinary Differential Equation (ODE) using similarity transformation as defined in (4.5). Note that ψ is the stream function and τ is the introduced dimensionless time

$$U_w(x) = ax, \qquad U_\infty(x) = bx \quad where\ a, b \in (s^{-1})\left(\frac{1}{t}\right), \qquad \tau = bt,$$

$$u = \frac{\partial \psi}{\partial y,}\ v = -\frac{\partial \psi}{\partial x}, \quad \psi = x\sqrt{\nu_f b}F(\xi,\tau), \quad \xi = y\sqrt{\frac{b}{\nu_f}}, \qquad \Theta(\xi,\tau) = \frac{T - T_\infty}{T_f - T_\infty}. \tag{4.5}$$

The terms in equations (4.2) and (4.3) are expanded in equation (4.6).

$$u = xbF'(\xi,\tau), v = -\sqrt{\nu_f b}F(\xi,\tau), \qquad \frac{\partial u}{\partial y} = xb\sqrt{\frac{b}{\nu_f}}F''(\xi,\tau),$$
$$\frac{\partial^2 u}{\partial y^2} = \frac{xb^2}{\nu_f}F'''(\xi,\tau), \tag{4.6}$$
$$\frac{\partial T}{\partial x} = \left(\Theta'(\xi,\tau)\left(T_f - T_\infty\right)\right)\left(\sqrt{\frac{b}{\nu_f}}\right), \qquad \frac{\partial^2 T}{\partial y^2} = \left(\Theta''(\xi,\tau)\left(T_f - T_\infty\right)\right)\frac{b}{\nu_f}.$$

Substituting the expanded from the equation (4.6) into equations (4.2) to (4.3) and simplifying it, we get the ODE of momentum and energy equation as (4.7),

$$\frac{\partial^3 f}{\partial \xi^3} - \frac{\rho_{nf}\upsilon_f}{\mu_{nf}}\left(\frac{\partial^2 f}{\partial \xi \partial \tau} + \left(\frac{\partial f}{\partial \xi}\right)^2 - f\frac{\partial^2 f}{\partial \xi^2} - 1\right) - \frac{\upsilon_f \sigma_{nf} B_0^2}{\mu_{nf} b}\left(\frac{\partial f}{\partial \xi} - 1\right) = 0,$$
$$\frac{\partial^2 \Theta}{\partial \xi^2} - \frac{\upsilon_f\left(\rho C_p\right)_{nf}}{k_{nf}}\frac{\partial \Theta}{\partial \tau} + \frac{\upsilon_f\left(\rho C_p\right)_{nf}}{k_{nf}}f\frac{\partial \Theta}{\partial \xi} + \frac{\mu_{nf}x^2b^2}{k_{nf}\left(T_f - T_\infty\right)}\left(\frac{\partial^2 f}{\partial \xi^2}\right)^2 \tag{4.7}$$
$$+ \frac{\upsilon_f \sigma_{nf} x^2 b B_0^2}{k_{nf}\left(T_f - T_\infty\right)}\left(\frac{\partial f}{\partial \xi} - 1\right)^2 = 0.$$

We introduce parameters and variables be defined as shown in equation (4.8),

$$A_1 = \frac{\mu_f}{\mu_{nf}}\frac{\rho_{nf}}{\rho_f}, A_2 = \frac{\sigma_{nf}\mu_f}{\sigma_f \mu_{nf}}, A_3 = \frac{\left(\rho C_p\right)_{nf} k_f}{\left(\rho C_p\right)_f k_{nf}}, A_4 = \frac{\mu_{nf} k_f}{\mu_f k_{nf}}, \gamma = \frac{\sigma_s}{\sigma_f}, M = \frac{\sigma_f B_0^2}{\rho_f b},$$

$$A_5 = \frac{\sigma_{nf} k_f}{\sigma_f k_{nf}}, Pr = \frac{\mu_f C_{pf}}{k_f}, \nu_f = \frac{\mu_f}{\rho_f}, Ec = \frac{x^2 b^2}{\left(C_p\right)_f\left(T_f - T_\infty\right)}, Bi = \frac{h_f}{k_f}\sqrt{\frac{\nu_f}{b}},$$

(4.8)

$$\frac{k_{nf}}{k_f} = \frac{(k_s + 2k_f) - 2\phi(k_f - k_s)}{(k_s + 2k_f) + \phi(k_f - k_s)}, \left(\rho C_p\right)_{nf} = (1-\phi)\left(\rho C_p\right)_f + \phi\left(\rho C_p\right)_s, S = L\sqrt{\frac{b}{\nu_f}},$$

$$\rho_{nf} = (1-\phi)\rho_f + \phi\rho_s, \ \ \mu_{nf} = \frac{\mu_f}{(1-\phi)^{2.5}}, \frac{\sigma_{nf}}{\sigma_f} = 1 + \frac{3(\gamma-1)\phi}{(\gamma+2) - (\gamma-1)\phi}, \lambda = \frac{a}{b},$$

where Pr is the base fluid Prandtl number $Pr = 6.2$; Bi is the Biot number, Ec is the Eckert number; M is the magnetic field parameter; S is the slip parameter; and λ is the shrinking parameter. Furthermore, parameters ρ_f is the density of the base fluid; ρ_s is the density of the solid nanoparticle; m is the nanoparticles shape factor; k_f is the base fluid thermal conductivity; k_s is the nanoparticles thermal conductivity; σ_f is the base fluid electrical conductivity; σ_s is the nanoparticles electrical conductivity; ϕ is the nanoparticles volume fraction; μ_f is the base fluid dynamic viscosity; C_{pf} is the base fluid specific heat capacity; and C_{ps} is the nanoparticles specific heat capacity. The equation (4.8) then simplifies as,

$$\frac{\partial^3 f}{\partial \xi^3} - A_1\left(\frac{\partial^2 f}{\partial \xi \partial \tau} + \left(\frac{\partial f}{\partial \xi}\right)^2 - f\frac{\partial^2 f}{\partial \xi^2} - 1\right) + A_2 M\left(\frac{\partial f}{\partial \xi} - 1\right) = 0,$$

$$\frac{\partial^2 \Theta}{\partial \xi^2} - A_3 Pr\frac{\partial \Theta}{\partial \tau} + A_3 Pr\, f\, \frac{\partial \Theta}{\partial \xi} + A_4 PrEc\left(\frac{\partial^2 f}{\partial \xi^2}\right)^2 + A_5 PrEc\, M\left(\frac{\partial f}{\partial \xi} - 1\right)^2 = 0, \tag{4.9}$$

with boundary condition

$$f(0,\tau) = 0, \ \frac{\partial f}{\partial \xi}(0,\tau) = \lambda + S\frac{\partial^2 f}{\partial\, \xi^2}(0,\tau), \ \frac{\partial f}{\partial \xi}(\infty,\tau) = 1,$$

$$\frac{\partial \Theta}{\partial \xi}(0,\tau) = Bi(\Theta(0,\tau) - 1), \qquad \Theta(\infty,\tau) = 0. \tag{4.10}$$

The solution of equations (4.9) under the influence of the small disturbances are given by,

$$f(\xi,\tau) = F(\xi) + e^{-\beta\tau}H(\xi),$$

$$\Theta(\xi,\tau) = \theta(\xi) + e^{-\beta\tau}G(\xi), \tag{4.11}$$

where the eigen-function $H(\xi)$ and $G(\xi)$ are closely related to $F(\xi)$ and $\theta(\xi)$ respectively. We get the eigen functions by solving equation (4.9) using equation (4.11) and the following results was obtained with β as the unknown eigenvalue to be determined.

$$\left(\frac{d^3F}{d\xi^3} - A_1\left(\frac{\partial^2 F}{\partial\xi\partial\tau} + \left(\frac{dF}{d\xi}\right)^2 - F\frac{d^2F}{d\xi^2} - 1\right) + A_2M\left(\frac{\partial d}{d\xi} - 1\right)\right)$$
$$+ e^{-\beta\tau}\left(\frac{d^3H}{d\xi^3} + F\frac{d^2H}{d\xi^2} + \frac{dH}{d\xi}\left(A_1\beta - 2A_1\frac{dF}{d\xi} - A_2M\right) + A_1H\frac{d^2F}{d\xi^2}\right) \quad (4.12)$$
$$= 0,$$
$$\left(\frac{d^2\theta}{d\xi^2} + A_3PrF\frac{d\theta}{d\xi} + A_4PrEc\left(\frac{d^2F}{d\xi^2}\right)^2 + A_5PrEc\,M\left(\frac{dF}{d\xi} - 1\right)^2\right)$$
$$+ e^{-\beta\tau}\left(\frac{d^2G}{d\xi^2} + A_3Pr\beta G + A_3\,\mathrm{Pr}\left(F\frac{dG}{d\xi} + H\frac{d\theta}{d\xi}\right)\right.$$
$$\left. + 2A_4PrEc\frac{d^2F}{d\xi^2}\frac{d^2H}{d\xi^2} + 2A_5PrEcM\frac{dH}{d\xi}\left(\frac{d\,F}{d\xi} - 1\right)\right) = 0.$$

The $F(\xi)$ and $\theta(\xi)$ are the basic steady state solution of the model problem and are obtained in the equation (4.13) below,

$$\frac{d^3F}{d\xi^3} - A_1\left(\left(\frac{dF}{d\xi}\right)^2 - F\frac{d^2F}{d\xi^2} - 1\right) + A_2M\left(\frac{dF}{d\xi} - 1\right) = 0,$$
$$\frac{d^2\theta}{d\xi^2} + A_3PrF\frac{d\theta}{d\xi} + A_4PrEc\left(\frac{d^2F}{d\xi^2}\right)^2 + A_5PrEc\,M\left(\frac{dF}{d\xi} - 1\right)^2 = 0, \quad (4.13)$$

together with boundary condition

$$F(0) = 0, \frac{dF}{d\xi}(0) = \lambda + S\frac{d^2F}{d\xi^2}(0), \frac{dF}{d\xi}(\infty) = 1, \frac{d\theta}{d\xi}(0) = Bi(\theta(0) - 1), \theta(\infty) = 0. \quad (4.14)$$

The system of linearized eigenvalue problem with a small disturbance is given by,

$$\frac{d^3H}{d\xi^3} + F\frac{d^2H}{d\xi^2} + \frac{dH}{d\xi}\left(A_1\beta - 2A_1\frac{dF}{d\xi} - A_2M\right) + A_1H\frac{d^2F}{d\xi^2} = 0,$$
$$\frac{d^2G}{d\xi^2} + A_3Pr\beta G + A_3\,\mathrm{Pr}\left(F\frac{dG}{d\xi} + H\frac{d\theta}{d\xi}\right) + 2A_4PrEc\frac{d^2F}{d\xi^2}\frac{d^2H}{d\xi^2}$$
$$+ 2A_5PrEcM\frac{dH}{d\xi}\left(\frac{dF}{d\xi} - 1\right) = 0, \quad (4.15)$$

along with boundary conditions

$$H(0) = 0, \frac{dH}{d\xi}(0) = S\frac{d^2H}{d\xi^2}(0), \frac{dH}{d\xi}(\infty) = 0, \frac{dG}{d\xi}(0) = Bi\mathrm{G}(0), G(\infty) = 0, \quad (4.16)$$

The interval of eigenvalue β can be evaluated by relaxing the boundary condition on $\frac{dH}{d\xi}$ and G . In this study the condition $\frac{dH}{d\xi} \to 0$ as $\xi \to \infty$ will be relaxed and imposed a new boundary condition $\frac{d^2H}{d\xi^2} = 1$ at $\xi = 0$ to obtain the solution of equation (4.15) with its boundary condition (4.16).

$$\begin{aligned} &\frac{d^3H}{d\xi^3} + F\frac{d^2H}{d\xi^2} + \frac{dH}{d\xi}\left(A_1\beta - 2A_1\frac{dF}{d\xi} - A_2M\right) + A_1H\frac{d^2F}{d\xi^2} = 0, \\ &\frac{d^2G}{d\xi^2} + A_3Pr\beta G + A_3\,\mathrm{Pr}\left(F\frac{dG}{d\xi} + H\frac{d\theta}{d\xi}\right) + 2A_4PrEc\frac{d^2F}{d\xi^2}\frac{d^2H}{d\xi^2} \\ &\qquad + 2A_5PrEcM\frac{dH}{d\xi}\left(\frac{dF}{d\xi} - 1\right) = 0, \end{aligned} \tag{4.17}$$

along with boundary condition

$$H(0) = 0, \frac{dH}{d\xi}(0) = S, \frac{dH}{d\xi}(\infty) = 0, \frac{d^2H}{d\xi^2}(0) = 1, \frac{dG}{d\xi}(0) = Bi\mathrm{G}(0), G(\infty) = 0. \tag{4.18}$$

Furthermore, the solution of equation (4.17) will produce a set of infinite numbers of eigenvalues $\{\beta_i, i = 1,2,\ldots\}$ such that $\beta_1 < \beta_2 < \beta_3 \ldots$ the temporal instability of the flow will occur due to the growth of the small disturbance that is determined by the negative value of the least eigenvalue β_1. If the least eigenvalue β_1 is the positive then the small disturbance will decay and the flow is temporal stable. Other quantities of interest with respect to the basic steady flow and heat transfer boundary layer are the skin friction coefficients (C_f) and the Nusselt number (Nu) which are given as,

$$C_f\sqrt{Re_x} = \frac{1}{(1-\phi)^{2.5}}\frac{d^2F}{d\xi^2}(0), \qquad \frac{Nu}{\sqrt{Re}} = -\frac{k_{nf}}{k_f}\frac{d\,\Theta}{d\xi}(0), \tag{4.19}$$

Where $C_f = \frac{T_w}{\rho_f U_\infty^2}$, $Nu = \frac{xq_w}{k_f(T_f - T_\infty)}$, $T_w = \mu_{nf}\frac{\partial u}{\partial y}$, $q_w = -k_{nf}\frac{\partial T}{\partial y}$ and $Re_x = \frac{xU_\infty}{\upsilon_f}$.

4.4 Numerical Procedure

The obtained boundary value problem (BVP) in the eigenvalue function (4.17) together with boundary condition equation (4.18) will be transformed to the initial value problem (IVP) by letting $x_1 = H(\xi)$, $x_2 = \frac{dH}{d\xi}$ and $x_3 = \frac{d^2H}{d\xi^2}$ then we have the following equations,

$$x_1' = x_2, x_2' = x_3, \qquad x_3' = -Fx_3 - x_2\left(A_1\beta - 2A_1\frac{dF}{d\xi} - A_2M\right) - A_1x_1\frac{d^2F}{d\xi^2}. \tag{4.20}$$

Which will be solved with the initial condition $x_1(0) = 0$, $x_2(0) = S$, $x_2(\infty) = 0$ and $x_3(0) = 1$, taking $\infty = 10$ note that $F(\xi) = \frac{\lambda-1}{Sn^2+n}\left(1 - e^{-n\xi}\right) + \xi$ where $n = -\frac{\delta m}{S\delta m+\lambda-1}$, thereafter, the system of first order ODEs is then solved by applying Runge-Kutta-Fehlberg integration scheme [62].

4.5 Results and Discussion

The results in Table 4.1 and Figure (4.1) - (4.3) will be discussed and note that the solid line represents the upper branch solution and the dotted line represents the lower branch solution. Furthermore, it is noticeable that the upper branch solution for shrinking surface is temporally stable and physically realizable since the value of the smallest eigenvalue $\boldsymbol{\beta}$ is positive while the negative value show the lower solution branch clearly revealed that it is unstable and unrealistic. Moreover, the positive value of $\boldsymbol{\beta}$ shows the decay rate of a small disturbance on the upper solution branch while the negative value of $\boldsymbol{\beta}$ for the lower solution branch shows the escalation of the disturbances. Table 4.1 illustrates that as the parameter values of magnetic field intensity (M), surface slipperiness (S) and nanoparticle volume fraction ($\boldsymbol{\phi}$) increases the magnitude of the smallest disturbance for upper solution branch escalates. This implies that the stability of the basic flow profiles for upper solution branch is enhanced with a rise in nanoparticles volume fraction, magnetic field intensity, and sheet surface slipperiness. It is clear from Figure (4.1 A), (4.2 A), and (4.3 A) that an increase in the value of magnetic field intensity (M), surface slipperiness (S) and nanoparticle volume fraction ($\boldsymbol{\phi}$) will decrease in the disturbance while the lower branch solution increase in disturbance. Figure (4.1 B), (4.2 B), and (4.3 B) shows that the upper branch solution gets stable quicker than the lower branch solution whilst the lower branch solution does not guarantee that it will be stable.

Table 4.1: Computations showing the Smallest Eigenvalues β (Cu-water).

S	ϕ	M	λ_c	λ	Upper branch β	Lower branch β
0.35	0.10	0.10	-1.08888125	-1.088	0.298148657388309	-0.90765143033749
0.40	0.10	0.10	-1.13059454	-1.088	0.557436560714014	-1.05014438401623
0.45	0.10	0.10	-1.27445889	-1.088	0.755102576762429	-1.14791083666851
0.40	0.00	0.10	-1.25435863	-1.188	0.440326214871573	-0.96441761152105
0.40	0.05	0.10	-1.26529459	-1.188	0.508507746496823	-1.02135100054917
0.40	0.10	0.10	-1.27445888	-1.188	0.557439515483268	-1.05014954262666
0.40	0.10	0.15	-1.31832136	-1.188	0.735094535307276	-1.24716464152716
0.40	0.10	0.20	-1.36228207	-1.188	0.885126600313630	-1.41697357183725

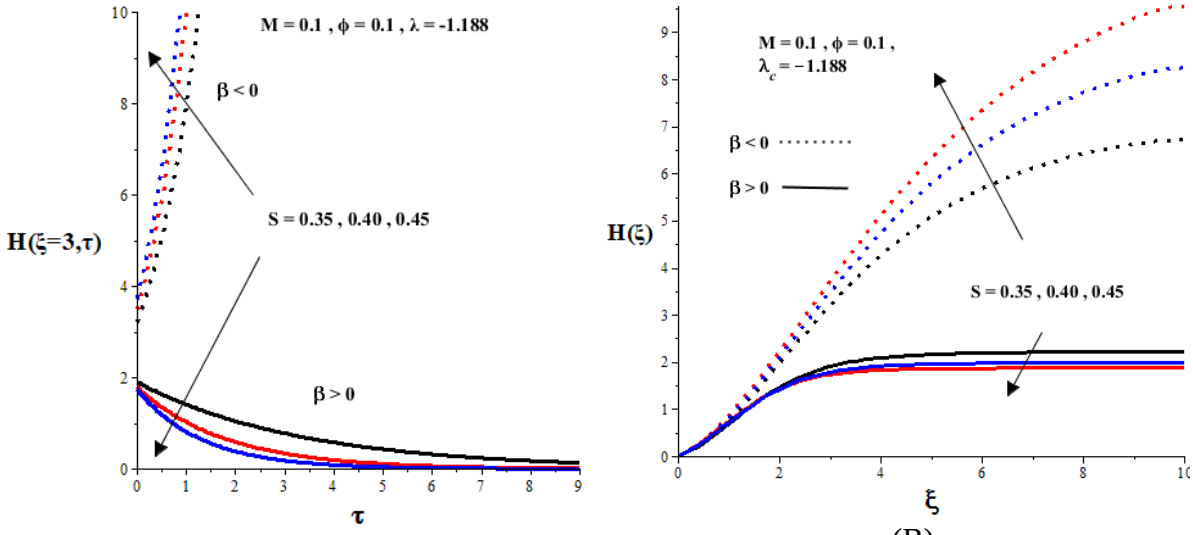

(A) (B)

Figure 4.2: The impact of Surface slippery (S) on the smallest eigenvalues β for both upper and lower branch solution.

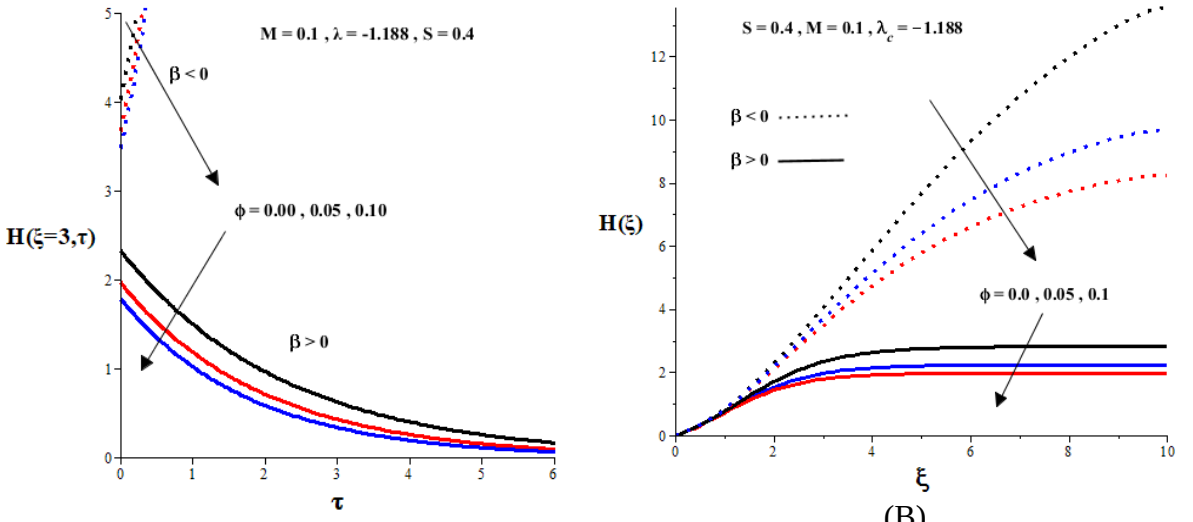

(A) (B)

Figure 4.3: The impact of nanoparticle volume fraction (ϕ) on the smallest eigenvalues β for both upper and lower branch solution.

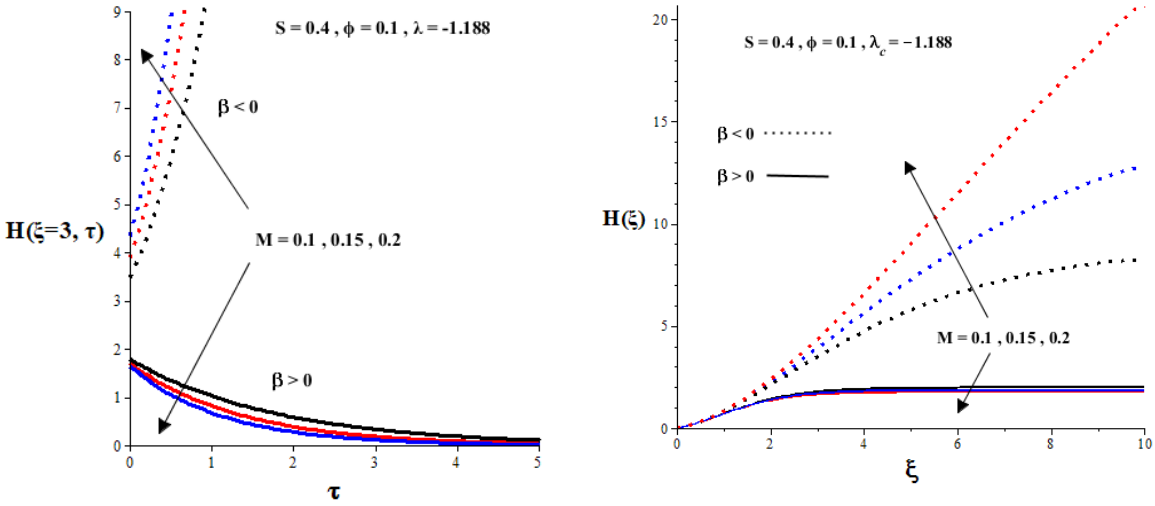

(A) (B)

Figure 4.4: The impact of magnetic field intensity (M) on the smallest eigenvalues β for both upper and lower branch solution.

CHAPTER 5: GENERAL DISCUSSION AND CONCLUSION

5.1 General Discussion

In this thesis, the problem of a nanofluid flow over a heated flat surface in the presence of an imposed magnetic field intensity were studied by using Cu-water, or Fe_3O_4-water, or Al_2O_3-water as a working nanofluid. The problems have been studied both numerically and analytically where the impact of magnetic field intensity (M), surface slipperiness (S), shrinking/stretching surface (λ), nanoparticle volume fraction (ϕ), Boit number (Bi), and Eckert number (Ec) was analysed on the velocity, temperature, skin friction and Nusselt number profiles. In Chapter 2, the computational modelling of MHD nanofluid flow over a stretching heated surface was numerical investigated. In Chapter 3, the dual solution for MHD stagnation point of nanofluid towards a heated shrinking surface was analysed. Lastly, in chapter 4 the MHD stability for stagnation point flow of nanofluid towards a heated shrinking surface was analysed. This mathematical model was conducted based on the theoretical concept of continuum mechanics, thermodynamics, electromagnetic theory, nanofluid thermophysical properties, Maxwell's equation, and numerical simulation techniques.

5.2 Conclusions

The current study examined the influence of a magnetic field on the thermal boundary layer flow of a conducting nanofluid consisting of Cu-water, Al_2O_3-water, and Fe_3O_4-water past a convectively shrinking and stretching slippery surface. The temporal stability of the obtained dual solutions to small disturbances were also investigated for the case of shrinking surface. The modelled mathematical equations were reduced to a system of ODEs and numerically tackled via the shooting method with the Runge-Kutta-Fehlberg integration scheme. The main findings of the present analysis are itemized as follows:

- Cu-water exhibited the highest heat transfer enhancement rate followed by Fe_3O_4-water and Al_2O_3-water. This implied that Cu-water may serve as a better coolant with more effective cooling properties as compared to Fe_3O_4-water and Al_2O_3-water.
- In all three nanofluids under examination, the obtained solution was unique for the flow over a stretched sheet, while dual solutions existed for a certain range of parameter ($\lambda_c < \lambda < 0$) in the case of flow over a shrinking sheet surface.

- A critical value of shrinking parameter *(λ_c)* occurred below which no real solution could be found. This critical value indicated the extent to which the surface can shrink during the cooling process.
- The smallest eigenvalue obtained based on temporal stability analysis revealed that only the upper solution branch was stable and physically realizable while the lower solution branch was unstable and unrealistic.
- The nanofluids velocity boundary layer thickness lessened with an increase in the surface slipperiness (*S*), magnetic field intensity (*M*) and nanoparticles volume fraction ($\boldsymbol{\phi}$).
- Thermal boundary layer thickness were amplified with an upsurge in magnetic field intensity (*M*) and Eckert number (*Ec*) due to viscous dissipation. Meanwhile, an increase in surface slipperiness (*S*), nanoparticles volume fraction ($\boldsymbol{\phi}$) and Biot number (*Bi*) due to sheet convective heating lessened the thermal boundary layer thickness.
- The skin friction on the sheet surface escalated with an increase in magnetic field intensity (*M*) and nanoparticles volume fraction ($\boldsymbol{\phi}$) but diminished with surface slipperiness (*S)*.
- The Nusselt number was enhanced with a rise in the nanoparticles volume fraction ($\boldsymbol{\phi}$), surface slipperiness (S) and Biot number (*Bi*) due to sheet convective heating, while an upsurge in magnetic field intensity (*M*) and Eckert number (*Ec*) due to viscous dissipation lessened the Nusselt number.

5.3. Recommendations

Finally, it is noteworthy that the heat transfer enhancement capability of a conducting nanofluid in the presence of magnetic field can be augmented by optimally regulating the values of various embedded parameters. This will innovatively boost the coolant effectiveness for engineering and industrial applications.

5.4. Future Research Work

In general, due to miniaturization-era of technology nonlinear materials is extremely important in the applied sciences and engineering areas and to explore the properties of flow and heat transfer the following future work may be proposed:

- Considering the different geometry of the surface of steady MHD flow consisting of Cu-water nanofluid coolants pass a heated stretching/stretching sheet.
- Considering the unsteady MHD flow of Cu-water nanofluid over a cylindrical body.
- The unsteady MHD flow of Al_2O_3-water nanofluid coolants pass a heated stretching flat surface.

REFERENCES

[1] L. Hosain, Fluid flow and heat transfer simulations for complex industrial applications malardalen university press dissertation,282 (2018).

[2] R. Shyam, Heat Transfer, An overview, International journal of science and research, 4(9), (2018), 910–915.

[3] Arpaci VS , Author, Salamet A , Author and, Kao Shu-Hsin , Author, and Jaluria Y , Reviewer, Introduction to heat transfer, Applied mechaninics reviews, 55(2), (2002), 37-38, doi: 10.1115/1.1451231.

[4] W. M. Okita, M. J. Reno, A. P. Peres, and J. V. Resende, Heat transfer analyses using computational fluid dynamics in the air blast freezing of guava pulp in large containers, B razilian journal of chemical engineering, 30(4), (2013), 811-824, doi: 10.1590/S010.

[5] C. T. O'Sullivan, Newton's law of cooling: A critical assessment, American journal of physics, 58(10), (1990), 956-960, doi: 10.1119/1.16309.

[6] P. A. Davidson, An Introduction to magnetohydrodynamics. Cambridge university press, (2001), doi: 10.1017/cbo9780511626333.

[7] A. Tamir, Conservation law of mass, Journal of chemical engineering, 4(8), (2013), 1-2, doi: 10.4172/2157-7048.1000e114.

[8] S. Gonen, Application of the first law of thermodynamics to the adiabatic processes of an ideal gas : Physics teacher candidates, Science educatiion international ,25(4),(2014),372–395.

[9] S. U. S. Choi, Enhancing thermal conductivity of fluids with nanoparticles, in american society of mechanical engineers, Fluids engineering division (Publication) FED, (1995).

[10] B. A. Bhanvase, D. P. Barai, S. H. Sonawane, N. Kumar, and S. S. Sonawane,Chapter 40 - Intensified heat transfer rate with the use of nanofluids in micro and nano technologies, C. B. T.-H. of N. for I. A. Mustansar Hussain, Ed. Elsevier, (2018), 739–750.

[11] W. Yu and H. Xie, A Review on nanofluids: preparation, stability mechanisms, and applications, Journal of nanomaterials, 2012, (2011), 17, doi: 10.1155/2012/435873.

[12] C. Pang, J. W. Lee, and Y. T. Kang, Review on combined heat and mass transfer characteristics in nanofluids, International journal of thermal sciences, 87, (2015), 49-67, doi: 10.1016/j.ijthermalsci.2014.07.017.

[13] S. K. Das, S. U. S. Choi, W. Yu, and T. Pradeep, Nanofluids: science and technology., (2007), DOI:10.1002/9780470180693.

[14] K. Schlichting, Hermann and Gersten, Boundary-layer theorytle. Springer, (2016).

[15] S. Ahmad, A. M. Rohni, and I. Pop, Blasius and Sakiadis problems in nanofluids, Acta mechanica, 218, (2011), 195-204., doi: 10.1007/s00707-010-0414-6.

[16] Z. Xiong and S. K. Lele, Stagnation-point flow under free-stream turbulence, Journal in . fluid mechanics, 590, (2007), 1–33, doi: DOI: 10.1017/S0022112007007768.

[17] C. L. Navier, Mémoire sur les lois du mouvement des fluides,Mémoires l'Académie R. des Sci. l'Institut Fr., 6, (1823), 389–440.

[18] K. Kamrin, M. Z. Bazant, and H. A. Stone, Effective slip boundary conditions for arbitrary periodic surfaces: The surface mobility tensor, Journal in . fluid mechanic., 658,

(2010) , 409–437, doi: 10.1017/S0022112010001801.

[19] S. N. Ha, A nonlinear shooting method for two-point boundary value problems, international journal of computers and mathematics with applications, 42,(10-11), (2001), 1411-1420, doi: 10.1016/S0898-1221(01)00250-4.

[20] M. R. Osborne, On shooting methods for boundary value problems, journal of mathematical analysis and application, 27, (1969), doi: 10.1016/0022-247X(69)90059-6.

[21] W. H. Press and S. A. Teukolsky, Adaptive Stepsize Runge-Kutta Integration, Computer and physics, 6, (1992), 188, doi: 10.1063/1.4823060.

[22] C. Mayo, Implementation of the Runge-Kutta-Fehlberg method for solution of ordinary differential equations on a parallel processor., California naval postgraduate school dissertation, (1987).

[23] J. Buongiorno, Convective transport in nanofluids, Journal of heat transfer, 128(3), (2006), 240-250, doi: 10.1115/1.2150834.

[24] O. D. Makinde, W. A. Khan, and Z. H. Khan, Stagnation point flow of MHD chemically reacting nanofluid over a stretching convective surface with slip and radiative heat, Process mechanical engineering, 231(4), (2017), 695-703, doi: 10.1177/0954408916629506.

[25] W. N. Mutuku-Njane and O. D. Makinde, Combined effect of buoyancy force and Navier slip on MHD flow of a nanofluid over a convectively heated vertical porous plate, The science world journal, 2013, (2013), 8, doi: 10.1155/2013/725643.

[26] L. A. Lund, Z. Omar, and I. Khan, Mathematical analysis of magnetohydrodynamic (MHD) flow of micropolar nanofluid under buoyancy effects past a vertical shrinking surface: dual solutions, Heliyon, 5(9), (2019),1-10, doi: 10.1016/j.heliyon.2019.e02432.

[27] W. A. Khan, O. D. Makinde, and Z. H. Khan, MHD boundary layer flow of a nanofluid containing gyrotactic microorganisms past a vertical plate with Navier slip, international journal of heta transfer, 74, (2014), 285-291, doi: 10.1016/j.ijheatmasstransfer.2014.03.026.

[28] L. A. Lund, Z. Omar, U. Khan, I. Khan, D. Baleanu, and K. S. Nisar, Stability analysis and dual solutions of micropolar nanofluid over the inclined stretching/shrinking surface with convective boundary condition, Symmetry, 12(1), (2020), 74, doi: 10.3390/sym12010074.

[29] C. S. K. Raju, N. Sandeep, M. Jayachandra Babu, and V. Sugunamma, Dual solutions for three-dimensional MHD flow of a nanofluid over a nonlinearly permeable stretching sheet, Alexandria engineering. Journal, 55(1)., (2016), 151-162, doi: 10.1016/j.aej.2015.12.017.

[30] S. Mansur, A. Ishak, and I. Pop, The magnetohydrodynamic stagnation point flow of a nanofluid over a stretching/shrinking sheet with suction, PLoS One, (2015), doi: 10.1371/journal.pone.0117733.

[31] S. S. Pillai and R. Yoshie, Flow velocity and surface temperature effects on convective heat transfer coefficient from urban canopy surfaces by numerical simulation, Journal of urban and environmental engineering, 7(1), (2013), 74-81,doi: 10.4090/juee.2013.v7n1.074081.

[32] B. Rostami, N. Freidoonimehr, and S. Abbasbandy, Free convective heat and mass transfer for MHD fluid flow over a permeable vertical stretching sheet in the presence of the radiation and buoyancy effects, Ain sham engineering journal, 5(3), (2014), 901-912,

doi: 10.1016/j.asej.2014.02.007.

[33] P. Ganesan, I. Behroyan, S. He, S. Sivasankaran, and S. C. Sandaran, Turbulent forced convection of Cu-water nanofluid in a heated tube: Improvement of the two-phase model, Numerical heat transfer part a application, 69(4), (2016), 401–420, doi: 10.1080/10407782.2015.1081019.

[34] T. Hayat, M. I. Khan, M. Farooq, A. Alsaedi, M. Waqas, and T. Yasmeen, Impact of Cattaneo–Christov heat flux model in flow of variable thermal conductivity fluid over a variable thicked surface, International journal of heat and mass transfer, 99, (2016), 702-710, doi: https://doi.org/10.1016/j.ijheatmasstransfer.2016.04.016.

[35] M. I. Khan, Transportation of hybrid nanoparticles in forced convective Darcy-Forchheimer flow by a rotating disk, international communication in heat and mass transfer, 122, (2021), 105177, doi: https://doi.org/10.1016/j.icheatmasstransfer.2021.105177.

[36] M. I. Khan, M. Waqas, T. Hayat, and A. Alsaedi, A comparative study of casson fluid with homogeneous-heterogeneous reactions, 498, (2017), 85-90, doi: https://doi.org/10.1016/j.jcis.2017.03.024.

[37] M. I. Khan and F. Alzahrani, Nonlinear dissipative slip flow of Jeffrey nanomaterial towards a curved surface with entropy generation and activation energy, mathematical and computers in simulation, 185, (2021), 47-61, doi: https://doi.org/10.1016/j.matcom.2020.12.004.

[38] M. I. Khan and F. Alzahrani, Dynamics of activation energy and nonlinear mixed convection in Darcy-Forchheimer radiated flow of carreau nanofluid near stagnation point region journal of thermal science and engineering application, 13(5), (2021) 8 , doi: 10.1115/1.4049434.

[39] M. I. Khan and F. Alzahrani, Free convection and radiation effects in nanofluid (silicon dioxide and molybdenum disulfide) with second order velocity slip, entropy generation, Darcy-Forchheimer porous medium, Intenational journal of hydrogen energy, 46(1), (2021), 1362-1369, doi: https://doi.org/10.1016/j.ijhydene.2020.09.240.

[40] A. U. Awan, M. Aziz, N. Ullah, S. Nadeem, and K. A. Abro, Thermal analysis of oblique stagnation point flow with slippage on second-order fluid, journal of thermal analysis and calorimetry, (2021) doi: 10.1007/s10973-021-10760-z.

[41] S. Ahmad, S. Nadeem, and M. N. Khan, Mixed convection hybridized micropolar nanofluid with triple stratification and cattaneo – Christov heat flux model, Physica scripta, 96(7), (2021), doi: 10.1088/1402-4896/abf615.

[42] A. Yasin, Naeem Ullah, S. Nadeem, and S. Saleem, Finite element simulation for free convective flow in an adiabatic enclosure: Study of Lorentz forces and partially thermal walls, Case studies in thermal engineering, 25, (2021), 100981, doi: https://doi.org/10.1016/j.csite.2021.100981.

[43] A. Hussain, Aysha Rehman, Sohail Nadeem, M. Y. Malik, Alibek Issakhov, Lubna Sarwar, Shafiq Hussain, A combined convection Carreau–Yasuda nanofluid model over a convective heated surface near a stagnation point: A numerical study, Mathematical problems in engineering, 2021, (2021), 14, doi: 10.1155/2021/6665743.

[44] N. Abbas, S. Nadeem, S. Saleem, and A. Issakhov, Transportation of modified nanofluid flow with time dependent viscosity over a riga plate: Exponentially stretching, Ain Shams engineering . journal, (2021), doi: https://doi.org/10.1016/j.asej.2021.01.034.

[45] M. N. Khan, S. Ahmad, and S. Nadeem, Flow and heat transfer investigation of bio–

convective hybrid nanofluid with triple stratification effects, Physica. Scripta., 96(6),(2021),65210, doi: 10.1088/1402-4896/abf305.

[46] S. Akhtar, L. B. McCash, S. Nadeem, and A. Saleem, Scientific breakdown for physiological blood flow inside a tube with multi-thrombosis, Scientific reports., 11, (2021), 6718, doi: 10.1038/s41598-021-86051-2.

[47] S. Saleem, S. Akhtar, S. Nadeem, A. Saleem, M. Ghalambaz, and A. Issakhov, Mathematical study of electroosmotically driven peristaltic flow of casson fluid inside a tube having systematically contracting and relaxing sinusoidal heated walls, Chinese Journal of physics, 71, (2021), 300-311, doi: https://doi.org/10.1016/j.cjph.2021.02.015.

[48] A. Yildirim and S. Sezer, Analytical solution of MHD stagnationpoint flowin porous media by means of the homotopy perturbation method, journal of porous media, 15, (2012), 83–94, doi: 10.1615/JPorMedia.v15.i1.70.

[49] E. Mureithi, J. Mwaonanji, and O. Makinde, On the boundary layer flow over a moving surface in a fluid with temperature-dependent viscosity, Open journal of fluid dynamivs., 3(2), (2013), 135–140, doi: 10.4236/ojfd.2013.32017.

[50] K. Bhattacharyya and G. C. Layek, Magnetohydrodynamic boundary layer flow of nanofluid over an exponentially stretching permeable sheet, Physical research international, 2014,(2014), 592536, doi: 10.1155/2014/592536.

[51] F. Achard, James clerk maxwell, a treatise on electricity and magnetism, first edition (1873), in Landmark Writings in Western Mathematics 1640-1940, Elsevier, (2005), 564–587.

[52] M. Ferdows, Steady laminar boundary layer flow over an impulsively stretching surface enclosed by strong magnetic field, Procedia Engineering, 56, (2013), 281-286, doi: 10.1016/j.proeng.2013.03.119.

[53] L. K. Saha, M. A. Hossain, and R. S. R. Gorla, Effect of hall current on the MHD laminar natural convection flow from a vertical permeable flat plate with uniform surface temperature, internation journal of thermal science, 46(8), (2007), 790-801, doi: 10.1016/j.ijthermalsci.2006.10.009.

[54] O. D. Makinde, Computational modelling of MHD unsteady flow and heat transfer toward a flat plate with navier slip and newtonian heating, Brazilian Journal of cheical engineering, 29(1), (2012), 159-166, doi: 10.1590/S0104-66322012000100017.

[55] O. A Ajala, L. O Aselebe, S. F Abimbade, A. W Ogunsola, Effect of magnetic fields on the boundary layer flow of heat transfer with variable viscosity in the presence of thermal radiation, intrernational journal of science and research publications, 9(5), (2019), 8904, doi: 10.29322/ijsrp.9.05.2019.

[56] S. Mondal, N. A. H. Haroun, S. K. Nandy, and P. Sibanda, MHD boundary layer flow and heat transfer of Jeffrey nanofluid over an unsteady shrinking sheet with partial slip, Journal of.Nanofluids, 6(2), (2017), 343-353, doi: 10.1166/jon.2017.1312.

[57] K. Jafar, R. Nazar, A. Ishak, and I. Pop, MHD mixed convection stagnation point flow of an upper convected maxwell fluid on a vertical surface with an induced magnetic field, Magnetohydrodynamics, 47(1), (2011), 61-78, doi: 10.22364/mhd.47.1.6.

[58] M. R. Eid, K. L. Mahny, A. Dar, and T. Muhammad, Numerical study for carreau nanofluid flow over a convectively heated nonlinear stretching surface with chemically reactive species, Physical A: Statistical mechenics and its application, 540, (2020), 13063, , doi: 10.1016/j.physa.2019.123063.

[59] A. Kamran, S. Hussain, M. Sagheer, and N. Akmal, A numerical study of

magnetohydrodynamics flow in casson nanofluid combined with Joule heating and slip boundary conditions, Results in physics, 7, (2017), 3037–3048, doi: 10.1016/j.rinp.2017.08.004.

[60] T. Hayat, A. Kiran, M. Imtiaz, and A. Alsaedi, Hydromagnetic mixed convection flow of copper and silver water nanofluids due to a curved stretching sheet,Results in Physics., 6, (2016), 904-910, doi: 10.1016/j.rinp.2016.10.023.

[61] T. V. S. Sekhar, R. Sivakumar, H. Kumar, and T. V. R. Ravi kumar, Effect of aligned magnetic field on the steady viscous flow past a circular cylinder, Applied mathematical modelling, 31(1), (2017), 130-139, doi: 10.1016/j.apm.2005.08.011.

[62] T. Cebeci and P. Bradshaw, Physical and computational aspects of convective heat transfer.(1984).

[63] C. Y. Wang, Stagnation flow towards a shrinking sheet, International. journal of non linear mechanics, 43(5), (2008), 377-382,.doi: 10.1016/j.ijnonlinmec.2007.12.021.

[64] A. Ishak, Dual solutions in the stagnation-point flow over a shrinking sheet, international journal of mathematical model and methods in applied science, 12, (2018), 56–59.

[65] C. Y. Wang, Stagnation flow towards a shrinking sheet, International. journal of non linear mechanics, 43(5), (2008), 377-382,.doi: 10.1016/j.ijnonlinmec.2007.12.021.

[66] H. Heidary, R. Hosseini, M. Pirmohammadi, and M. J. Kermani, Numerical study of magnetic field effect on nano-fluid forced convection in a channel, Journal of. magnetism and magnetc material, 374, (2015), 11-17 doi: 10.1016/j.jmmm.2014.08.001.

[67] M. M. Rashidi, M. Nasiri, M. Khezerloo, and N. Laraqi, Numerical investigation of magnetic field effect on mixed convection heat transfer of nanofluid in a channel with sinusoidal walls, Journal of. Magnetism and magnetc material, 401., (2016), 159-168, doi: 10.1016/j.jmmm.2015.10.034.

[68] N. S. Akbar, S. Nadeem, R. U. Haq, and S. Ye, MHD stagnation point flow of carreau fluid toward a permeable shrinking sheet: Dual solutions, Ain Shams engineering. journal, 5(4), (2014), 1233-1239 doi: 10.1016/j.asej.2014.05.006.

[69] M. N. Rostami, S. Dinarvand, and I. Pop, Dual solutions for mixed convective stagnation-point flow of an aqueous silica–alumina hybrid nanofluid, Chinese journal of physics, 56(5), (2018), 2465-2478, doi: 10.1016/j.cjph.2018.06.013.

[70] N. S. Akbar, Z. H. Khan, R. U. Haq, and S. Nadeem, Dual solutions in MHD stagnation-point flow of Prandtl fluid impinging on shrinking sheet, Applied. mathematics and.mechanics, 35(7), (2014), 813-820, doi: 10.1007/s10483-014-1836-9.

[71] R. Dhanai, P. Rana, and L. Kumar, Critical values in slip flow and heat transfer analysis of non-Newtonian nanofluid utilizing heat source/sink and variable magnetic field: Multiple solutions, Journal of the Taiwan institute of chemical engineers, 58, (2016), 155-164,. doi: 10.1016/j.jtice.2015.06.026.

[72] K. Bhattacharyya and K. Vajravelu, Stagnation-point flow and heat transfer over an exponentially shrinking sheet, Communications in nonlinear science and numerical simulation, 17(7), (2012), 2728-2734, doi: 10.1016/j.cnsns.2011.11.011.

[73] K. Bhattacharyya, Dual solutions in boundary layer stagnation-point flow and mass transfer with chemical reaction past a stretching/shrinking sheet, International .communications in Heat Mass Transf., 38(7), (2011), 917-922, doi: 10.1016/j.icheatmasstransfer.2011.04.020.

[74] O. D. Makinde, Stagnation point flow with heat transfer and temporal stability of ferrofluid past a permeable stretching/shrinking sheet, Defect diffusion. forum, 387,

(2018), 510-522, doi: 10.4028/www.scientific.net/DDF.387.510.

[75] L. A. Lund, Z. Omar, S. Dero, Y. Chu, I. Khan, and K. S. Nisar, Temporal stability analysis of magnetized hybrid nanofluid propagating through an unsteady shrinking sheet: Partial slip conditions, Computer. Materials and. continua., 66(2), (2020), 1963–1975.

[76] O. D. Makinde and M. S. Tshehla, Analysis of thermal stability in a convecting and radiating two-step reactive slab, Advances in. mechanical engineering, 2013, (2015), 294961, doi: 10.1155/2013/294961.

[77] O. D. Makinde, Thermal stability of a reactive viscous flow through a porous-saturated channel with convective boundary conditions, Applied. thermal engineering, 29(8-9), (2009), 1773-1777, doi: 10.1016/j.applthermaleng.2008.08.012.

[78] O. D. Makinde, Thermal stability of a reactive third grade fluid in a cylindrical pipe: An exploitation of Hermite-Padé approximation technique, Applied. mathematical and compution, 189(1), (2007), 690-697, doi: 10.1016/j.amc.2006.11.124.

[79] O. D. Makinde, Magneto-hydrodynamic stability of plane-Poiseuille flow using multideck asymptotic technique, Mathematical and. computer modelling, 37(3-4), (2003), 251-259, doi: 10.1016/S0895-7177(03)00004-9.

[80] O. D. Makinde, On thermal stability of a reactive third-grade fluid in a channel with convective cooling the walls, Applied. mathematical and compution, 213(1), (2009), 170-176, doi: 10.1016/j.amc.2009.03.003.

[81] L. A. Lund, Z. Omar, I. Khan, A. H. Seikh, E. S. M. Sherif, and K. S. Nisar, Stability analysis and multiple solution of Cu-Al2O3/H2O nanofluid contains hybrid nanomaterials over a shrinking surface in the presence of viscous dissipation, Journal of. materials. research and . technology, 9(1), (2020), 421-432, doi: 10.1016/j.jmrt.2019.10.071.

[82] Y. Liu, S. Luo, and F. Liu, Multiple solutions and stability of the steady transonic small-disturbance equation, Theoretical and applied mechanics letters, 7(5), 265-16, (2017), doi: 10.1016/j.taml.2017.09.011.

[83] I. Mustafa, Z. Abbas, A. Arif, T. Javed, and A. Ghaffari, Stability analysis for multiple solutions of boundary layer flow towards a shrinking sheet: Analytical solution by using least square method, Physica A: Statistical. mechanics and its applitions, 540, (2020), 123028., 2020, doi: 10.1016/j.physa.2019.123028.

[84] S. Samanta and A. Guha, Analysis of heat transfer and stability of magnetohydrodynamic natural convection above a horizontal plate with heat flux boundary condition, international journal of heat and mass transfer, 70, (2014), 793-802, doi: 10.1016/j.ijheatmasstransfer.2013.10.049.

[85] https://www.google.com/url?sa=i&url=https%3A%2F%2Fwww.sciencelearn.org.nz%2Fresources%2F1909-observing-water-introduction&psig=AOvVaw3NjMA4Nrr_wAAqyc9O44ew&ust=1621359894575000&source=images&cd=vfe&ved=0CAIQjRxqFwoTCMjvzsOi0fACFQAAAAAdAAAAABAL

[86] https://www.google.com/url?sa=i&url=http%3A%2F%2Fwww.goldenbricks.co.zw%2Fproduct%2Fsolid-common-bricks&psig=AOvVaw3XZY5OYrV21IAq5dJPbNnh&ust=1621360088515000&sourc

e=images&cd=vfe&ved=0CAIQjRxqFwoTCPCkmpyj0fACFQAAAAAdAAAAABAD

[87] https://www.google.com/url?sa=i&url=https%3A%2F%2Fsciencing.com%2Fcure-smoke-pollution-factories-23979.html&psig=AOvVaw29Tw0TYq4-Ii13ahP3n6aU&ust=1621360189649000&source=images&cd=vfe&ved=0CAIQjRxqFwoTCKiH8sqj0fACFQAAAAAdAAAAABAD

[88] https://www.google.com/imgres?imgurl=https%3A%2F%2Fwww.universetoday.com%2Fwp-content%2Fuploads%2F2010%2F07%2FOur-Sun.jpg&imgrefurl=https%3A%2F%2Fwww.universetoday.com%2F84361%2Fplasma%2F&tbnid=_6yk5A5ck3XHYM&vet=10CBMQxiAoAmoXChMIgPDLiaTR8AIVAAAAAB0AAAAAEAc..i&docid=SxopRsVVCO6u5M&w=1280&h=1024&itg=1&q=plasmas%20liquid&hl=en&ved=0CBMQxiAoAmoXChMIgPDLiaTR8AIVAAAAAB0AAAAAEAc

[89] https://www.google.com/imgres?imgurl=https%3A%2F%2Fexaircorp.files.wordpress.com%2F2018%2F09%2F13580963114_f222b3cdd9_z.jpg%3Fw%3D640&imgrefurl=https%3A%2F%2Fblog.exair.com%2F2018%2F09%2F12%2Fheat-transfer-3-types%2F&tbnid=e6N7NOH8JdLFuM&vet=10CAMQxiAoAGoXChMImNzT26TR8AIVAAAAAB0AAAAAEAc..i&docid=dw1RkOK0FkPTaM&w=640&h=223&itg=1&q=heat%20transfer%20in%20conduction%20electrons&ved=0CAMQxiAoAGoXChMImNzT26TR8AIVAAAAAB0AAAAAEAc

[90] https://www.google.com/imgres?imgurl=x-raw-image%3A%2F%2F%2F0f51d4ef68e79df1c78f78dbe000f7312f757466ebe4408e9ac0f1ab23bb7e96&imgrefurl=http%3A%2F%2Fmrszeches.weebly.com%2Fuploads%2F2%2F6%2F6%2F1%2F26611576%2Fheat_transfer_worksheet_with_article.pdf&tbnid=8Z3naO_UUQ-pLM&vet=10CAMQxiAoAGoXChMI-MLHiKXR8AIVAAAAAB0AAAAAEAY..i&docid=WoGPg_1n7K3FyM&w=225&h=148&itg=1&q=heat%20transfer%20in%20conduction%20hand%20on%20hot%20pot&ved=0CAMQxiAoAGoXChMI-MLHiKXR8AIVAAAAAB0AAAAAEAY

[91] https://www.google.com/url?sa=i&url=https%3A%2F%2Fwww.britannica.com%2Fscience%2Fsea-and-land-breeze&psig=AOvVaw0CY5u3QuWpLphSJkQ-UmWN&ust=1621360717203000&source=images&cd=vfe&ved=0CAIQjRxqFwoTCID38b6l0fACFQAAAAAdAAAAABAD

[92] https://www.google.com/url?sa=i&url=https%3A%2F%2Fhandwiki.org%2Fwiki%2FPhysics%3AForced_convection&psig=AOvVaw2jsDjCkLIH4GVSQ0XSiL9E&ust=1621360797478000&source=images&cd=vfe&ved=0CAIQjRxqFwoTCMi6r-al0fACFQAAAAAdAAAAABAD

[93] https://www.google.com/imgres?imgurl=https%3A%2F%2Fyoursafetyexperts.com%2Fwp-content%2Fuploads%2F2018%2F08%2FFire-Extinguisher-with-border.jpg&imgrefurl=https%3A%2F%2Fyoursafetyexperts.com%2Fsafety-training%2Ffire-extinguisher-training%2F&tbnid=lTAD4n3DDTPnIM&vet=10CBMQxiAoCGoXChMIiKX5qqbR8AIVAAAAAB0AAAAAEAY..i&docid=4ETlFG2vVcI8PM&w=819&h=552&itg=1&q=fire%20extinguisher%20as%20forced%20convection&ved=0CBMQxiAoCGoXChMIiKX5qqbR8AIVAAAAAB0AAAAAEAY

[94] https://www.google.com/imgres?imgurl=https%3A%2F%2Fi.pinimg.com%2Foriginals%2Fd0%2Fb4%2F13%2Fd0b41328f264efffa8eca02fb8ff6dbb.png&imgrefurl=https%3A%2F%2Fwww.pinterest.com%2Fpin%2F470344754830832385%2F&tbnid=fWmmUlXw9vt5MM&vet=12ahUKEwjcl52dp9HwAhUIdxoKHVm-DqwQMygAegQIARA9..i&docid=7yUsbu33mUa2-M&w=640&h=488&q=radiation%20heat%20transfer%20mirror%20and%20asphalt&ved=2ahUKEwjcl52dp9HwAhUIdxoKHVm-DqwQMygAegQIARA9

[95] https://www.google.com/url?sa=i&url=https%3A%2F%2Fphysicsabout.com%2Fradiation%2F&psig=AOvVaw3dS60mtzTCBfbHHdEMvVXV&ust=1621361112443000&source=images&cd=vfe&ved=0CAIQjRxqFwoTCNDkv4en0fACFQAAAAAdAAAAABAD

[96] https://www.google.com/url?sa=i&url=https%3A%2F%2Fintl.siyavula.com%2Fread%2Fscience%2Fgrade-7%2Fheat-energy-transfer%2F13-heat-energy-transfer&psig=AOvVaw18-ZLMq2OqiYZMTZecM7Rk&ust=1621361241655000&source=images&cd=vfe&ved=0CAIQjRxqFwoTCNCvi7qn0fACFQAAAAAdAAAAABAD

[97] https://www.google.com/url?sa=i&url=https%3A%2F%2Fwww.hindawi.com%2Fjournals%2Fjnm%2F2018%2F6978130%2F&psig=AOvVaw1WOZ3dPiHi95kfZE-muT8-&ust=1621361449478000&source=images&cd=vfe&ved=0CAIQjRxqFwoTCOiLiZ-o0fACFQAAAAAdAAAAABAD

[98] https://www.google.com/url?sa=i&url=https%3A%2F%2Fwww.electronicsforu.com%2Ftechnology-trends%2Ftech-focus%2Fthermal-management-techniques-optimal-design&psig=AOvVaw32TGaDGg_9qcZNvTaxGuTM&ust=1621361718801000&source=images&cd=vfe&ved=0CAIQjRxqFwoTCJibvaOp0fACFQAAAAAdAAAAABAD

[99] https://www.google.com/url?sa=i&url=https%3A%2F%2Fwww.pinterest.com%2Fpin%2F369365606913581458%2F&psig=AOvVaw3X87XAMGbRstVOob7WHbCa&ust=1621361834099000&source=images&cd=vfe&ved=0CAIQjRxqFwoTCLD4qdap0fACFQAAAAAdAAAAABAD

[100] https://www.google.com/imgres?imgurl=https%3A%2F%2Fwww.aviationcentral.co.za%2Fwp-content%2Fuploads%2F2018%2F09%2FIMG_1523.jpg&imgrefurl=https%3A%2F%2Fwww.aviationcentral.co.za%2Fafrica-aerospace-and-defence-airshow-2018%2F&tbnid=lUz_5DERo5f5LM&vet=12ahUKEwjQpLqpqtHwAhUS04UKHeaKDmYQMygBegUIARC6AQ..i&docid=7nYud4r013KchM&w=4848&h=3356&q=sandf%20air%20show&hl=en&ved=2ahUKEwjQpLqpqtHwAhUS04UKHeaKDmYQMygBegUIARC6AQ

[101] https://www.google.com/url?sa=i&url=http%3A%2F%2Fplateandfinheatexchanger.sell.everychina.com%2Fp-101402318-aluminum-compact-high-performance-radiators-for-cars-air-heat-exchanger.html&psig=AOvVaw1khU7Dv8D-U_1xOQFcA2mQ&ust=1621362191089000&source=images&cd=vfe&ved=0CAIQjR

xqFwoTCPjmjoWr0fACFQAAAAAdAAAAABAD

[102] https://www.google.com/imgres?imgurl=https%3A%2F%2Flookaside.fbsbx.com%2Flookaside%2Fcrawler%2Fmedia%2F%3Fmedia_id%3D845465779141764&imgrefurl=https%3A%2F%2Fwww.facebook.com%2Ftranemyanmar%2Fposts%2Ftrane-super-nano-coolant%2F845466759141666%2F&tbnid=61pyGP45fY0b9M&vet=12ahUKEwiHzorxqtHwAhUU7xoKHbHzCUcQMygBegUIARC3AQ..i&docid=KN8_Q_8C5g0PkM&w=310&h=600&q=super%20nano%20coolant&hl=en&ved=2ahUKEwiHzorxqtHwAhUU7xoKHbHzCUcQMygBegUIARC3AQ

[103] https://www.google.com/url?sa=i&url=https%3A%2F%2Fwww.thermal-engineering.org%2Fwhat-is-boundary-layer-definition%2F&psig=AOvVaw26otx2Shx1UNAH1nfLD0zL&ust=1621362285723000&source=images&cd=vfe&ved=0CAIQjRxqFwoTCNCxtK6r0fACFQAAAAAdAAAAABAD

[104] https://www.google.com/url?sa=i&url=https%3A%2F%2Fen.m.wikipedia.org%2Fwiki%2FFile%3AAerodynamics_of_model_car.jpg&psig=AOvVaw1NTiXpud-XT-j8Doogr_qL&ust=1621362466536000&source=images&cd=vfe&ved=0CAIQjRxqFwoTCLD5zoms0fACFQAAAAAdAAAAABAP

[105] https://www.google.com/url?sa=i&url=https%3A%2F%2Fwww.researchgate.net%2Ffigure%2FIllustration-showing-stagnation-point-flow-field_fig2_224107981&psig=AOvVaw0WcmnYfXr7pLYnD9Xv_QG0&ust=1621362661852000&source=images&cd=vfe&ved=0CAIQjRxqFwoTCMDdk-Cs0fACFQAAAAAdAAAAABAD